Reduced power output in skeletal muscles devoid of skMLCK:

RLC phosphorylation contributes to peak performance

Josh Bowslaugh, Bkin

Submitted in partial fulfillment of the requirements for the degree of

Master of Science in Applied Health Sciences

(Kinesiology)

Faculty of Applied Health Sciences,

Brock University

500 Glenridge Ave.

St. Catharines, ON

L2S 3A1

© January 2016

ABSTRACT

Regulatory light chain (RLC) phosphorylation in fast twitch muscle is catalyzed by skeletal myosin light chain kinase (skMLCK), a reaction known to increase muscle force, work, and power. The purpose of this study was to explore the contribution of RLC phosphorylation on the power of mouse fast muscle during high frequency (100 Hz) concentric contractions. To determine peak power shortening ramps (1.05 to 0.90 L_o) were applied to Wildtype (WT) and skMLCK knockout ($skMLCK^{-/-}$) EDL muscles at a range of shortening velocities between 0.05-0.65 of maximal shortening velocity (V_{max}), before and after a conditioning stimulus (CS). As a result, mean power was increased to 1.28 ± 0.05 and 1.11 ± .05 of pre-CS values, when collapsed for shortening velocity in WT and $skMLCK^{-/-}$, respectively (n = 10). In addition, fitting each data set to a second order polynomial revealed that WT mice had significantly higher peak power output (27.67 ± 1.12 W/ kg^{-1}) than $skMLCK^{-/-}$ (25.97 ± 1.02 W/ kg^{-1}), ($p < .05$). No significant differences in optimal velocity for peak power were found between conditions and genotypes ($p > .05$). Analysis with Urea Glycerol PAGE determined that RLC phosphate content had been elevated in WT muscles from 8 to 63 % while minimal changes were observed in $skMLCK^{-/-}$ muscles: 3 and 8 %, respectively. Therefore, the lack of stimulation induced increase in RLC phosphate content resulted in a ~40 % smaller enhancement of mean power in $skMLCK^{-/-}$. The increase in power output in WT mice suggests that RLC phosphorylation is a major potentiating component required for achieving peak muscle performance during brief high frequency concentric contractions.

ACKNOWLEDGEMENTS

This thesis is not simply the work of one author, but rather, it is the product of endless collaboration, deliberation, and input from others who cared to support me during my graduate work. Every individual brought something forth that aided in the betterment of this thesis and I must thank you all for your advice:

Firstly, to my supervisor Dr. Rene Vandenboom for all of your input over the past two years. From ball-hockey to lab meetings, you always had advice to give me that motivated me to achieve a high standard of performance - both in my thesis and ball hockey. I learned a great deal from your teaching and mentoring style.

To my thesis advisory committee - who truly represented an inter-disciplinary and well-rounded panel of experts - your feedback was undoubtedly the most important tool during the writing and re-writing of this work.

I must also thank the Boom Squad and their tireless effort to prevent the 'Bows-law' from over-analyzing every situation. Dr. William Gittings (Bill) was nothing short of an inspiration to me in every aspect of my life. He was a role model and teacher to me in the early portion of my degree and for that I am extremely grateful. Then there were the other two mouseketeers: Jordan and Steve. Jordan, who was my roommate for several years, saved me from myself in the form of "the roommate pact". We constantly encouraged one another and also found sanctity in our Wednesday night store runs. I would not have completed this thesis without you. As for Steve, he acted as both friend and third roommate during my Master's degree. We would have late-night sing along/ jam sessions and the three of us would speak in the form of movie quotes until exhaustion.

Erika, from as early as our picnic bench lunches, you supported me in so many ways, through tough times and tougher times. It was a journey I am glad to have spent with you by my side and I am appreciative of your kind words.

Last but not least, I would like to thank my family for believing in me and showing me support in whatever facet was needed. You all mean so much to me.

TABLE OF CONTENTS

LIST OF FIGURES

LIST OF TABLES

LIST OF ABBREVIATIONS

ACh = Acetylcholine

ADP = Adenosine Diphosphate

AP = Action Potential

ATP = Adenosine Triphosphate

Ca^{2+} = Calcium Ions

CNS = Central Nervous System

CS = Conditioning Stimulus

DHPR = Dihydropyridine Receptor

ECC = Excitation Contraction Coupling

ELC = Essential Light Chain

Fapp = Forward Rate Constant of Crossbridge Attachment

FT = Fast Twitch

Gapp = Reverse Rate Constant of Crossbridge Attachment

Hz = Stimulation Frequency

ICT = Intracellular Calcium Transient

KO = skMLCK Knockout Mice

L_o = Optimal Length

MLCP = Myosin Light Chain Phosphatase

mN = Millinewtons

Ms = Milliseconds

P_i = Inorganic Phosphate

P_o = Maximum Tetanic Force

PO = Power Output

PTP = Post-tetanic Potentiation

RLC = Regulatory Light Chain

RyR = Ryanodine Receptor

SkMLCK = Skeletal Myosin Light Chain Kinase

$SkMLCK^{-/-}$ = Skeletal Myosin Light Chain Kinase Knockout Mice

SR = Sarcoplasmic Reticulum

ST = Slow Twitch

TA = Tibialis Anterior

Tm = Tropomyosin

TnC = Troponin C

Vmax = Maximum Shortening Velocity

WT = Wildtype Mice

+dF/dt = Rate of Force Development

-dF/dt = Rate of Force Relaxation

REVIEW OF LITERATURE

1.1 Introduction

Muscle contraction is a means to move or resist a given load by applying force, whether it is in the form of locomotion or moving an external object. The underlying trigger for movement is a series of motor signals carried through the central nervous system causing muscles to contract. Depending on the load, muscles will either contract by creating force without a change in length (isometrically), or dynamically, by creating force while lengthening (eccentrically) or shortening (concentrically). Isometric contractions are useful in many settings; however, they do not comprise a high portion of the contractions used during movement. In lieu of this, it is essential to our fundamental understanding of the musculoskeletal system, as well as to aspects of locomotion, to study dynamic contraction as it pertains to mechanical performance in mammals.

One of the most important aspects of muscle performance is power, which can be defined as the speed of muscle shortening against any given load (Josephson, 1993; Seow, 2013). In order to reach peak muscle power, muscle fibers that can produce the most amount of force in the shortest period of time must be recruited. These muscle fibers are aptly named fast-twitch fibers (type 2), and these become increasingly activated during more powerful and forceful muscle contractions. Unlike other muscle fiber types these fibers have the ability to potentiate, a mechanism suggested to assist fast twitch muscle fibers in achieving high forces very rapidly (Gittings et al., 2014). Potentiation may occur anytime these fibers are activated; a process that enhances mechanical power and thus improves performance. The following review will detail the major intracellular

mechanisms of muscle contractile functioning, with specific detail to the mechanisms of potentiation and how it can affect the attainment of peak power in mammalian skeletal muscle.

1.2 Excitation-Contraction Coupling

The molecular process by which vertebrate skeletal muscle converts chemical energy into mechanical force, work, and power is known as excitation-contraction coupling (Vandenboom, 2004), and is the basis for mammalian locomotion. Skeletal muscle contraction is induced by changes in resting membrane potential as a result of innervation from the central nervous system in the form of an action potential (AP) released down the spinal cord where it synapses directly/indirectly with a motor neuron. The motor neuron then transmits the AP down the length of its axon where it converges with the target muscle cell at the neuromuscular junction (Huxley, 1974). Release of acetylcholine (ACh) into the synaptic cleft results in the opening of ligand-gated sodium release channels on the motor end plate. A wave of Na^+ depolarizes the sarcolemma and ensures further AP propagation down into the t-tubules of the cell (Huxley & Taylor, 1958; Westerblad et al., 2010). The t-tubule network is continuous throughout the length of the cell with regular intervals extending inward for vast and hastily transmission of the chemo-electrical signal (Schneider & Chandler, 1973). During depolarization of the t-tubules, both a voltage-sensing dihydropyridine receptor (DHPR) and its linked SR bound Ca^{2+} release Ryanodine (RyR_1) receptor becomes activated (Allen, Lamb, & Westerblad, 2008; Chin, 2005; Dulhunty, 2006). The mechanism of connection between the two proteins is still unclear, albeit a conformational coupling process seems to be the likely cause (Beam & Bannister, 2010; Rebbeck, Karunasekara, Board, Beard, Casarotto,

& Dulhunty, 2014). Consequently, the SR releases an efflux of Ca^{2+} into the myoplasm (Allen et al., 2008). Released Ca^{2+} will bind to troponin C (TnC) on the actin filament allowing for weak binding of myosin heads to actin (Mckillop & Geeves, 1993; Vandenboom, 2004). Force is then generated through the hydrolysis of ATP within the myosin head, which acts as a molecular motor, and the subsequent movement of myosin against the actin filament powers contraction. When the activating stimulus is removed the decay of force is regulated by re-sequestration of Ca^{2+} into the SR by the Ca^{2+} ATPase pumps, leading to unbound myosin heads and muscle relaxation (Allen et al., 2008; Lamb, 2000).

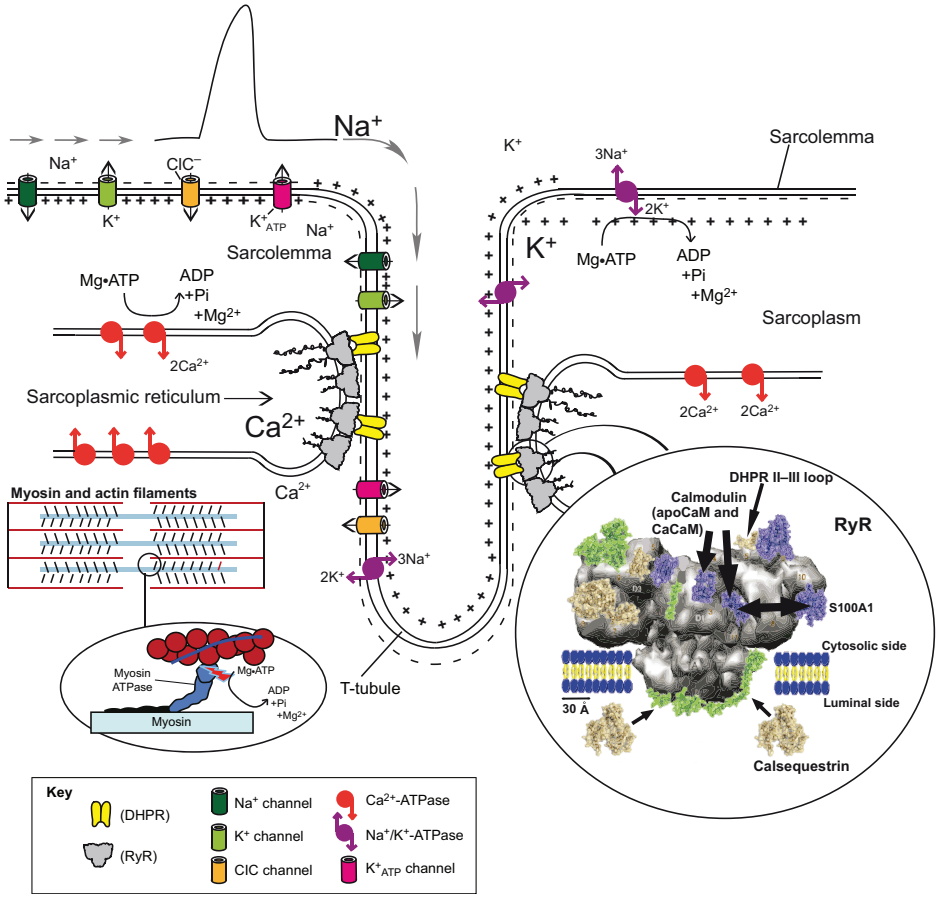

Figure 1. (MacIntosh, B. R., Holash, R. J., & Renaud, J. M. 2012) Excitation–contraction coupling and ATP usage in a skeletal muscle cell.

1.3 Contractile Apparatus Microanatomy

The sarcomere is known as the functional unit of the muscle cell. Within each sarcomere lies two distinct series of filaments, actin and myosin, that interact to produce force (Rayment et al., 1993a). It was originally hypothesized in 1954 that myosin and actin slid past each other forming a connection that generated force and muscle shortening (Huxley & Hanson, 1954; Huxley & Neidegerke, 1954). These research findings became the basis of the underlying mechanism of the sliding filament theory known today as crossbridge cycling (Craig & Woodhead, 2006). With regards to the potentiation of muscle force (see section **1.5**), knowing the biochemical makeup of myosin will further the understanding of its role during potentiation and therefore is discussed below.

1.3.1 Myosin Structure

The skeletal isoform of myosin, the myosin 2, is part of the superfamily of myosin motor proteins (Vandenboom, 2004). Skeletal myosin dimers are long protein chains that consist of two identical motor proteins (Kendrel & Mooseker, 2005). Each dimer is composed of two individual myosin molecules with winding tails, which projects from the larger thick filament base. The other end of the tail splits to form separate necks, each consisting of two light chain proteins, and two heads (Uyeda, Abramson, & Spudich, 1996). The tail of one myosin molecule runs anti-parallel to its adjacent neighboring myosin in a helical coiled-coil structure, thus forming the dimer. The distal portion of the tail is known as the C-terminus or light meromyosin region and provides self-association with the thick-filament backbone. The proximal portion of the tail segment known as the S2 subunit, acts as a flexible and mobile rod (Craig & Woodhead, 2006). It is the S2

portion of the tail that connects to the N-terminus globular head (motor domain) and is partly responsible for contractile and motility functions. As stated above, the neck of the molecule - at the base of the head - contains two light chains: the regulatory light chain (RLC), and the essential light chain (ELC); together they constitute the light-chain binding domain (LCD).

Each myosin heavy chain carries a molecular mass of ~220kD with the addition of the two light chains (~17-23kD each) making the overall myosin 2 molecule roughly 520kD (Rayment et al., 1993b; Schiaffino & Reggiani, 1994). Fastidious detail is called for when describing the myosin head region, as it is the key functioning segment of the myosin molecule. The head encompasses a nucleotide binding domain (25kD) used to store and release energy in the form of adenosine triphosphate (ATP). The hydrolysis of this high energy phosphate is used to drive contraction (Rayment et al., 1993b). The head of myosin also forms a cleft from a 50kD heavy chain segment, as well as a 20kD segment, that hold positive charges that bind to the negatively charged amino acids within the actin molecule, in preparation for crossbridge cycling.

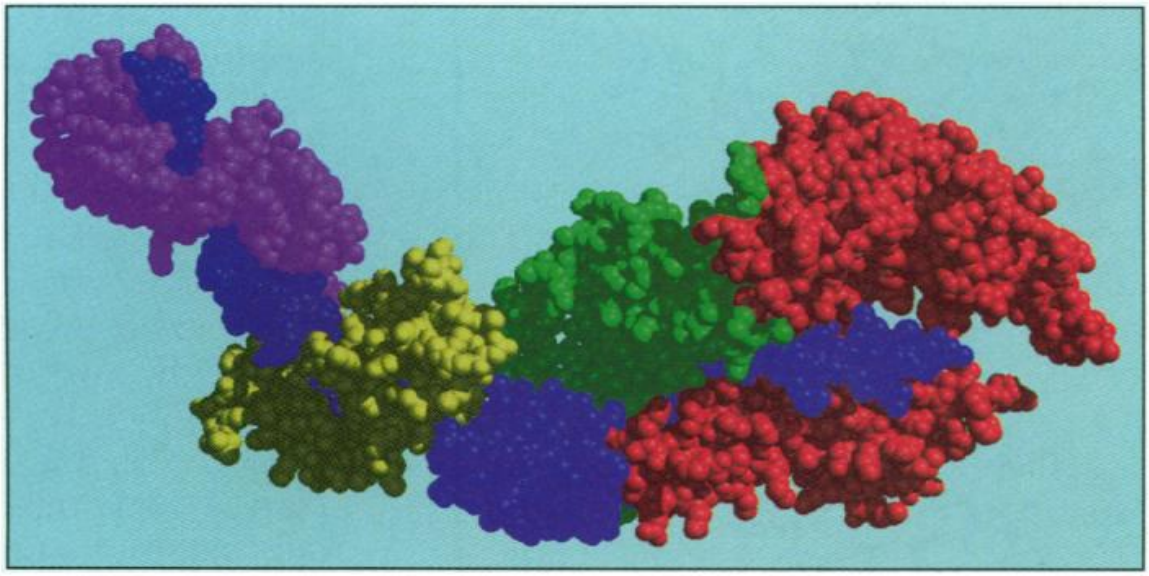

Figure 2. (Rayment et al., 1993*a*) A coloured myosin S1 schematic. Red represents the 50-kD actin binding cleft, blue represents the 20-kD actin binding region, and green represents the 25-kD nucleotide binding domain. The essential and regulatory light chains are shown in yellow and purple, respectively.

1.4 Crossbridge Cycling

The transduction of chemical-to-mechanical energy is facilitated by the interaction of the myofilaments. The putative mechanism of contraction is the cycling crossbridges that utilizes the energy from ATP hydrolysis to create force via filament sliding.

1.4.1 ATP Hydrolysis

The crossbridge cycle begins when Ca^{2+} binds to TnC on tropomyosin resulting in a change in position along actin. When tropomyosin (Tm) twists and 'rolls' off of its previous location on actin, it reveals a binding site where the head of myosin will dock to actin, pulling it towards the centre of the sarcomere (Gordon, Regnier, & Homsher, 2001). The acto-myosin complex is stabilized by docking of the S1 of myosin to actin, removing the steric-hindrance and forcing Tm away form the active site. This occurs

following the hydrolysis of ATP, and the resultant ADP and inorganic phosphate (P_i) become transiently captured within the nucleotide pocket (Gordon, Homsher, & Regnier, 2000). The release of free energy during this time is also harnessed by conformational changes within S1. The relay helix, for example, responds to changes in the lower 50kDa domain by creating a kink that rotates the converter region 60° (reverse stroke) into the pre-power stroke position, in preparation for force production (Rayment, Smith & Yount, 1996; Schiaffino & Reggiani, 2011).

1.4.2 Actin Binding and Product Release

The 50kDa domain of myosin strongly binds to actin by fully closing the actin binding cleft. This causes the converter domain to rotate again, releasing the kink made during the pre-power stroke, straightening the neck, and releasing P_i from the nucleotide-binding pocket. Release of P_i initiates the power stroke by relaying the information through the converter domain to the lever arm of the S1; this amplifies small changes at the active site into large changes within the neck region needed to transport actin 4-10nm closer to the sarcomere centre (Geeves & Holmes, 1999; Gordon et al., 2001; Uyeda et al., 1996). The release of P_i provides the final chemical to mechanical link that results in force production.

Several loops and switches within the myosin head are also highly important during actin binding and P_i release. For example, loop 2 may contribute to the stereospecific binding to actin and trigger P_i release. Furthermore, Sweeney and Houdusse (2010) offer that P_i release may be central to the role of switch one. After myosin-actin binding, movement of switch one provides a ‘back door’ escape for P_i,

which is then pinched off and removed without movement of the neck region or alteration of ADP release (Sweeney & Houdusse, 2010).

1.4.3 ADP Release

Force generation can occur irrespective of ADP release from myosin; however, continuous crossbridge cycling is dependent upon full release of ADP from the nucleotide pocket. As shown in *figure 3*, once P_i is released from myosin and the power stroke has occurred, ADP is left clinging within the nucleotide pocket. Upon release of ADP, the crossbridge enters the nucleotide-free rigor conformation. Under these conditions myosin is weakly bound to actin, very briefly, and shortly after, ATP will then rebind to the myosin head (post-rigor) causing rapid dissociation from actin due to a loss in affinity (Rayment et al., 1993a). The post rigor state is also short-lived and precedes the hydrolysis of ATP to ADP+P_i where the myosin heads re-cock and prepares for future binding to actin (see *Figure 3*).

Interestingly, the release of ADP is believed to be strain dependent and therefore is affected by contraction parameters. For example, it is postulated that when muscles are stimulated to contract against a heavy load ADP is held within the pocket for a longer duration than at low loads, and under this heavy strain a further rotation of the converter domain is needed to release ADP. As a result of the prolonged ADP bound state, an increase in force occurs without further ATP utilization (Nyitrai & Geeves, 2004). Consequently, when the muscle produces high forces, speed becomes sacrificed; in contrast, as absolute force drops, velocity of muscle shortening rises (Sweeney & Houdusse, 2010). This phenomenon is in part related to the Fenn effect, which describes how muscle shortening is more metabolically costly than isometric contractions (Geeves

and Holmes, 1999; Sweeney and Houdusse, 2010). If speed or movement - in the form of shortening - is the end goal of contraction, ADP will be released faster than at high forces (isometric) and will therefore increase liberated energy (Gordon et al., 2001; Sweeney & Houdusse, 2010). In fast twitch skeletal fibers myosin is able to maximize shortening velocity and power production by rapid detachment of ADP from myosin and myosin dissociation from actin. This is followed by rapid ATP binding to myosin and the crossbridge cycle can continue as myosin docks to actin farther up the filament.

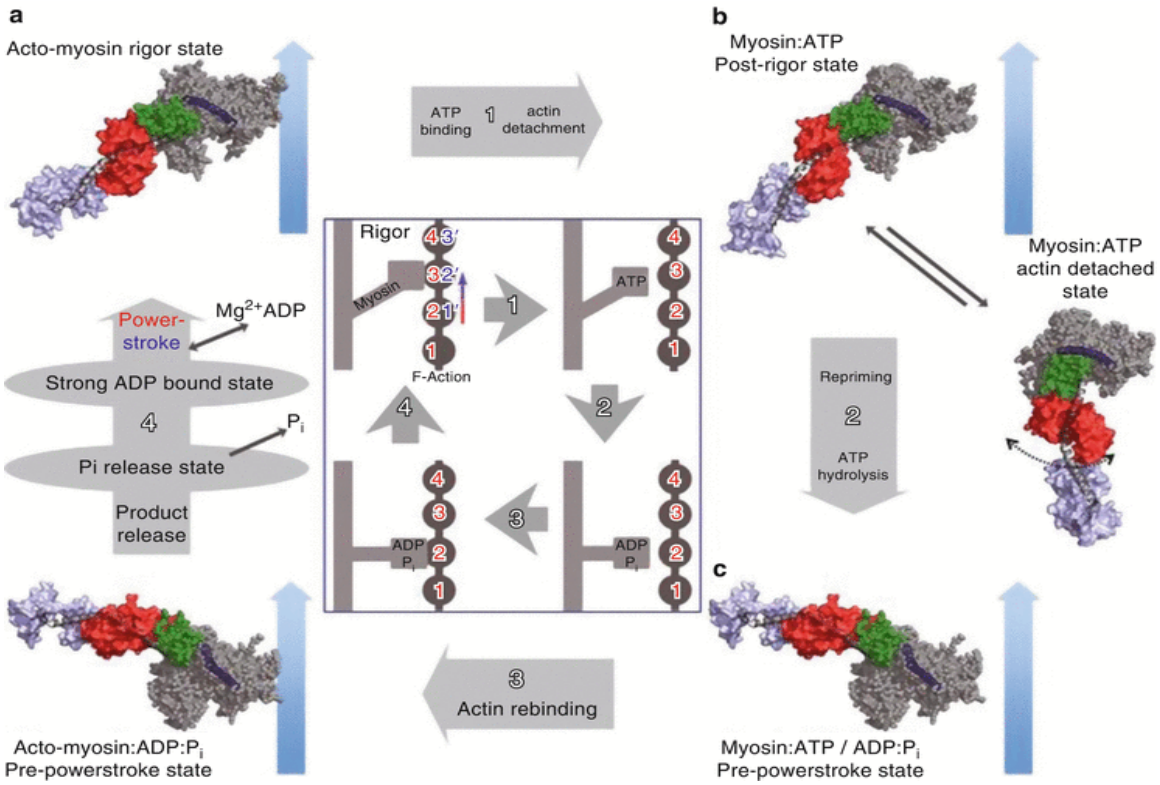

Figure 3. Llinas, Pylypenko, Isabet, Mukherjea, Sweeney, & Houdusse (2009). Crossbridge cycle of skeletal muscle contraction showing the hydrolysis of ATP. The inner schematic represents transitional states of actomyosin complex proposed by Lymn and Taylor (1971).

1.5 Potentiation

Muscle activation can lead to two very different states/changes in performance: fatigue, the decrease of expected force or work, or potentiation, the enhancement of expected force or work (Abbate et al., 2001; Grange et al., 1995; Westerblad et al., 1991).

Although opposing, fatigue and potentiation may also coexist and mask the presence of the other during prolonged or high frequency activation (Krarup, 1981; Rassier & MacIntosh, 2000). Potentiation can be defined as the transient increase in muscle force observed after contractile activity (Brown & Loeb, 1999; Close & Hoh, 1968; Vandenboom, Gittings, Smith, Grange, & Stull, 2013). As a fundamental property of fast twitch skeletal muscle fibers, potentiation enhances muscle performance under a variety of conditions.

1.5.1 Background

The mechanism for twitch force potentiation has been studied for over 100 years (Lee, 1907) and is known to be an intrinsic muscle phenomenon (Botelho & Cander, 1953; Ramsey & Street, 1941; Standaert, 1964). Potentiation was first believed to be the result of accumulated chemical mediators in the muscle (Guttman et al., 1937). Work by Brown and von Euler (1938), Rosenblueth and Morison, (1937) and Zingoni (1954), implicated sources such as sodium, potassium, and acetylcholine as the causes for the heightened contractile response after repeated stimulation. More recent work, however, suggests that phosphorylation of myosin and changes in Ca^{2+} homeostasis may be responsible (Gittings et al., 2011; Smith et al., 2013; Vandenboom et al., 2014). Both of these divergent mechanisms are suggested to occur in concert with one another in a stimulus frequency and duration dependent manner (Moore & Stull, 1984). In contrast, stimulation of slow-twitch muscle produces minimal potentiation or even depressed responses to stimulation (Moore & Stull, 1984). This fiber type dependence may resonate in differences in myofilament structure, interfilament spacing, or excitation-contraction coupling process (Stull et al., 2011; Vandenboom et al., 2013).

The two most common forms of activity dependent potentiation are staircase and post-tetanic potentiation (PTP). Originally termed 'treppe', staircase potentiation is characterized as a progressive increase in twitch force during a prolonged period of low frequency stimulation (Moore & Stull, 1984), whereas post-tetanic potentiation (PTP) is an increase of twitch force after a brief period of high frequency stimulation (Close & Hoh, 1968). Not surprisingly, as the result of different stimulation paradigms, both exhibit a different time course of dissipation. For instance, upon cessation of the contractile stimulus, staircase potentiation displays a slow initial decrease in force followed by a more rapid drop thereafter (Krarup, 1981a). For PTP the twitch force following a tetanic conditioning stimulus is rapidly subdued followed by a slower dissipation over several minutes (Vandenboom et al., 2013).

Regardless of the form, it appears that potentiation selectively enhances muscle function. For example, there are potentiation dependent differences in contraction type (concentric>isometric>eccentric), length (shorter than L_o >longer than L_o), temperature (higher temperatures>lower temperatures), as well as sporadic differences between species (Abbate Sargeant, Verdijk, & De Haan, 2000; Caterini, Gittings, Huang, & Vandenboom, 2011; Gittings, Huang, & Vandenboom, 2012; Xeni et al., 2011). Post-tetanic potentiation also exhibits a concentric speed dependence such that twitch force increases with faster sliding velocities (Caterini et al., 2011; Gittings et al., 2012; Xeni et al., 2011). Thus, a multitude of experimental conditions may alter potentiation and therefore care must be taken when attributing results to specific mechanisms (see **Appendix B**: Compilation of studies examining potentiation)

1.6 RLC Function

The light-chain binding domain is part of the S1 subunit of myosin and is dedicated to modulating contractile dynamics and providing mechanical stability. In addition to its structural role, post-translational modification of the RLC modulates myosin motor function, an effect that increases the calcium sensitivity of the thin filament during submaximal force generation (Persechini, Stull, & Cooke, 1985; Sweeney & Kushmerick, 1985; Sweeney & Stull, 1990).

1.6.1 RLC Phosphorylation Pathway

Existence of a phosphorylatable site on the myosin regulatory light chain (Blumenthal & Stull, 1980; Perrie, Smillie, Perry, 1973; Stuart et al., 1998) provided a plausible intracellular mechanism for potentiation, and in particular, during PTP. Interestingly, the same Ca^{2+} signal that initiates contraction also employs a signaling cascade that phosphorylates the RLC (Klug, Botterman, & Stull, 1982; Zhi et al., 2005). As part of this cascade Ca^{2+} binds to calmodulin: a ubiquitous Ca^{2+} binding protein. Calmodulin contains four resident Ca^{2+} binding sites that when occupied enables it to bind to and form a holoenzyme with skeletal myosin light-chain kinase (skMLCK) (Blumenthal & Stull, 1980). Binding of calmodulin to skMLCK occurs almost simultaneous with contraction although activation of the catalytic process and RLC phosphorylation is slower (Stull, Kamm, & Vandenboom, 2011). After a series of conformational changes the calmodulin-skMLCK connection prompts the catalytic segment of skMLCK to displace from its regulatory sub-unit allowing the RLC N-terminus to bind the catalytic segment. Upon RLC binding, the cleft within the catalytic

segment closes and the ATP within skMLCK transfers P_i to the RLC (see *figure 4* for pathway).

1.6.2 skMLCK Kinetics

Similar to the steric blocking mechanism displayed by the thin filament, skMLCK has an auto-inhibitory component existing between the large catalytic core and the calmodulin binding sequence (Padre & Stull, 2000a; Padre & Stull, 2000b). In essence, this component is an intrasteric regulator, which controls the activity of skMLCK by remaining inactive without calmodulin binding; yet allows ATP binding (Krueger, Padre, & Stull, 1995). Under steady state conditions (Ca^{2+} present) both the RLC and ATP are allowed as substrates of the calmodulin-skMLCK complex.

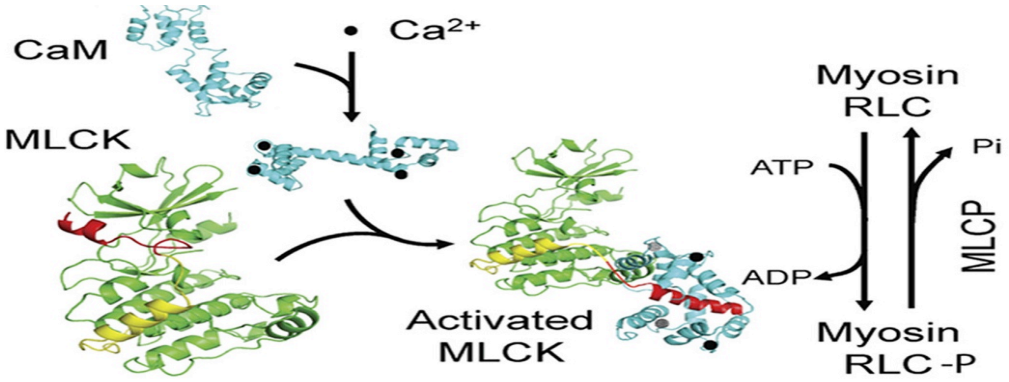

Figure 4. (Kamm and stull, 2011) The molecular signaling cascade initiating phosphorylation of the myosin regulatory light chain.

The time between periods of activation and the frequency of stimulation (Hz), determines the percentage of skMLCK activated. This is due to the slow rate of calmodulin dissociation from skMLCK that in turn affects dissociation of Ca^{2+} from calmodulin (Ryder et al., 2007). The result is an increased fraction of phosphorylated myosin heads. In addition, the activity of the protein phosphatase (MLCP) that cleaves the phosphate from the RLC is much slower (~50 fold) than skMLCK-induced

phosphorylation (Manning & Stull, 1982; Moore & Stull, 1984). Therefore, during brief activation (<10secs), the MLCP activity is offset by skMLCK activity, an effect that may enhance contractile performance by increasing the fraction of cycling crossbridges in the force generating state (Stull et al., 2011). Stull et al. (2011) referred to the history dependent nature of phosphorylation as a biochemical memory that improves the future contractile response within fast twitch muscle fibers. After cessation of the stimulus and a period of relaxation, the unregulated MLCP activity (Morgan, Perry, & Ottaway, 1976) continues to slowly de-phosphorylate the RLC until it returns to resting levels.

1.6.3 RLC Phosphorylation-Mediated Potentiation

As described by Stull and colleagues, RLC phosphorylation catalyzed by skMLCK, may be the principle mechanism of PTP. In support of this, stimulation induced increases in RLC phosphate content has been temporally correlated with increases in twitch force potentiation, (Abbate, Van Der Velden, Steinen, & De Haan, 2001; Grange, Cory, Vandenboom, & Houston, 1995; Klug et al., 1982; Moore & Stull, 1984; Xeni et al., 2011) in some cases, phosphorylation has increased ~5 fold from rest following a tetanic conditioning stimulus (Grange et al., 1995; 1998). However, the link between RLC phosphorylation and the precise modification of crossbridge dynamics is still unclear. For example, RLC phosphorylation has been suggested to increase the rate of cross-bridge attachment to actin (Sweeney & Stull, 1990); yet also may increase the force per cross-bridge (Childers & MacDonald, 2004). It has been thought that the latter change occurs by augmenting the power stroke portion of the crossbridge cycle (Davis et al., 2002; Sweeney et al., 1993), however, considering that tetanic force is unaltered when potentiated, this mechanism is unlikely. The first mechanism, however, which is based on

alterations to F_{app}, is the most likely source of force enhancement. This model is based on work by Huxley (1957), who proposed that there are two states of crossbridge cycling represented by rate constants: F & G. Modified by Brenner (1988), F_{app} represents the transition of crossbridges from a non-force generating to a force generating state. G_{app} on the other hand, represents the reverse transition where crossbridges cycle from a force generating to a non-force generating state. Similar to Ca^{2+} binding on TnC, it is suggested that RLC phosphorylation enhances force production by increasing F_{app} without affecting G_{app} (Brenner, 1988; 1990; Sweeney & Stull, 1990) and will therefore increase the fraction of cycling crossbridges able to attain the force generating state (Metzger, Greaser, & Moss, 1989; Sweeney & Stull, 1990). In addition to this, research examining the flight pattern of *drosophila melanogaster* (fruit fly) found decreased flight fluency in mutated RLC's incapable of phosphorylation. It was determined that the reduced number of attached crossbridges in mutated flies links to a reduction in F_{app} and reflects the reduction in power output. As a result, sufficient power output for flight was lost without the ability to phosphorylate the RLC (Dickinson et al., 1997), indicating that this mechanism is required for normal/ optimal functioning in some species.

The increased rate of crossbridge attachment is also corroborated by structural studies on myosin thick filaments. These studies have shown that when the RLC is phosphorylated the myosin head moves away from the thick filament backbone and is displaced towards the thin filament (Alamo et al., 2008; Brito et al., 2011; Levine, Kensler, Yang, Stull, & Sweeney, 1996; Levine et al., 1998). Similarly, the orderly arrangement of myosin heads may be disrupted by phosphorylation by weakening the inter-molecular interactions between adjacent heads (Alamo et al., 2008). Furthermore,

work form Sweeney, Yang, Zhi, Stull, and Trybus (1994) suggested the addition of a phosphate moiety to the RLC may reverse the electrostatic interaction of the surrounding positively charged amino acids and another yet to be determined structure. Regardless of mechanism, the closer association of actin to myosin promotes crossbridge formation at a given submaximal level of $[Ca^{2+}]$.

1.7 Force-Frequency Relationship of Potentiation

The potentiation of force is directly influenced by stimulation frequency and duration. For example, although dependent on experimental conditions (e.g., temperature and species), potentiation of muscle force has been observed at all sub-tetanic frequencies; however, as stimulation frequency increases there is a simultaneous decrease in potentiation (Abbate et al., 2000; Brown & Loeb, 1998; Burke et al., 1976; Krarup, 1981; Gittings et al., 2012; MacIntosh et al., 2008). Thus, while force production in both fast and slow fibres is proportional to stimulation frequency, the influence of RLC phosphorylation on force is inversely related to stimulation frequency. Furthermore, this signifies that the influence of potentiation diminishes as muscle force nears maximal, even for high levels of RLC phosphorylation. Similarly, during isotonic contractions when the muscle shortens, MacIntosh and Bryan (2002) detected a large increase in shortening amplitude and shortening velocity at the onset of contraction that faded towards the end of a 7s contraction. They attributed this to the muscle approaching near maximal shortening amplitude and shortening velocity for the given stimulation paradigm; yet during this time, RLC phosphorylation still increased in a linear manner. These findings support the role of RLC phosphorylation in increasing F_{app} at submaximal but not maximal Ca^{2+} activation levels (Sweeney et al., 1993), and furthermore, is

consistent with studies showing that potentiation does not improve maximal shortening velocity (Butler et al., 1983; Gittings et al., 2011; Palmar & Moore, 1989). Indeed, during isovelocity shortening contractions of mouse EDL, potentiation seems to be inversely related to force (Gittings et al., 2014). This is consistent with increased potentiation for concentric than isometric contractions at a given frequency, as well as increased potentiation present as shortening velocity increases (Caterini et al., 2011; Gittings et al., 2012; 2014; Xeni et al., 2011). Moreover, skinned fiber data showing that potentiation is inversely proportional to the strongly bound crossbridge population supports the idea that RLC phosphorylation mediated potentiation is force dependent (i.e., more force, less potentiation) for all contractions (Sweeney & Kushmerick, 1985; Sweeney & Stull, 1990).

1.8 Secondary Mechanism of Potentiation

Development of knockout mice devoid of the skMLCK enzyme ($skMLCK^{-/-}$), which are unable to phosphorylate the RLC, has provided a negative control for comparison to WT mice. This genotype enables the relative contribution of RLC phosphorylation to potentiation to be separated from other potential mechanisms. For example, in 2005, Zhi et al. compared isometric twitch force potentiation in EDL of WT and $skMLCK^{-/-}$ mice. In all cases $skMLCK^{-/-}$ mice had severely attenuated PTP and a 50% reduction in staircase responses when compared with WT, signifying that RLC phosphorylation is the largest, but not the only, component of isometric twitch force potentiation. Gittings et al., (2011) also found that potentiation of isometric twitch force caused by PTP was selectively inhibited by the ablation of the skMLCK gene in fatigued muscle.

The residual staircase potentiation seen in skMLCK$^{-/-}$ mice implicates an alternate mechanism for potentiation (Zhi et al., 2005). To this end, a stimulation induced increase in myoplasmic [Ca^{2+}] has been suggested. To study this effect, Smith et al. (2013) used the mouse lumbrical, a unique WT muscle that displays isometric twitch force potentiation in the absence of RLC phosphorylation. This model is therefore able to isolate the contribution of altered [Ca^{2+}] to potentiation. Increases in resting myoplasmic [Ca^{2+}] were correlated with PTP in the absence of RLC phosphorylation although the exact mechanism still remains unknown. It has been hypothesized that an increased resting myoplasmic [Ca^{2+}] that reduces the buffering capacity of parvalbumin enables a larger quantity of free Ca^{2+} released from the sarcoplasmic reticulum to bind TnC (MacIntosh, Taub, Dormer, & Tomaras, 2008; Smith et al., 2013). Future research should seek to quantify the calcium potentiated force potentiation during dynamic contractions to further improve understanding of potentiation during locomotion and possibly the role in vivo.

1.9 Muscle Power Output & Locomotion

Power, as it relates to muscle, is the product of speed of shortening and the force produced during shortening. It is essential for locomotion and has varying demands as the mode of locomotion changes. For example, as movement speed increases in rodents from a walk to a trot and again to a gallop, the type of muscle fibers required for movement changes from slow to fast twitch fibers (Armstrong et al., 1997). This occurs because fast twitch fibers are able to shorten against loads at faster speeds of shortening than slow twitch fibers. During fast cyclical movements muscles must stretch and shorten very rapidly while maintaining power output. In order to move faster, frequency of stimulation

must increase to provide more force; alternatively, fast twitch fibers can also potentiate, which may effectively reduce power loss during the shortening portion of locomotion.

Locomotion shares many traits among different species; some of which are not mammals. For example, comparisons can be drawn between the gait patterns of lizards, crabs, dogs, and humans alike. During a running gait pattern each of these species uses stored elastic energy created from kinetic and gravitational potential energy to propel them forward into flight. Unfortunately, most circumstances requiring locomotion are not as simple as exchanging stored potential energy into movement. For most species the environment is dynamic and constant bombardment with external perturbations is the norm. As such, the motor system must modulate muscle output relentlessly to achieve smooth locomotion. Importantly, understanding the role of a particular muscle, including the stimulation frequency and the timing of activation, will allow for better study and understanding of the in vivo functioning. For example, some muscles act as motors while others work as brakes to provide a well-rounded system for locomotion (Azizi, 2014).

1.9.1 Potentiation and Crossbridge Kinetics

Results from skinned fibers demonstrate that RLC phosphorylation enhances submaximal forces by altering crossbridge kinetics during isometric contractions. This manifests as an increase in the rate of force development ($+dF/dt_{max}$) during potentiated isometric twitches and tetanic contractions (Vandenboom, Grange, & Houston, 1995; Vandenboom, Xeni, Bestic, & Houston, 1997). The increase in $+dF/dt_{max}$ is greater at shorter lengths, while the rate of relaxation is independent of length (Brown and Loeb, 1999). Together, these kinetic changes augment peak twitch force and prolong the state of tetanic force generation. The enhancement of peak force may extend to brief tetanic

stimulation also (MacIntosh & Willis, 2000). Similarly, during potentiated concentric contractions the $+dF/dt_{max}$ may increase independent of stimulation frequency and shortening velocity (Gittings et al., 2012). This allows for greater sub-tetanic forces during fast shortening velocities elicited by high frequency pulses (Abbate et al., 2000). In doing so, the total work and power done by the muscle over the period of a contraction also increases. In contrast, $skMLCK^{-/-}$ mice display no increase in $+dF/dt_{max}$ during concentric contractions (Gittings et al., 2014) and during isometric tetani, and furthermore, tetanic $-dF/dt_{max}$ is quickened rather than slowed (Gittings et al., 2011). Thus, a reduction in power output may be seen in these mice compared with WT, implicating a positive role for RLC phosphorylation.

1.9.2 Potentiation of Power Output

It has been proposed that the potentiated state may actually be the normal working state of fast-twitch muscle fibers (Brown & Loeb, 1998). Under this assumption, a physiological role for RLC phosphorylation must include dynamic contractions. Interestingly, PTP has a greater effect during concentric contractions compared to that of isometric contractions (Caterini et al., 2011; Grange et al., 1995; 1998; Xeni et al., 2011). Contrary to this, the effects of PTP during eccentric contractions are severely attenuated in both skinned fibers and isolated skeletal muscle preparations (Caterini et al., 2011; Childers & McDonald, 2004). Therefore, the potentiation of power output during dynamic functioning is selective to concentric contractions. This is most likely the result of the inverse relationship between magnitude of potentiation and thin filament activation (Davis & Sartorius, 2002; Gittings et al., 2014; Metzger et al., 1989; Patel et al., 1996; Sweeney & Kushmerick, 1985; Sweeney & Stull, 1990), an effect that may be enhanced

during shortening by sensitizing the contractile apparatus to RLC phosphorylation via thin filament deactivation or increases in G_{app} (Gittings et al., 2012; Stull et al., 2011).

The relative force attained for a given frequency of stimulation is lower when shortening than isometric. Considering that potentiation is inversely related to force (Gittings et al., 2014) this suggests that higher stimulation frequencies will potentiate shortening compared to isometric contractions. This is corroborated by data from intact rat gastrocnemius muscle displaying larger increases in force potentiation from brief high frequency pulses (200-400Hz) during isotonic shortening compared with isometric contractions (MacIntosh, Taub, Dormer, & Tomaras, 2008). These results are in agreeance with the rightward shift in the force-frequency curve during shortening compared to isometric contractions, implying that higher stimulation frequencies are needed to fully activate muscle while shortening (Abbate et al., 2000). Furthermore, potentiation also shifts the force-velocity relationship such that force is increased at almost every shortening velocity and vice versa (Gittings et al., 2012; Grange et al., 1995; 1998). Therefore, it is plausible that power output may be positively influenced over the range of physiological shortening speeds and high frequency activation patterns such as that observed by Abbate et al. (2000).

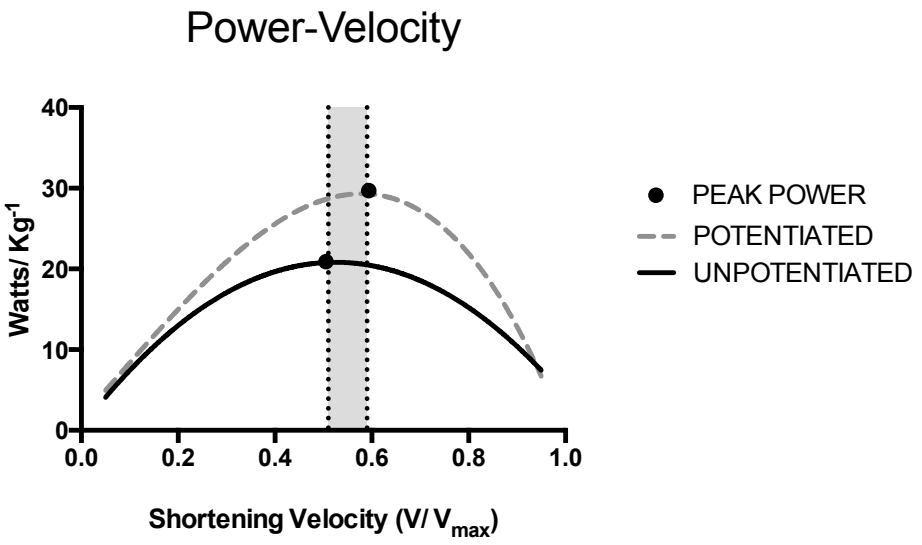

Figure 5. Schematic representing the hypothetical shift in power output between different states of muscle activation i.e., unpotentiated and potentiated. Shaded area (grey-fill) denotes the potential range that optimal velocity may occur at, depending on level of potentiation. Figure is based on 'in vitro' mouse EDL muscle stimulated at 100Hz.

Interestingly, the shift in the force-velocity relationship also occurs, albeit, to a lesser extent, in skMLCK$^{-/-}$ mice (Gittings, Bunda, & Vandenboom, unpublished); this indicates that changes in resting myoplasmic [Ca^{2+}] may also potentiate force, work, and power. Nonetheless, given that RLC phosphorylation may enhance tetanic +dF/dt_{max} and decrease -dF/dt_{max}, prolonging force production at contraction end, this mechanism may play an important role in modulating muscle performance in vivo (Grange et al., 1995).

STATEMENT OF PROBLEM

Historically, PTP has been mostly studied using isometric contractions at low frequencies of stimulation (Krarup, 1981; Klug et al., 1982; Manning & Stull; Moore et al., 1990; Vandenboom et al., 1993; 1995). Interestingly, when studied using dynamic contractions these have been shown to potentiate to a greater extent than isometric in both rat and mouse muscle (Abbate et al., 2000; Caterini et al., 2011; Childers & McDonald, 2004; Grange et al., 1995; 1998; Xeni et al., 2011). In addition to this, many of these studies noted a pronounced augmentation of power when muscles were in the potentiated state (Abbate et al., 2000; Caterini et al., 2011; Grange et al., 1995; 1998), however, these studies have not been able to directly examine the contribution of RLC phosphorylation to power during shortening contractions. Therefore, a main impetus of this study is to separate the impact of RLC phosphorylation from other possible mechanisms of potentiation through use of skMLCK$^{-/-}$ mice. Lastly, deciphering which mechanisms contribute to the rightward shift observed in the power-velocity curve to higher shortening velocities (i.e., Abbate et al., 2000) still remains unknown. Therefore, these factors need to be examined further before we can fully understand the physiological utility of the RLC phosphorylation mechanism in enhancing mechanical function in vertebrate striated muscle.

2.1 Purpose

1. The main purpose of this study was to determine the impact of RLC phosphorylation mediated force potentiation on mechanical power of mouse EDL muscle (*in vitro*, 25° C). To this end we compared both the mean and peak resting and

stimulated power outputs of WT and skMLCK$^{-/-}$ muscles (with and without RLC phosphorylation, respectively) under experimental conditions designed to mimic physiologically relevant contractions.

2. A secondary purpose of these experiments was to determine whether the absence of RLC phosphorylation negated the shift in the power-velocity curve to higher shortening velocities expected to occur in potentiated WT muscles.

Note: Mean power is a measure used to describe an entire contraction. As an added measure to delineate genotypic differences in mean power we analyzed the contractile kinetics of each muscle: maximum rate of force development (+dF/d*t*), maximum rate of force relaxation (-dF/d*t*), time to peak tension (TPT), and half relaxation time (½RT), were used to assess these differences. Furthermore, as a confirmatory measure, RLC phosphorylation content was analyzed for differences between genotypes pre and post-CS.

2.2 Hypotheses

1. Concentric power output of potentiated EDL muscles will increase to a greater extent in WT than skMLCK$^{-/-}$ muscles at all speeds of shortening.

2. Peak concentric power output of potentiated EDL muscles will increase to a greater extent in WT than skMLCK$^{-/-}$ muscles.

3. The shift in the power-velocity relationship to higher speeds of shortening will be observed in WT but not in skMLCK$^{-/-}$ EDL muscles.

2.3 Assumptions

There are no phenotypic differences other than the skMLCK gene knockout and the coat colour (black and agouti) i.e., body weight and composition.

There are no cellular adaptations in skMLCK$^{-/-}$ that result in RLC phosphorylation.

Length changes will not induce large variations in passive tension since the elastic components will not be stretched and the contractions will be shortening from slightly over optimal length (1.05-0.90L_o).

Any potentiation in skMLCK$^{-/-}$ mice will be due to altered ($Ca^{2+}_{resting}$) homeostasis.

2.4 Limitations

The use of only one stimulation frequency during the experimental protocol minimizes extrapolation of findings to a narrower range than if a range of frequencies were used.

Not all contractions will produce force over the entire shortening cycle. As a consequence of constant pulse number, only the contractions that use the fastest percentage of maximum shortening velocity will create force over the majority of the shortening ramp.

METHODS

3.1 Mice

Adult male wildtype and skMLCK$^{-/-}$ mice were used in these studies. All mice were selected at a minimum age that accorded with sexual maturation, as previously described

(Fox, 2006). Wildtype C57BL/6 mice (male, age 3-6 months, 27.6 ± 2.0 g) were ordered from Charles River- Drummondville, QC, Canada, and were housed at Brock for ~1-2 week before experiments began. The skMLCK$^{-/-}$ mice (C57BL/6 background) were obtained from our own breeding colony at Brock University (male, age 2-5 months, 23.2 ± 1.2 g) and were housed in the Comparative Biology Facility. Coat colour in the skMLCK$^{-/-}$ mice were backcrossed to the C57BL/6 genotype for nine generations to ensure subsequent generations were homozygous dominant for the agouti coat colour. This enables a clear visual distinction between the two genotypes. More details regarding the generation and characterization of the skMLCK$^{-/-}$ mice have been presented previously (Zhi et al. 2005; Gittings et al. 2011). All mice were fed standard chow and water *ad libitum* and were maintained on a 12h/12h night/day cycle. All procedures utilized during the experimental protocol received full ethical approval from the Brock University Animal Care and Use Committee (Protocol # 13-03-02).

3.2 Surgical Intervention and Cardiac Injection

On the day of an experiment adult mice were transported from caging in the Comparative Biology Facility to the experimental area in our laboratory. Following this, the mice were anaesthetized with a peritoneal injection of sodium pentobarbital (0.025 ml/g body weight), diluted with 0.9 % saline in a 1 ml syringe. The extensor digitorum longus (EDL) muscle was then surgically removed with both proximal and distal tendons tied off by non-absorbable braided silk suture (4-0) and then the muscle was suspended in a jacketed vertical organ bath (Radnoti Glass Technology, Inc.). The bath contained Tyrode's solution (in mM): 121 NaCl, 5 KCl, 24 $NaHCO_3$, 0.4 NaH_2PO_4, 0.5 $MgCl_2$, 1.8$CaCl_2$, 5.5 D-Glucose, and 0.1 EDTA, that was continuously gassed (95% O_2, 5%

CO_2), maintaining a stable pH (7.4) and maintaining the muscle preparation at 25^o C, using an Isotemp 3013S circulator. After suspension, the second EDL muscle was extracted and placed in a separate oxygenated bath (95% O_2, 5% CO_2) containing Tyrode's solution, surrounded by ice. After the muscle had been carefully excised from the hind limb, the mouse was euthanized with a lethal intracardiac injection of sodium pentobarbital (0.025 ml/g body weight), diluted with 0.9 % saline in a 1 ml syringe, and was properly disposed of according to the Brock University animal care facility procedures. After collection of contractile data for the first EDL muscle and before mounting of the second EDL muscle, a fresh aliquot of Tyrode's solution was added to the vertical bath.

3.3 Experimental Apparatus

All experiments utilized a customized in vitro muscle testing system (Aurora Scientific Incorporated) capable of adjusting muscle length and controlling a variety of environmental factors. After surgery was performed within each experiment, muscle stimulation of the EDL was applied using flanking platinum electrodes, provided by a Model 701B biphasic stimulator (ASI) with voltage set to 1.25 times the threshold required to elicit maximal twitch force (refer to equilibration protocol for determination of threshold, section **3.4**). Following muscle suspension, the isometric resting muscle length was determined, within 0.01 mm, using a horizontal stereo zoom microscope (Bausch and Lomb) and a sliding micrometer (Velmex, Inc.). A 20-30 minute equilibration period then took place followed by measurement of the muscle's optimal length (L_o), deemed to be the length associated with maximal isometric twitch force. During experiments, muscle length and force data was monitored via LINUX software

and controlled by a dual mode servomotor (Model 305B, Aurora Scientific Inc., Aurora ON). All experiments were collected at 2000 Hz and saved to computer for further analysis (ASI 600a software).

3.4 Equilibration & Finding Optimal Length

Each experiment began with a preliminary set of protocols devised to reduce unsystematic error by monitoring muscle viability and by ensuring proper experimental set up i.e., muscle placement and suture tying. Initially, optimal length (L_o) for maximal isometric twitch force production was roughly estimated by measurement through the stereo zoom microscope (tendon to tendon) and set as 'reference length' in the computer. The EDL was then stimulated with a 400 ms (150 Hz) tetanus, to remove any slack or compliance within the muscle and to test for possible slipping of the suture on the tendon. Muscles were then equilibrated for 30 minutes during which a 1 Hz, 100 ms twitch was elicited every 3 minutes, whereby intensity of stimulation (current) was gradually increased until a maximal twitch force was observed. The stimulus intensity was then increased 25% to confirm activation of all muscle fibers. Following the 30 minute equilibration period, optimal length for isometric twitch force (L_o) was determined by administering twitches to the muscle at varying lengths between 1.1-0.90 L_o via written 'optimal length' protocol. The resting tension that corresponded with the highest peak was used to set the muscle for a secondary observation of length under the stereo zoom lens. The new 'adjusted' length was set as L_o and used as reference for the remainder of the experimental protocol in order to normalize force values between experiments.

3.5 Extensor Digitorum Longus

The Extensor Digitorum Longus (EDL) is a highly studied muscle model for investigating rodent muscle biophysics (Wilson & James, 2004). Traditionally the EDL was examined for assessing locomotion, work and power output of hindlimb muscles; more recently it has been used to investigate mammalian skeletal muscle potentiation, as a result of the high quantity of fast glycolytic fibres existing within the muscle. In order to properly understand the use of the EDL within the existing scientific literature, a brief synopsis of the underlying physiological properties, as well as the more visible mechanical properties of the muscle, must be illustrated.

The mouse EDL muscle is located in the hindlimb and acts to extend the toe and raise the foot into dorsi flexion. In the instance of locomotion the EDL provides a spring like motion to the foot at the beginning of the swing phase, slightly after the foot has propelled itself from contact with the ground. Neural activation begins during flight and ends shortly after landing (James, 1995). From this standpoint, the muscle's main action during movement is to play a synergistic role in maintaining steady limb movement. Structurally, all of the dorsi-flexors of the hindlimb have longer fiber lengths with small cross-sectional areas that provide high velocities of shortening, and thus, movement during the swing phase becomes easily modulated based on locomotor needs (Lieber, 1997).

By implanting electrodes in freely moving rats, Hennig and Lomo (1985) determined that EDL motor units are active for approximately 5-22% of a 24hour period (Hennig and Lomo, 1985). This is indicative of the high quantity of fast-twitch fibers within the muscle: 5.3% (2a), 3.3% (2a/x), 24.5% (2x), 6.8% (2x/b), 59.7% (2b),

(Gittings et al., 2011). Combined with work from other hindlimb muscles, this model will further our understanding of the dynamics of movement.

Lastly, this muscle model was chosen because it is small enough to maintain viability over a long period of time through diffusion of sufficient oxygen and substrates into the cell (Barclay, 2005). Moreover, it has previously been demonstrated that rodent intact muscle preparations (EDL) remain stable for > 1 hour when maintained at 25^{o}C (Segal & Faulkner, 1985).

3.6 Experimental Design

The mouse EDL was used to investigate the effects of RLC phosphorylation mediated potentiation on peak power output of mouse skeletal muscle. The choice of EDL muscle used for collection of contractile data first i.e., left vs. right leg, was alternated between mice to minimize confounding variables.

Two identical sets of experiments were performed: one with the use of C57bl/6 wildtype mice, the other using C57bl/6 skMLCK$^{-/-}$ mice. As previously stated, skMLCK$^{-/-}$ mice provide a unique negative control since the gene coding for skeletal myosin light chain kinase has been removed, and therefore they display no stimulation induced RLC phosphorylation.

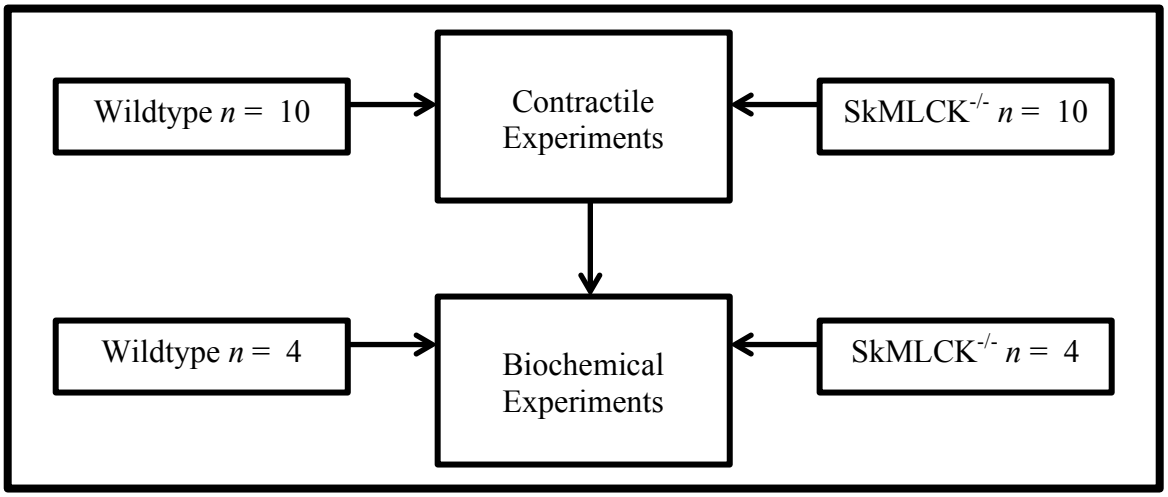

Figure 6. An overview of the sample size used for each experiment and the assignment of groups based on genotype. Each 'subject, (*n*)' represents a single EDL muscle; in some cases only one muscle was taken from the mouse dependent on proficiency of surgical removal.

3.6.1 Experimental Design and Protocol

Experiments investigated the effects of PTP on concentric power output at a range of shortening velocities (0.05-0.65 V_{max}) in both wildtype (WT) and skMLCK$^{-/-}$ mice. The protocol had identical sets of shortening-ramps before and after the CS to illustrate the effects of PTP on power. Shortening-ramp amplitude was controlled by a dual-mode servomotor that shortened muscle length to simulate a concentric contraction in vivo. All muscles (n = 10) were stimulated at the same frequency (100 Hz), representing a value that was considered to be physiological (Abbate et al., 2000; Henig & Lomo, 1985) and has previously been shown to cause variations in power output after a tetanic conditioning stimulus (Gittings, 2012).

The conditioning stimulus consisted of four independent brief high frequency bursts (100Hz) lasting 400ms each, within a total duration of 10 seconds. This type of stimulus paradigm has been previously shown to induce reproducible near maximal potentiation in mouse EDL muscles at 25^{o} C, with minimal fatigue: denoted by a decrease in expected force, work, or power (Caterini et al., 2011; Gittings et al., 2012;

Vandenboom et al. 1997; Xeni et al., 2011). Each set of experimental conditions i.e., CS bracketed by shortening ramps, was separated by 15 minute rest periods to prevent fatigue and allow RLC phosphorylation to dissipate (Abbate et al., 2000).

The protocol consisted of closely spaced concentric shortening ramps: the first ramp proceeding without stimulation, the second while being stimulated. The passive tension from the first ramp was subtracted from the total tension of the second ramp, thus giving active tension of the muscle during contraction. Active force was then used to calculate all contractile measures. Furthermore, every stimulated shortening ramp was activated by an equal number of pulses (3) in order to accurately compare work and power accomplished across the entire contraction. After the first set of ramps had finished, the muscle was subjected to a second set of ramps shortening at a different velocity. Each set of ramps was then tested after a potentiating stimulus (CS), making up a 'single protocol', for each WT and KO muscle, as shown in Figure 6. The order in which shortening ramps were administered over the course of an experiment i.e., 0.05-0.65 V_{max} was chosen at random and was strategically altered between muscles to control for the possibility of order effects.

Each ramp shortened for a different period of time, corresponding to the time it took the muscle to shorten from 1.05 to 0.90 L_o at the desired shortening velocity. Within each stimulated ramp (active), stimulation began after shortening had begun (~1.045 L_o). Furthermore, this stimulation paradigm allowed for complete relaxation from concentric force by the end of each shortening ramp. The average/ peak force developed over the course of each contraction was then used in conjunction with velocity of shortening to find the PO of each muscle contraction. The starting length for shortening ramps (1.05

L_o) was chosen to prevent large variations in passive tension. As suggested by James (1995), starting lengths above 20% of L_o will create large-scale changes in viscoelastic tension within muscle. Furthermore, Longer muscle lengths also increase the calcium sensitivity of the myofilaments and will have force-modulating consequences that may confound the results of the shortening ramps used (Josephson, 1999).

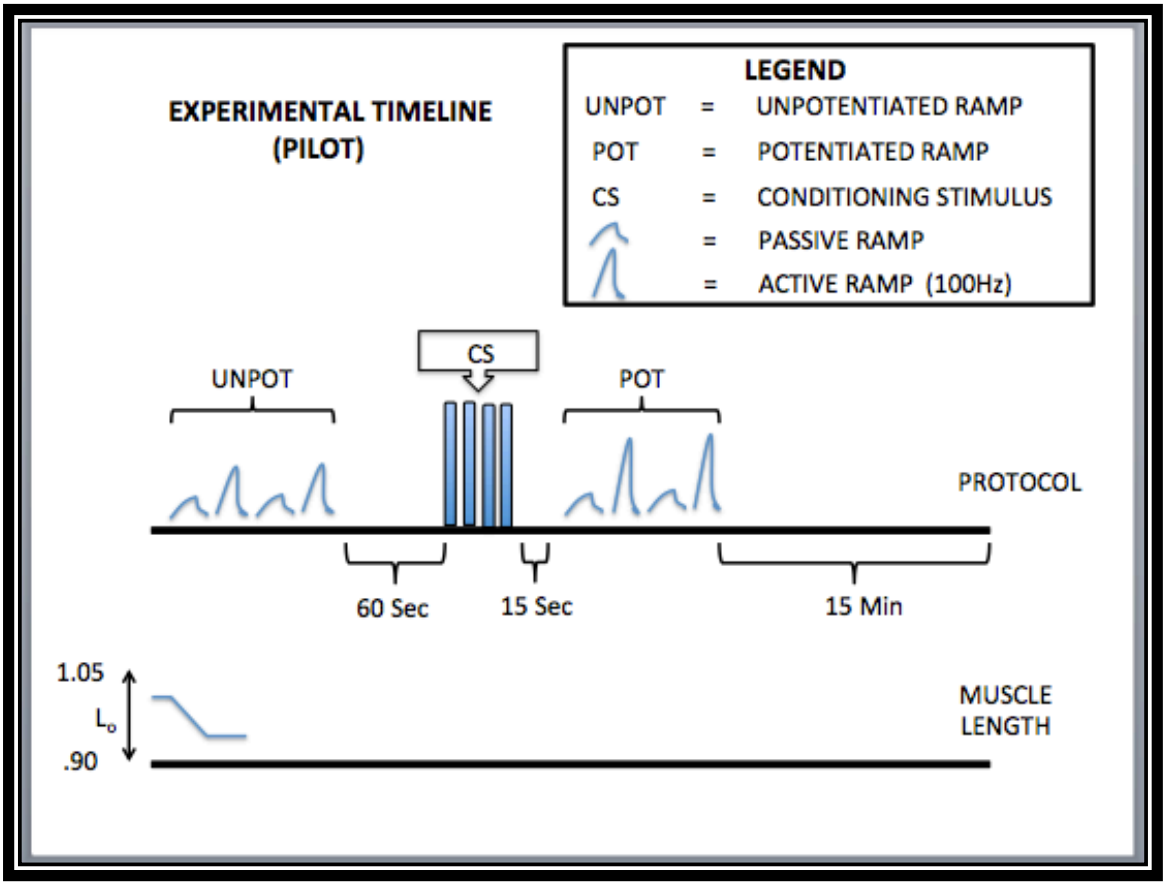

Figure 7. The experimental timeline for collection of contractile data (n = 10). Upper line represents force traces of shortening ramps (in blue) at rest and post CS. Each was paired (rest & stimulated) in order to acquire the active force produced by the contractile unit. Two different speeds were assessed during each protocol to reduce the length of the entire experimental procedure and prevent muscle damage/fatigue. The order of shortening ramp speed e.g. 0.10 & 0.35 Vmax, 0.65 & 0.20 V_{max} etc., was manipulated between protocols to prevent order effects. Lower line represents the change in muscle length for each shortening ramp, which was set at a constant 15% L_o (1.05-.90 L_o).

3.7 Determining Muscle Shortening & Ramp Velocity

The maximum velocity of shortening for intact whole muscle preparations are quantified in two ways: 1) The slack test, pioneered by Edman (1979) as a measure of the unloaded shortening velocity (V_o) of the fastest fibers within a muscle. 2) Maximum shortening velocity (V_{max}) extrapolated from force-velocity properties of skeletal muscles fit to a curve using the Hill equation, (1937). Considering mouse EDL is a heterogeneous muscle, V_{max} is therefore a better representation of the whole muscle's maximum velocity of shortening. The current study used a V_{max} value of 9.8 fiber lengths per second (fl/s) (Gittings et al., 2012) that is consistent with other studies for mouse EDL (Brooks & Faulkner, 1988, 1991). This value was then converted to muscle lengths per second (ml/s) using a ratio (0.44-0.45:1) proposed by previous studies (Brooks & Faulkner, 1988; 91; Grange et al., 1995; McCully & Faulkner, 1985), (*see below for equation*). This value was then converted to maximal percentage of optimal lengths per second (ex. 444% L_o/s), another unit equating to V_{max}. Converting to this unit is instrumental in determining the time it will take each ramp to shorten from 1.05 L_o to 0.90 L_o. Every shortening speed was then calculated as a percentage of the maximum L_o/s at which the muscle could shorten. Dividing the percentage of L_o/s by the distance of length change i.e., 1.05 L_o - 0.90 L_o, calculates the duration of the length ramp. Example using 0.20 V_{max} shortening ramp:

$$fl/s \cdot 0.44 = Vmax\ (ml/s) = 4.31$$

$$\frac{4.31}{Ml/s} \times \frac{100}{\%\ L_o/s} = 431$$

$$0.20\ Vmax = \frac{431 L_o}{s} \cdot 0.20\ \% = 86.2\ \%L_o/s$$

$$\frac{15\ \%L_o}{86.2\ \%L_o/s} = 0.174 s \cdot \frac{1000}{ms} = 174\ ms$$

174 ms represents the duration of the shortening ramp (1.05-0.90 L_o) at 0.20 V_{max}.

The speed of each shortening ramp was expressed in two separate units: an absolute value, expressed in mm/s, or as a relative value, expressed as a percentage of maximum shortening velocity (% V_{max}).

3.8 Determining Active Force

Active force is a complex function of sarcomere length, velocity, activation history, state of potentiation, and fatigue (Brown & Loeb, 1999). It is the contribution of the myofilaments to force production; found by changing muscle length while using electrical stimulation (Marsh, 1999). Whereas the passive tension of a muscle, found by changing the muscle length without stimulation, is the contribution of the series elastic components (e.g., tendons and cytoskeleton) to total force (Josephson, 1999). By separating the determinants of total tension, the contribution of potentiation to active tension can be analyzed. This was accomplished by subtracting passive tension from the total force trace record, leaving active force.

3.9 Determining Mean & Peak Force

Peak force was defined as the maximum tension the muscle produced in response to 100 Hz stimulation during shortening, measured in Millinewtons (mN); whereas mean force was defined as the sum of force over the shortening ramp divided by the number of scores. The mean and peak force during shortening provides insight into the physiological changes between the physical states of rest and potentiation, in particular with reference to RLC phosphorylation. Both values were normalized to specific tension for accurate comparison between genotypes.

Specific tension is acquired by dividing muscle mass by the product of muscle fiber length (mm) and muscle density (1.06g cm^{-3}), as specified by Mendez and Keys (1960), as well as Brooks and Faulkner (1988), giving physiological cross-sectional area (PCSA). Specific tension is then given by dividing mean force by PCSA and expressed in (mN/ mm^2).

Peak force during tetanic stimulation (CS) was used to assess fatigue (section 3.12) and muscle viability throughout the experimental protocol.

3.10 Determining Rate of Force Development (+dF/d*t*) and Relaxation (-dF/d*t*)

Rates of force development (+dF/d*t*) and force relaxation (-dF/d*t*) were calculated as the instantaneous rates of development and relaxation over the displacement during muscle shortening i.e., the integral of the active force record. The maximal responses of each contraction were taken and the means for each shortening velocity were pooled and compared according to genotype (WT vs. skMLCK$^{-/-}$). In all cases, the use of relative values eliminated changes in muscle size, strength, and tissue viability and allowed for consistent evaluation between muscles and mouse genotypes.

3.11 Determining Time to Peak Tension and Half Relaxation Time

Time to peak tension (TPT) was calculated as the time it took to reach peak force from the time active force production began during each shortening ramp (ms). Half relaxation time (½RT) was calculated as the time it took for force to diminish to 50 % of peak force levels (ms). The responses of each contraction were then collected and the means for each shortening velocity were pooled and compared according to genotype (WT vs. skMLCK$^{-/-}$).

3.11 Determining Work and Power

Due to large differences in force output between genotypes work and power were normalized to muscle mass and scaled to Joules per kilogram (J kg^{-1}) and Watts per kilogram (W kg^{-1}). This was accomplished by taking the wet weight of each muscle post experimentally using an electronic balance and was expressed in milligrams (mg). Work done by the muscle was determined by calculating the average force over the distance of length change during each contraction (mN·m). Two methods were then used to calculate

Power output: multiplying mean force by shortening velocity and multiplying peak force by shortening velocity.

3.12 Determining Potentiation and Fatigue

Dividing the value of a contractile measure i.e., force, work, dF/d*t*, or power output when potentiated (post-CS) by the value of unpotentiated contractions (pre-CS) provided the relative difference (potentiation) for each contractile parameter.

Comparing force output from the first tetanus of the first CS with the first tetanus of the last CS assessed fatigue (Grange et al., 1995). The value is given as a percentage of the initial maximal tetanic force. This measurement estimated relative muscle fatigue and ensured muscle viability throughout the experiment (Gittings et al., 2011). Any tetanic responses yielding less than 90% of the force from the initial tetanus were considered to be fatigued (Abbate et al., 2000) and any data collected during that experiment were not used for analysis (WT, $n = 1$).

3.13 Myosin Phosphorylation Timeline

A 2nd set of identical experiments were performed to measure the amount of phosphorylated RLC within the muscle at two time points within the protocol i.e., before and after the potentiating CS. Immediately following each event, the muscles were frozen by tongs precooled with liquid nitrogen and stored in microcentrifuge tubes at -80^{o}C until analysis using urea-glycerol polyacrylamide gel electrophoresis.

To ensure that changes in RLC phosphate content during the experimental protocol were due to the conditioning stimulus, and nothing else, the time points were strategically chosen as indicators of RLC phosphorylation. The first time point was taken after the CS to indicate that potentiation of force, work, and power is coincident with high levels of

RLC phosphorylation. The second was used as a baseline measure for RLC phosphorylation values corresponding to the state of the muscle at rest; taken 15 minutes post experiment. Selecting these two time points permitted biochemical samples to be collected within the same experiment as the collection of contractile data. This design reduced the number of mice used for the entire research project.

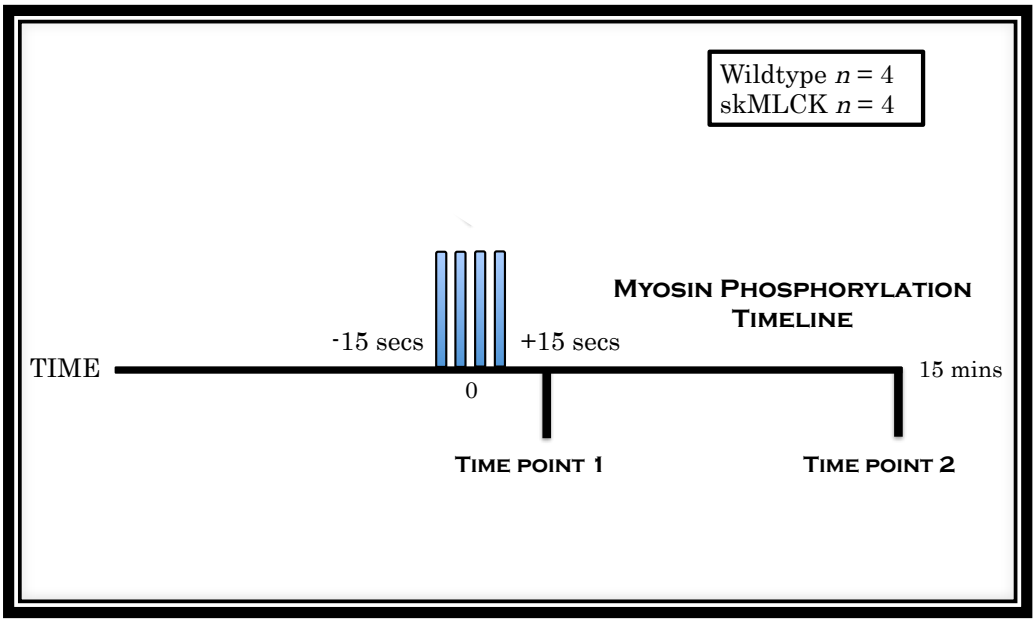

Figure 8. The experimental timeline for collection of RLC phosphorylation content. Time point 1 represents the peak of potentiation post CS (15 secs), whereas time point 2 represents the resting state of muscles during the experimental protocol. (*n)* Represents one EDL muscle; muscle selection for time-points (left vs. right) were randomized.

3.14 Determining Myosin Phosphorylation Content

The following is a brief overview of the methods used to determine myosin phosphorylation content (in mol phosphate per mol RLC) using the urea-glycerol PAGE western blot technique. For a detailed list of chemicals used and description of the methods see **Appendix C**: Western Blotting.

Muscles that were freeze-clamped during the experimental protocol were stored in the freezer (-80^{o}C) and then were extracted from isolated microcentrifuge tubes,

denatured using dithiothreitol (DTT) and trichloroacetic acid (TCA), homogenized, and prepped for gel electrophoresis. Each muscle was homogenized by mortar and pestle (Wheaton, USA) until a consistent mixture was obtained. After centrifugation at 2000 rpm for 2 minutes, the supernatant was poured off leaving a 'pellet'. The remaining tissue pellet was then washed using ethyl ether to remove excess TCA. Following this, the pellet was resuspended in a urea based sample buffer and urea crystals were added, as necessary, to achieve complete saturation. After the RLC's of each sample had been solubilized by urea the samples were pipetted into separate 'wells' of a BIO RAD minigel electrophoresis apparatus (10 μL per sample) containing a polyacrylamide gel with the addition of glycerol for density. Gels were run for 85 min at 400 V, and then electrophoretically transferred (60 min at 25 V) to a nitrocellulose membrane using a non-conducting gel-membrane cassette submerged in transfer buffer. After transfer, the membranes were washed with Tris buffered saline + Tween 20 (TBST), followed by incubation in blocking buffer for 1 hour to prevent blocking of non-specific protein binding. Lastly, the nitrocellulose gels were incubated with 1^{o} (1:7500) antibody (RLC) and were then stored overnight at 4^{o}C.

The next day the membranes were washed with TBST to remove 1^{o} antibody; immediately followed by incubation with 2^{o} (1:10000) goat anti-rabbit IgG-horseradish peroxidase (Santa Cruz Biotechnology, Inc.) in TBST for 1 hour at room temperature. The membranes were then incubated with a detection buffer (enhanced chemiluminescence prime) for 3 minutes. Membranes were then rinsed with dH_20, drained, and placed in a FLUORCHEM 5500 for exposure of the membrane and photo-analysis of the blot. Each lane represented a different sample and was characterized by

three separate bands: non-phosphorylated RLC, an unknown band, and mono-phosphorylated RLC. Sample content was quantified using 'Image Studio Lite' (Li-Core) western blotting software.

3.15 Data Analysis and Statistics

The main purpose of the study was to investigate the effects of skMLCK gene ablation on peak power of mouse fast muscle. Several indicators of muscle performance were tested (mean and peak force, rate of force development/relaxation, time to peak tension, and work and power output) to provide a robust comparison between WT and skMLCK$^{-/-}$ mouse muscle. IBM SPSS Statistics analyzer, Version 21.0. was used to assess whether the data fit the Gaussian distribution (Shapiro Wilk test), as well as to examine measures of central tendency (skewness and kurtosis) and search for outliers; statistical analysis and hypothesis-significance testing were determined using Prism 6 Graph Pad (La Jolla, CA). After examining the data for fit of the normal distribution, the results of the Shapiro Wilk test produced non-significant test results for each level of each of the independent variables. Therefore, no corrections were made to the data for analysis of parametric statistics.

For contractile experiments, a two-way factorial ANOVA (2x8) was used to examine the influence of shortening speed (0.05, 0.10, 0.20, 0.30, 0.35, 0.45, 0.55, & 0.65 V_{max}) and genotype (WT vs. skMLCK$^{-/-}$) on the relative change in each of the contractile measures (force, contractile kinetics, work, and power).

Separate two-way ANOVAs tested the influence of shortening speed (0.05, 0.10, 0.20, 0.30, 0.35, 0.45, 0.55, & 0.65 V_{max}) and activation state (pre-CS vs. post-CS) on the

absolute change in each contractile measure (force, contractile kinetics, work, and power). This was repeated for each genotype i.e., WT and skMLCK$^{-/-}$.

A two-way ANOVA was then used to examine the influence of genotype (WT vs. skMLCK$^{-/-}$) and activation state (pre-CS vs. post-CS) on RLC phosphorylation content in mol/phos per mol/RLC.

All statistics are reported using means accompanied by standard error of the mean, when appropriate. A value will was considered significant if ($p < .05$).

3.14.1 Sample Size Predictions

Based on a one-tailed test comparing the means for unpotentiated ($M = 51.80 \pm 10.10$) vs. potentiated ($M = 68.10 \pm 11.50$) WT force values ($n = 12$) with a p value set to .05 and a power value of 0.9, the critical t-value was = 1.943, $Df = 6$, giving a sample size of $n = 4$ (Gittings et al., 2012).

RESULTS

4.1 Animal Characteristics

4.1.1 Body Mass

An unpaired t-test was conducted to determine if there were significant differences in body mass between mouse genotypes (WT vs. skMLCK$^{-/-}$). The test revealed a significant increase in body mass for WT (27.56 ± 0.65 g, $n = 10$) compared to skMLCK$^{-/-}$ mice (23.25 ± 0.38 g, $n = 10$), [$t = 5.74$, $df = 18$, $p < 0.0001$, $r^2 = .65$]. We normalized force to specific tension (mN·mm^2) and work and power were normalized to

muscle mass (kg), therefore, we assumed mass differences did not impact the outcome measures.

4.1.2 Muscle Mass

An unpaired t-test was conducted to determine if there were significant differences in muscle mass between genotypes (WT vs. skMLCK$^{-/-}$). The test revealed a significant increase in muscle mass for WT (15.09 ± 0.91 g, n = 10) compared to skMLCK$^{-/-}$ muscles (11.82 ± 0.44 g, n = 10), [t = 3.25, df = 18, p = 0.0044, r^2 = 0.37]. This result of this test was expected given the increase in body mass for WT mice.

4.1.3 Muscle Length

An unpaired t-test was conducted to determine if any differences in muscle fiber length existed between genotypes (WT vs. skMLCK$^{-/-}$). The test revealed that there were no significant differences in WT (10.78 ± 0.31) and skMLCK$^{-/-}$ muscles (10.70 ± 0.23), [t = 0.20, df = 18, p = 0.84, r^2 = 0.002]. As a result, no further measures were taken to prevent confounding variables.

4.1.4 PCSA

An unpaired t-test was conducted to determine if any differences in muscle fiber physiological cross-sectional area were present between the two genotypes (WT vs. skMLCK$^{-/-}$). The tests revealed that WT muscles had significantly larger PCSA values (1.33 ± 0.09) than skMLCK$^{-/-}$ muscles (1.04 ± 0.05), [t = 2.86, df = 18, p = 0.01, r^2 = 0.31]. This difference was expected considering that PCSA is a function of muscle mass (mg) divided by the product of mammalian muscle density 1.06mg mm^{-3} and muscle fiber length (mm). No follow up measures were required.

4.1.5 Age

An unpaired t-test was conducted to determine if there were significant differences in age between genotypes (WT vs. skMLCK$^{-/-}$). The test revealed that WT mice were significantly older (143.5 ± 6.18 days) than skMLCK$^{-/-}$ mice (91.40 ± 15.34 days), [$t = 3.15$, $df = 18$, $p = 0.006$, $r^2 = 0.36$].

4.2 Contractile Measures

4.2.1 Relative Concentric Force Potentiation

A two-way ANOVA was conducted to assess the effects of shortening velocity (0.05, 0.10, 0.20, 0.30, 0.35, 0.45, 0.55, & 0.65 V_{max}) and genotype (WT vs. skMLCK$^{-/-}$) on the relative change in concentric force after a tetanic conditioning stimulus (CS). Results revealed significant main effects for velocity, [F (7, 144) = 20.98, $p < 0.0001$, n^2 = .41] and for genotype, [F (1, 144) = 68.93, $p < 0.0001$, $n^2 = 0.19$] on force. Post-hoc tests (Holm-Sidak) were then conducted to reveal the differences in force between genotypes, among levels of shortening velocity. WT force values were found to be significantly higher than skMLCK$^{-/-}$ at all shortening velocities when compared at the same velocity ($p < 0.05$).

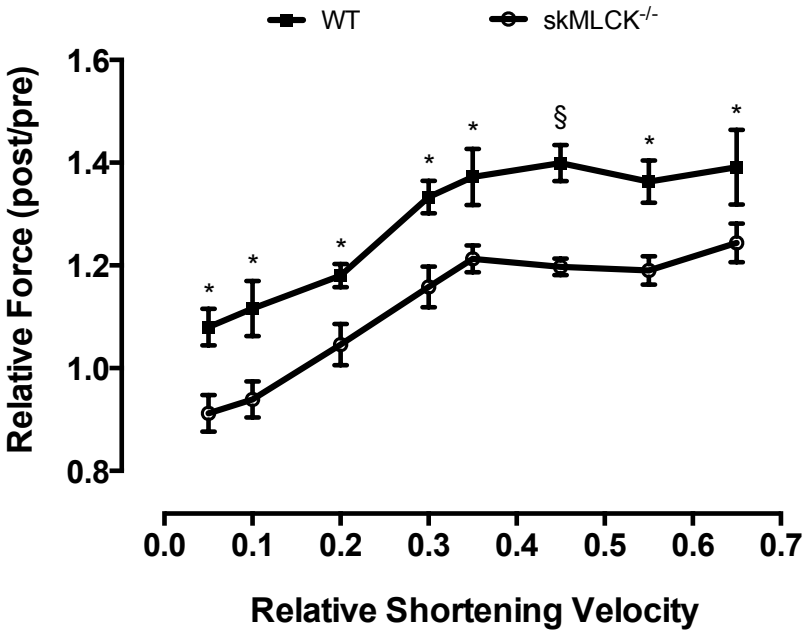

Figure 9. Relative concentric force (post-CS/ pre-CS) of mouse EDL at different shortening velocities (%Vmax), after tetanic stimulation (CS). * Indicates significant difference from skMLCK$^{-/-}$ value at the same velocity, ($p < 0.05$); § ($p < .01$). Values are presented as means and ± SEM ($n = 10$).

4.2.2 Absolute Concentric Force Potentiation

A two-way RM ANOVA was conducted for each genotype to test the effects of shortening velocity (0.05, 0.10, 0.20, 0.30, 0.35, 0.45, 0.55, & 0.65 V_{max}) and activation state (pre-CS vs. post-CS) on concentric force. Results for WT revealed a significant interaction effect and [F, (7, 63) = 4.611, $p = 0.0003$, $n^2 = 0.005$] significant main effects for shortening velocity [F (7, 63) = 91.78, $p < 0.0001$, $n^2 = 0.56$] and for activation state [F (1, 9) = 48.90, $p < 0.0001$, $n^2 = 0.062$] on concentric force. Post-hoc comparisons (Holm-Sidak) revealed that forces post-CS were significantly higher than pre-CS values when compared at the same velocity ($p < 0.001$), furthermore, this increase was greater at shortening speeds above 0.05 V_{max} ($p < 0.0001$).

Results for skMLCK$^{-/-}$ revealed a significant interaction effect [F, (7, 63) = 14.45, $p < 0.0001$, $n^2 = 0.02$] and significant main effects for shortening velocity [F (7, 63) = 99.38, $p < 0.0001$, $n^2 = 0.55$] on concentric force. Post-hoc comparisons (Holm-Sidak) revealed that post-CS forces were significantly higher than pre-CS, at shortening velocities 0.30 V_{max} and above ($p < 0.01$), however, at 0.20 V_{max} there was no significant change in force between conditions ($t = 0.8028$, $p > 0.05$). At slow shortening velocities of 0.05 ($p < 0.0001$) and 0.10 V_{max} ($p < 0.01$) there was a significant decrease in force post-CS.

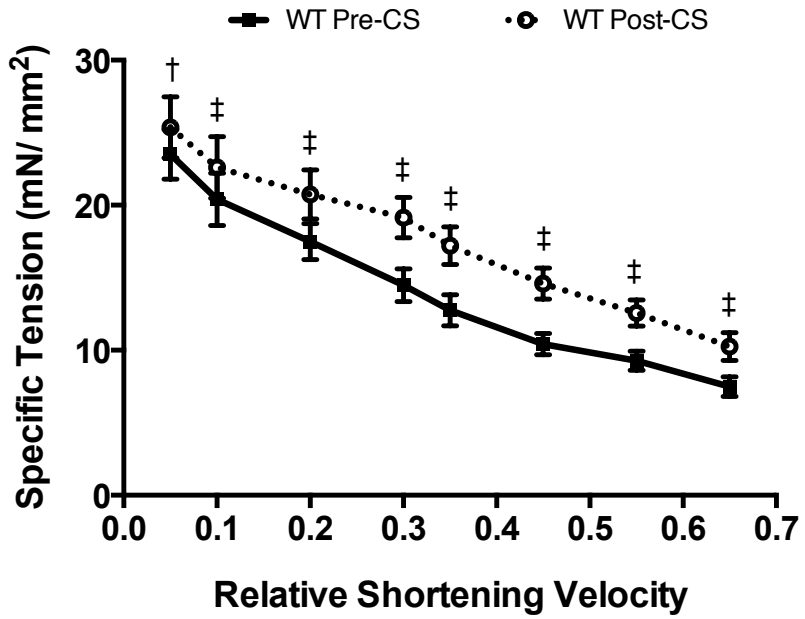

Figure 10. Specific Tension of WT mouse EDL muscle at different shortening velocities (%Vmax), before (solid line) and after (dashed line) tetanic stimulation (CS). † Indicates significant difference from pre-CS value at same velocity, ($p < 0.001$); ‡, ($p < 0.0001$). Values are presented as means and ± SEM ($n = 10$).

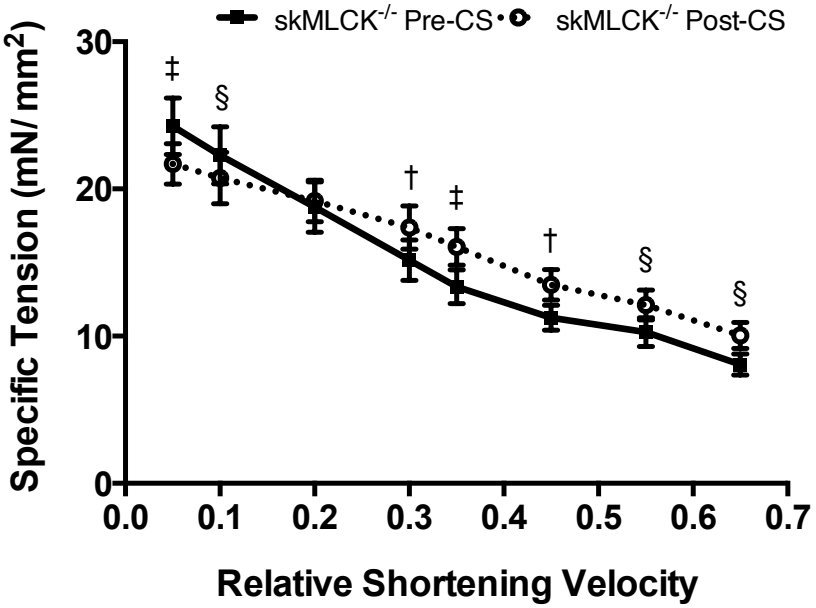

Figure 11. Specific tension of skMLCK$^{-/-}$ mouse EDL muscle at different shortening velocities (%Vmax), before (solid line) and after (dashed line) tetanic stimulation (CS). § Indicates significant difference from Pre-CS value at the same velocity, ($p < 0.01$); †, ($p < 0.001$); ‡, ($p < 0.0001$). Values are presented as means and ± SEM ($n = 10$).

Table 1. Mean forces (specific tension) of mouse EDL in WT and skMLCK$^{-/-}$ mice.

		0.05 Vmax	0.10 Vmax	0.20 Vmax	0.30 Vmax	0.35 Vmax	0.45 Vmax	0.55 Vmax	0.65 Vmax
Before	*skMLCK-/-*	24.2 ± 1.93	22.2 ± 1.93	18.8 ± 1.71	15.2 ± 1.38	13.4 ± 1.15	11.3 ± 0.85	10.3 ± 0.98	8.1 ± 0.71
After		21.6 ± 1.38 ‡	20.7 ± 1.75 §	19.2 ± 1.40	17.5 ± 1.47 †	16.1 ± 1.25 ‡	13.5 ± 1.04 †	12.1 ± 1.02 §	10.0 ± 0.89 §
Before	*WT*	23.5 ± 1.72	20.3 ± 1.81	17.5 ± 1.25	14.5 ± 1.14	12.8 ± 1.08	10.4 ± 0.74	9.3 ± 0.65	7.5 ± 0.68
After		25.3 ± 2.11 †	22.6 ± 2.13 ‡	20.8 ± 1.70 ‡	19.1 ± 1.39 ‡	17.2 ± 1.29 ‡	14.6 ± 1.08 ‡	12.6 ± 0.91 ‡	10.3 ± 0.96 ‡
Relative	*skMLCK-/-*	0.91 ± .04	0.94 ± .03	1.04 ± .04 [a]	1.16 ± .04 [a]	1.21 ± .03 [a]	1.20 ± .02 [a]	1.19 ± .03 [a]	1.24 ± .04 [a]
	WT	1.08 ± .03 *	1.12 ± .05 *	1.18 ± .02 [a]*	1.33 ± .03 [a]*	1.37 ± .05 [a]*	1.40 ± .04 [a]*	1.36 ± .04 [a]*	1.39 ± .07 [a]*

Note: Mean concentric force was normalized to specific tension and expressed as mN·mm^2. Values are presented as means and ± SEM (n = 10). Relative change is calculated as post-CS (**After**) value divided by pre-CS value (**Before**). Muscles were stimulated with 2 pulses.

After: § Indicates a significant increase above Pre-CS values, ($p < 0.01$); † ($p < .001$); ‡ ($p < .0001$).

Relative: * Indicates a significant increase above skMLCK$^{-/-}$ values, ($p < 0.05$).

[a] Indicates a significant relative difference from 0.05 Vmax, ($p < 0.0001$).

4.2.3 Relative Contractile Kinetics

Separate two-way ANOVAs were conducted to assess the effects of shortening velocity (0.05, 0.10, 0.20, 0.30, 0.35, 0.45, 0.55, & 0.65 V_{max}) and genotype (WT vs. skMLCK$^{-/-}$) on the relative change in rate of force development (+dF/d*t*) and rate of force relaxation (-dF/d*t*). Results for +dF/d*t* revealed a main effect for genotype [*F*, (7, 144) = 94.34, $p < 0.0001$, $n^2 = 0.38$] on the maximum rate of force development. Sidak's comparison revealed that WT values were significantly higher than skMLCK$^{-/-}$ at all shortening velocities, when compared at the same shortening velocity, ($p < 0.05$). Results for -dF/d*t* revealed a main effect for velocity [*F*, (7, 144) = 40.97, $p < 0.0001$, $n^2 = 0.65$]; however, no effect for genotype was present ($p = 0.8011$) and therefore no post-hoc tests were conducted.

4.2.4 Absolute Contractile Kinetics

A two-way RM ANOVA was conducted for each genotype to test the effects of shortening velocity (0.05, 0.10, 0.20, 0.30, 0.35, 0.45, 0.55, & 0.65 V_{max}) and activation state (pre-CS vs. post-CS) on the maximum rate of force development (+dF/d*t*). Separate two-way ANOVAs were then conducted for the rate of relaxation (-dF/d*t*). Results for (+dF/d*t*) in WT revealed a significant interaction effect [*F*, (7, 63) = 10.37, $p < 0.0001$, $n^2 = .002$], a main effect for velocity [*F*, (7, 63) = 64.43, $p < 0.0001$, $n^2 = 0.17$], and a main effect for activation state [*F*, (1, 9) = 87.09, $p < 0.0001$, $n^2 = 0.37$] on the rate of force development. As a result, post-hoc tests (Holm-Sidak) were conducted to compare pre-CS and post-CS values at each shortening velocity. The tests revealed a significant increase in +dF/d*t* after the CS, at every shortening velocity, ($p < 0.0001$).

Results for (+dF/d*t*) in skMLCK$^{-/-}$ revealed a significant interaction [*F*, (7, 63) = 2.355, $p = 0.033$, $n^2 = 0.002$] and significant main effects for shortening velocity [*F*, (7, 63) = 77.10, $p < 0.0001$, $n^2 = 0.33$] and for activation state [*F*, (1, 9) = 69.43, $p < 0.0001$, $n^2 = 0.04$]. Post-hoc tests (Holm-Sidak) were conducted to reveal the differences in (+dF/d*t*) between genotypes, among levels of shortening velocity. The tests revealed a significant increase in +dF/d*t* after the CS, at every shortening velocity, $p < .0001$.

Results for -dF/d*t* in WT revealed a significant a significant interaction effect [*F*, (7, 63) = 21.76, $p < 0.0001$, $n^2 = 0.06$] and significant main effects for velocity [*F* (7, 63) = 51.28, $p < 0.0001$, $n^2 = 0.35$] and for activation state [*F* (1, 9) = 45.51, $p < 0.0001$, $n^2 = 0.12$] on the rate of force relaxation. As a result, post-hoc tests (Holm-Sidak) were conducted to compare pre-CS and post-CS values at each shortening velocity. The tests revealed a significant increase in -dF/d*t* after the CS, between shortening velocities of 0.05-0.30 V_{max}, ($p < 0.0001$); a significant increase was also seen at 0.35 V_{max}, ($p < 0.05$).

Results of the ANOVA for -dF/d*t* in skMLCK$^{-/-}$ revealed a significant interaction effect [*F*, (7, 63) = 22.08, $p < 0.0001$, $n^2 = 0.07$] and significant main effects for velocity [*F*, (7, 63) = 22.64, $p < 0.0001$, $n^2 = 0.23$] and activation state [*F* (1, 9) = 29.83, $p = 0.12$, $n^2 = 0.13$] on the rate of force relaxation. As a result, post-hoc tests (Holm-Sidak) were conducted to compare pre-CS and post-CS values at each shortening velocity. The tests revealed a significant increase in -dF/d*t* after stimulation, between shortening velocities of 0.05-0.30 V_{max}, ($p < 0.0001$); a significant increase was also seen at 0.35 V_{max}, ($p < 0.05$). A summary of results for contractile kinetics is expressed in Tables 1 and 2.

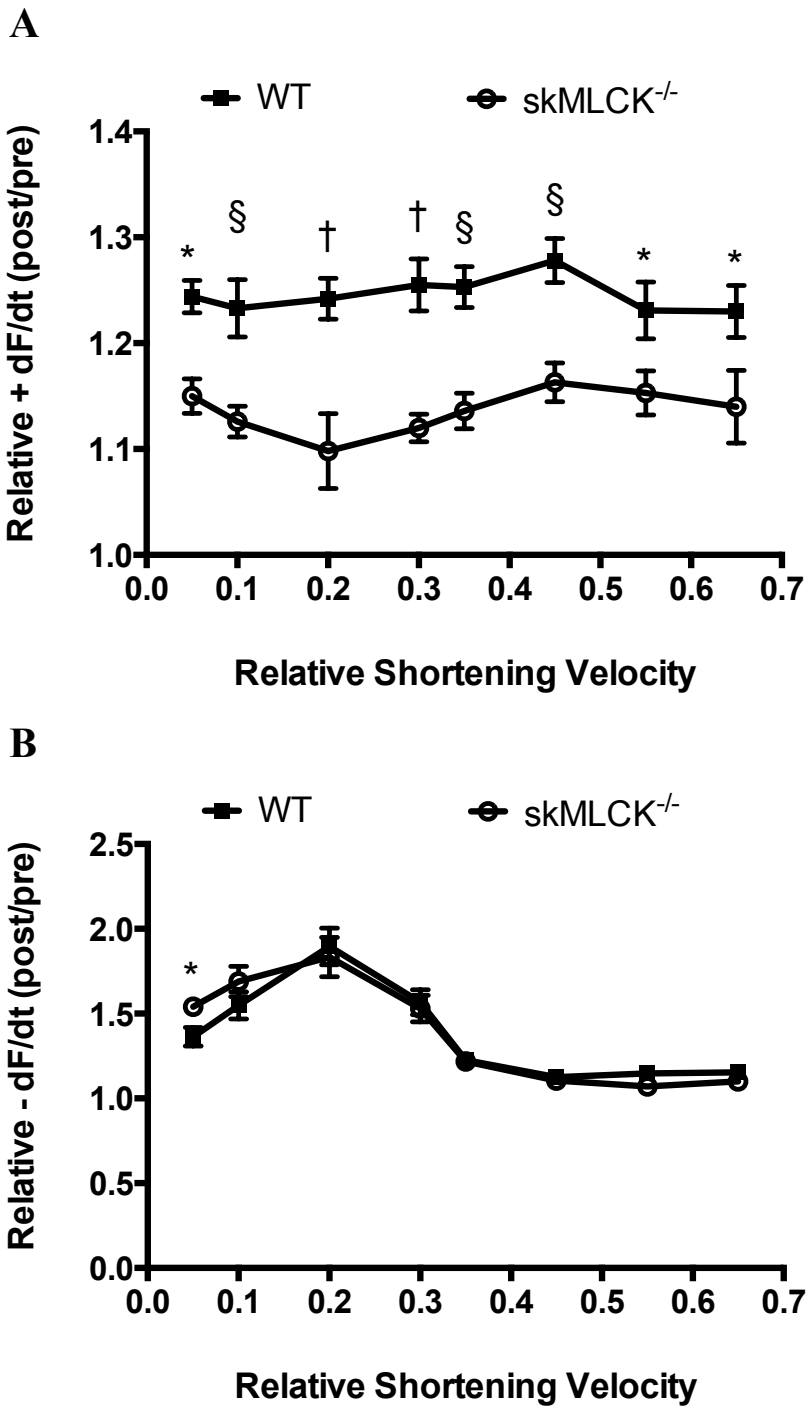

12. **A)** Relative change (post-CS/ pre-CS) in maximum rate of force development (+dF/d*t*) and **B)** maximum rate of force relaxation of mouse EDL in WT and skMLCK$^{-/-}$ mice after tetanic stimulation (CS). Values are presented as means and ± SEM for each velocity (n = 10). **A)** * Indicates significantly different from skMLCK$^{-/-}$, ($p < 0.05$); §, ($p < 0.01$); †, ($p < 0.001$). **B)** * Indicates significantly different from pre-CS in WT only, ($p < 0.05$).

Table 2. Rate of force development (+dF/d*t*) in mouse EDL of WT and skMLCK$^{-/-}$ mice.

		0.05 Vmax	0.10 Vmax	0.20 Vmax	0.30 Vmax	0.35 Vmax	0.45 Vmax	0.55 Vmax	0.65 Vmax
Before	*skMLCK$^{-/-}$*	2250 ± 177	2218 ± 181	2138 ± 175	1934 ± 153	1792 ± 133	1596 ± 116	1515 ± 122	1337 ± 112
	WT	2319 ± 254	2240 ± 280	2047 ± 226	1868 ± 232	1709 ± 220	1536 ± 184	1466 ± 179	1301 ± 149
After	*skMLCK$^{-/-}$*	2579 ± 196 ‡	2497 ± 205 ‡	2311 ± 167 ‡	2169 ± 177 ‡	2034 ± 151 ‡	1850 ± 131 ‡	1731 ± 121 ‡	1515 ± 122 ‡
	WT	2875 ± 305 ‡	2713 ± 302 ‡	2521 ± 265 ‡	2313 ± 270 ‡	2121 ± 262 ‡	1946 ± 224 ‡	1790 ± 212 ‡	1617 ± 204 ‡
Relative	*skMLCK$^{-/-}$*	1.15 ± 0.02	1.13 ± 0.01	1.10 ± 0.04	1.12 ± 0.01	1.14 ± 0.02	1.16 ± 0.02	1.15 ± 0.02	1.14 ± 0.03
	WT	1.25 ± 0.01 *	1.23 ± 0.03 §	1.24 ± 0.02 †	1.25 ± 0.02 †	1.25 ± 0.02 §	1.28 ± 0.02 §	1.23 ± 0.03 *	1.23 ± 0.02 *

Note: Rate of force development expressed as +mN·mm^{-2}·s^{-1}. Values are presented as means and ± SEM (n = 10). Relative change is calculated as post-CS (**After**) value divided by pre-CS value (**Before**). Muscles were stimulated with 2 pulses.

After: ‡ Indicates a significant increase above Pre-CS values, ($p < 0.0001$).

Relative: * Indicates a significant increase above skMLCK$^{-/-}$ values, ($p < 0.05$); § ($p < 0.01$); † ($p < 0.001$).

Table 3. Rate of force relaxation (-dF/d*t*) in mouse EDL of WT and skMLCK$^{-/-}$ mice.

		0.05 Vmax	0.10 Vmax	0.20 Vmax	0.30 Vmax	0.35 Vmax	0.45 Vmax	0.55 Vmax	0.65 Vmax
Before	*skMLCK*$^{-/-}$	1115 ± 157	989 ± 124	845 ± 86	818 ± 78	826 ± 77	780 ± 67	747 ± 69	648 ± 69
	WT	1290 ± 118	1108 ± 106	868 ± 88	845 ± 82	829 ± 84	813 ± 73	662 ± 67	659 ± 66
After	*skMLCK*$^{-/-}$	1708 ± 246 ‡	1690 ± 246 ‡	1580 ± 213 ‡	1286 ± 164 ‡	1019 ± 113 *	870 ± 84	804 ± 77	712 ± 77
	WT	1761 ± 191 ‡	1713 ± 184 ‡	1616 ± 173 ‡	1301 ± 116 ‡	1002 ± 92 *	916 ± 83	760 ± 76	751 ± 67
Relative	*skMLCK*$^{-/-}$	1.54 ± 0.05	1.69 ± 0.09	1.83 ± 0.12	1.53 ± 0.08	1.22 ± 0.04	1.11 ± 0.02	1.07 ± 0.01	1.10 ± 0.02
	WT	1.36 ± 0.06	1.55 ± 0.08	1.90 ± 0.11	1.57 ± 0.07	1.22 ± 0.03	1.13 ± 0.02	1.15 ± 0.02	1.15 ± 0.03

Note: Rate of force relaxation expressed as -mN·mm^{-2}·s^{-1}. Values are presented as means and ± SEM (n = 10). Relative change is calculated as post-CS (**After**) value divided by pre-CS value (**Before**). Muscles were stimulated with 2 pulses.

After: * Indicates a significant increase above pre-CS values, ($p < 0.05$); ‡ ($p < 0.0001$).

4.2.5 Gross Changes in Contractile Kinetics

In order to display the overall effect of genotype (WT vs. skMLCK$^{-/-}$) and activation state (pre-CS vs. post-CS) on +dF/d*t* and -dF/d*t* irrespective of shortening velocity, a two-way RM ANOVA was conducted for each measure. The results of the ANOVA for +dF/d*t* revealed a significant interaction effect [F, (1, 14) = 31.29, p < 0.0001, n^2 = 0.01] and main effect for activation state [F, (1, 14) = 389.90, p < 0.0001, n^2 = 0.17]. Post-hoc tests (Holm-Sidak) were then conducted to examine the differences between genotypes and activation state. The results revealed significant increases in +dF/d*t* after the CS in WT and skMLCK$^{-/-}$ mice, p < .0001. No differences between genotypes were present pre-CS (t = 0.1906, p > 0.05) or post-CS (t = 0.7841, p > 0.05).

The results for -dF/d*t* revealed a significant main effect for activation state [F, (1, 14) = 26.04, p < 0.0002, n^2 = 0.21]. Post-hoc tests (Holm-Sidak) were then conducted to examine the differences between pre-CS and post-CS. The results revealed significant increases in -dF/d*t* after the CS, (p < 0.01). No differences between genotypes were present pre-CS (t = 1.451, p < 0.05) or post-CS (t = 1.863, p < 0.05).

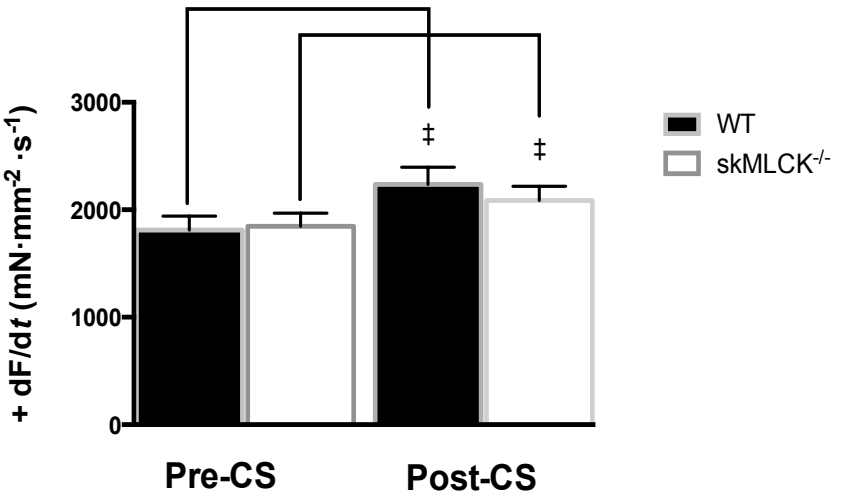

Figure 13. The maximum rate of force development (+dF/d*t*) in WT and skMLCK$^{-/-}$ mice when collapsed for shortening velocity. Values are presented as pooled means and ± SEM (n = 10). ‡ Indicates a significant difference between pre-CS and post-CS, ($p < 0.0001$).

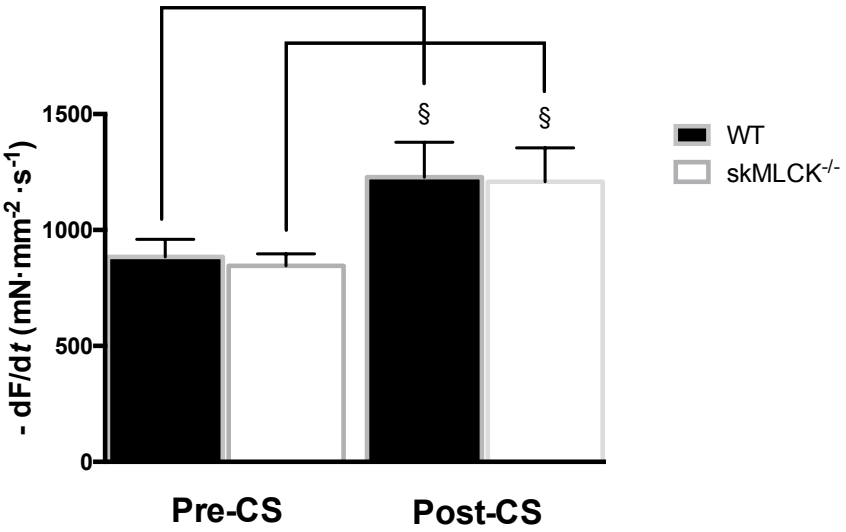

Figure 14. The maximum rate of force relaxation (-dF/d*t*) in WT and skMLCK$^{-/-}$ mice when collapsed for shortening velocity. Values are presented as means and ± SEM (n = 10). § Indicates a significant difference between pre-CS and post-CS, ($p < 0.01$).

4.2.6 Relative Time to Peak Tension

A two-way ANOVA was conducted to assess the effects of shortening velocity (0.05, 0.10, 0.20, 0.30, 0.35, 0.45, 0.55, & 0.65 V_{max}) and genotype (WT vs. skMLCK$^{-/-}$) on the relative change in time to peak tension (TPT) for each muscle. The ANOVA revealed significant main effects for shortening velocity [F (7, 144) = 31.89, $p < 0.0001$, $n^2 = 0.54$] and for genotype [F (1, 144) = 35.77, $p < 0.0001$, $n^2 = 0.09$] on TPT. Post-hoc tests were then conducted to reveal differences in TPT, between genotypes, among levels of shortening velocity. Using Holm-Sidak's Test, WT values were found to take significantly longer to reach peak than skMLCK$^{-/-}$ at 0.20 V_{max} ($p < 0.001$) and 0.35 V_{max} ($p < 0.01$).

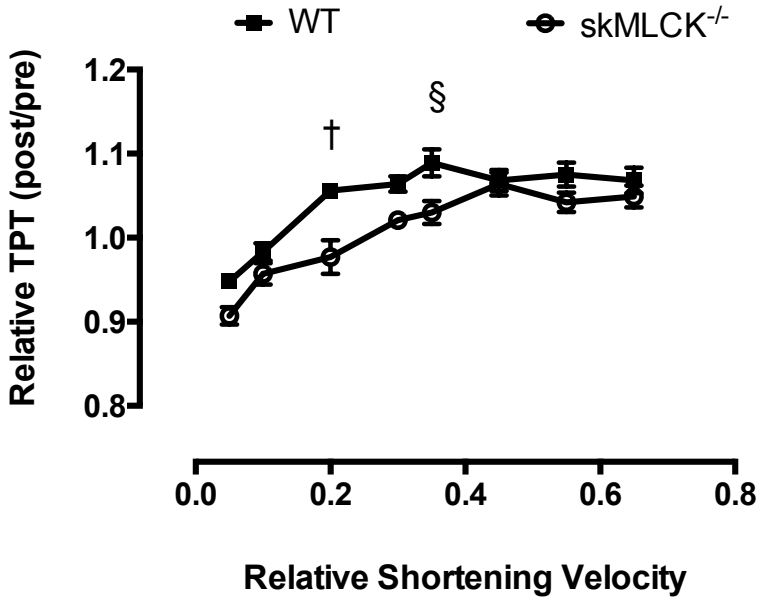

Figure 15. Relative change (post-CS/ pre-CS) in time to peak tension (TPT) of mouse EDL in WT and skMLCK$^{-/-}$ mice after tetanic stimulation (CS). Values are presented as means and ± SEM for each velocity (n = 10). § Indicates a significant difference between pre-CS and post-CS, $p < .01$; †, $p < .001$.

4.2.7 Absolute Time to Peak Tension

A two-way RM ANOVA was conducted for each genotype to assess the effects of shortening velocity (0.05, 0.10, 0.20, 0.30, 0.35, 0.45, 0.55, & 0.65 V_{max}) and activation state (pre-CS vs. post-CS) on absolute TPT. Results of the ANOVA for WT revealed a significant interaction [F (7, 63) = 30.70, $p < 0.0001$, $n^2 = 0.02$] and significant main effects for velocity, [F (7, 63) = 994.3, $p < 0.0001$, $n^2 = 0.88$] and for activation state, [F (1, 9) = 28.77, $p = 0.0005$, $n^2 = 0.08$] on TPT. Post-hoc tests (Holm-Sidak) revealed a significant increase in TPT pre-CS compared with post-CS at 0.05 ($p < 0.001$) and 0.10 V_{max} ($p < 0.05$). For shortening velocities between 0.20-0.65 V_{max}, post-CS values were significantly higher than Pre-CS ($p < 0.0001$).

The ANOVA for skMLCK$^{-/-}$ revealed a significant interaction [F (7, 63) = 20.23, $p < .0001$, $n^2 = 0.03$] and a significant main effect for velocity, [F (7, 63) = 422.3, $p < 0.0001$, $n^2 = 0.92$] on TPT. Post-hoc tests (Holm-Sidak) revealed a significant increase in TPT pre-CS compared with post-CS values at shortening velocities of 0.05 ($p < 0.0001$) and 0.10 V_{max} ($p < 0.01$). On the other hand, at 0.45 and 0.65 V_{max}, post-CS TPT was significantly longer than pre-CS ($p < 0.01$, $p < 0.05$, respectively).

Table 4. Mean time to peak tension (TPT) of mouse EDL in WT and skMLCK$^{-/-}$ mice.

		0.05 Vmax	0.10 Vmax	0.20 Vmax	0.30 Vmax	0.35 Vmax	0.45 Vmax	0.55 Vmax	0.65 Vmax
Before	*skMLCK-/-*	29.1 ± 0.36‡	27.9 ±0.48§	25.7 ± 0.42	22.9 ± 0.26	20.9 ± 0.36	19.1 ± 0.37	18.3 ± 0.31	17.3 ± 0.35
	WT	29.0 ± 0.23‡	28.0 ±0.24*	24.9 ± 0.24	22.8 ± 0.24	20.9 ± 0.27	19.5 ± 0.15	18.3 ± 0.21	17.5 ± 0.17
After	*skMLCK-/-*	26.4 ± 0.46	26.7 ± 0.45	25.0 ± 0.41	23.35 ± 0.40	21.6 ± 0.38	20.3 ± 0.32§	19.0 ± 0.39	18.2 ± 0.43*
	WT	27.5 ± 0.28	27.5 ± 0.28	26.3 ± 0.26‡	24.2 ± 0.23‡	22.7 ± 0.15‡	20.8 ± 0.30‡	19.6 ± 0.3 ‡	18.7 ± 0.33‡
Relative	*skMLCK-/-*	0.91 ± 0.01	0.96 ± 0.01	0.98 ± 0.02	1.02 ± 0.01	1.03 ± 0.01	1.06 ± 0.01	1.04 ± 0.01	1.05 ± 0.01
	WT	0.95 ± 0.01	0.98 ± 0.01	1.06 ± 0.01†	1.06 ± 0.01	1.09 ± 0.02§	1.07 ± 0.01	1.07 ± 0.01	1.07 ± 0.02

Note: Time to peak tension expressed in milliseconds (ms). Values are presented as means and ± SEM (n = 10). Relative change is calculated as post-CS (**After**) value divided by pre-CS value (**Before**). Muscles were stimulated with 2 pulses.

Before; After: * Indicates a significant increase above other condition, ($p < 0.05$); § ($p < 0.01$); ‡ ($p < 0.0001$).

Relative: § Indicates a significant increase above skMLCK$^{-/-}$ values, ($p < 0.01$); † ($p < 0.001$).

4.2.8 Relative Half Relaxation Time (½RT)

A two-way ANOVA was conducted to assess the effects of shortening velocity (0.05, 0.10, 0.20, 0.30, 0.35, 0.45, 0.55, & 0.65 V_{max}) and genotype (WT vs. skMLCK$^{-/-}$) on the relative change in ½RT after a tetanic conditioning stimulus (CS). Results revealed a significant interaction [F (7, 144) = 2.082, p = 0.0491, n^2 = 0.01] and significant main effects for velocity, [F (7, 144) = 119.2, p < 0.0001, n^2 = 0.75] and for genotype, [F (1, 144) = 122.3, p < 0.0001, n^2 = 0.11] on ½RT. Post-Hoc tests revealed significantly longer ½RT for WT than skMLCK$^{-/-}$ muscles at 0.05 (p < 0.0001), 0.10 (p < 0.01), 0.30 (p < 0.01), 0.45 (p < 0.0001), 0.55 (p < 0.0001), and 0.65 V_{max} (p < 0.0001).

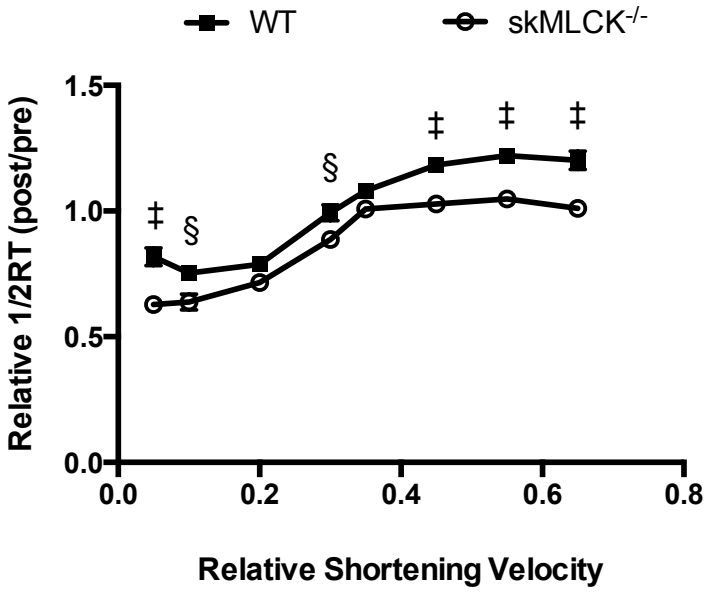

Figure 16. Relative change (post-CS/ pre-CS) in half relaxation time (½RT) of mouse EDL in WT and skMLCK$^{-/-}$ mice after tetanic stimulation (CS). Values are presented as means and ± SEM for each velocity (n = 10). § Indicates a significant difference between pre-CS and post-CS, (p < 0.01); ‡, (p < 0.001).

Table 5. Mean half relaxation time (1/2RT) of mouse EDL in WT and skMLCK$^{-/-}$ mice.

		0.05 Vmax	0.10 Vmax	0.20 Vmax	0.30 Vmax	0.35 Vmax	0.45 Vmax	0.55 Vmax	0.65 Vmax
Before	*skMLCK-/-*	25.9 ± 0.78‡	24.1 ± 0.63‡	20.9 ± 0.49‡	17.2 ± 0.39‡	14.75 ± 0.32	13.0 ± 0.34	12.0 ± 0.24	11.1 ± 0.24
	WT	23.0 ± 1.32‡	22.4 ± 0.69‡	20.7 ± 0.38‡	17.1 ± 0.33	14.8 ± 0.25	12.4 ± 0.23	11.2 ± 0.21	10.4 ± 0.22
After	*skMLCK-/-*	16.3 ± 1.08	15.4 ± 0.72	15.0 ± 0.40	15.2 ± 0.30	14.9 ± 0.44	13.3 ± 0.25	12.6 ± 0.20	11.2 ± 0.34
	WT	18.8 ± 1.02	16.9 ± 0.88	16.3 ± 0.64	16.9 ± 0.37	16.0 ± 0.35*	14.6 ± 0.19‡	13.7 ± 0.16‡	12.5 ± 0.25‡
Relative	*skMLCK-/-*	0.63 ±0 .03	0.64 ± 0.02	0.72 ± 0.02	0.89 ± 0.03	1.01 ± 0.03	1.03 ± 0.02	1.05 ± 0.02	1.01 ± 0.04
	WT	0.82 ± 0.02‡	0.75 ± 0.03§	0.79 ± 0.02	0.99 ± 0.02§	1.08 ± 0.01	1.18 ± 0.01‡	1.22 ± 0.02‡	1.20 ± 0.02‡

Note: Time to half-relaxation from peak tetanic force, expressed in milliseconds (ms). Values are presented as means and ± SEM (n = 10). Relative change is calculated as post-CS (**After**) value divided by pre-CS value (**Before**). Muscles were stimulated with 2 pulses.

Before; After: * Indicates a significant increase above other condition, ($p < 0.05$); ‡ ($p < 0.0001$).

Relative: § Indicates a significant increase above skMLCK$^{-/-}$ values, ($p < 0.01$); ‡ ($p < 0.001$).

4.2.9 Absolute Half Relaxation Time

A two-way RM ANOVA was conducted for each genotype to assess the effects of shortening velocity (0.05, 0.10, 0.20, 0.30, 0.35, 0.45, 0.55, & 0.65 V_{max}) and activation state (pre-CS vs. post-CS) on absolute ½RT. Results of the ANOVA for WT revealed a significant interaction [F (7, 63) = 58.12, $p < 0.0001$, $n^2 = 0.16$] and significant main effects for velocity, [F (7, 63) = 101.5, $p < 0.0001$, $n^2 = 0.68$] and for activation state, [F (1, 9) = 11.30, $p = 0.0084$, $n^2 = 0.01$] on ½RT. Post-hoc tests (Holm-Sidak) revealed a significant increase in ½RT pre-CS compared with post-CS for 0.05-0.20 V_{max} ($p < 0.0001$); no significant differences were seen between conditions at 0.30 V_{max} ($t = 0.455$, $p < 0.05$). On the other hand, at 0.35 V_{max}, post-CS ½RT was significantly longer than pre-CS values ($p < 0.05$), and between 0.45-0.65 V_{max} ($p < 0.0001$).

The ANOVA for skMLCK$^{-/-}$ revealed a significant interaction [F (7, 63) = 108.4, $p < 0.0001$, $n^2 = 0.19$] and a significant main effect for velocity, [F (7, 63) = 75.59, $p < 0.0001$, $n^2 = 0.55$] and activation state [F (1, 9) = 266.1, $p < 0.0001$, $n^2 = 0.12$] on ½RT. Post-hoc-tests (Holm-Sidak) revealed a significant increase in ½RT pre-CS compared with post-CS values at shortening velocities between 0.05-0.30 V_{max} ($p < 0.0001$).

4.2.10 Relative Muscle Work

A two-way ANOVA was conducted to assess the effects of shortening velocity (0.05, 0.10, 0.20, 0.30, 0.35, 0.45, 0.55, & 0.65 V_{max}) and genotype (WT vs. skMLCK$^{-/-}$) on the relative change in muscle work after a tetanic conditioning stimulus (CS). Results revealed significant main effects for velocity, [F (7, 144) = 71.49, $p < 0.0001$, $n^2 = 0.55$] and for genotype, [F (1, 144) = 260.2, $p < 0.0001$, $n^2 = 0.28$] on work. Post-hoc tests were then conducted to reveal the differences in work, between genotypes, among levels of shortening velocity. Using Holm-Sidak's test, WT work values were found to be significantly higher than skMLCK$^{-/-}$ at all shortening velocities when compared at the same velocity, ($p < .0001$); with the exception of 0.10 V_{max} ($p < 0.05$). All shortening velocities were then compared to the slowest shortening velocity (0.05 V_{max}) of each genotype (WT & skMLCK$^{-/-}$) to examine the differences in speed within genotypes. Results of the tests (Holm-Sidak) revealed a significant difference in WT muscles between 0.05 V_{max} and all shortening velocities ($p < 0.01$), except at 0.10 V_{max} ($p = 0.8393$); however the relative change was still higher than at 0.05 V_{max} (1.04 vs. 1.00).

In skMLCK$^{-/-}$ muscles, every shortening velocity was found to be significantly different from 0.05 V_{max} ($p < 0.05$). The largest relative difference in each genotype was trending towards 0.65 V_{max} (WT, 1.53%; skMLCK$^{-/-}$, 1.20%).

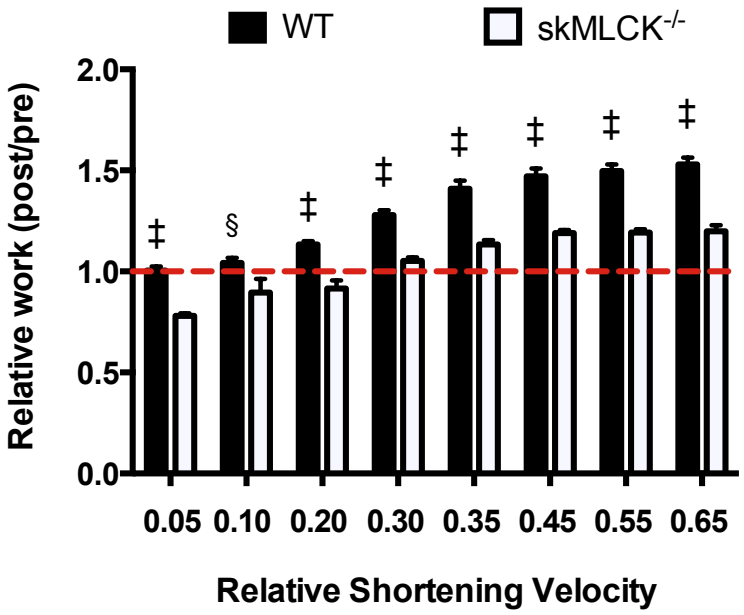

Figure 17. Relative work output (post-CS/ pre-CS) of EDL in WT and skMLCK$^{-/-}$ mice. Values are presented as means and ± SEM (n = 10). Red dashed line indicates maximal pre-CS work output for each velocity. § Indicates significant increase in WT work output above skMLCK$^{-/-}$, (p < 0.01); ‡, (p < 0.0001).

4.2.11 Absolute Muscle Work

A two-way RM ANOVA was conducted for each genotype to assess the effects of shortening velocity (0.05, 0.10, 0.20, 0.30, 0.35, 0.45, 0.55, & 0.65 V_{max}) and activation state (pre-CS vs. post-CS) on absolute muscle work. Results of the ANOVA for WT revealed a significant interaction [F (7, 63) = 83.68, (p < 0.0001), n^2 = 0.05] and significant main effects for velocity, [F (7, 63) = 128.7, p < 0.0001, n^2 = 0.49] and for activation state, [F (1, 9) = 138.5, p < 0.0001, n^2 = 0.11] on work. Post-hoc tests were then conducted to reveal the differences in work between activation states, among levels of shortening velocity. The tests (Holm-Sidak) revealed that work values were significantly higher post-CS than pre-CS at shortening velocities of 0.20 V_{max} and above,

when compared at the same velocity, ($p < 0.0001$). At 0.05 and 0.10 V_{max} there were no significant changes between activation states, $t = 0.073$ and $t = 1.137$, respectively ($p > 0.05$).

Results for skMLCK$^{-/-}$ revealed a significant interaction [F (7, 63) = 33.04, $p < 0.0001$, $n^2 = 0.03$] and significant main effects for velocity, [F (7, 63) = 86.78, $p < 0.0001$, $n^2 = 0.52$] and for activation state, [F (1, 9) = 11.57, $p = 0.0079$, $n^2 = 0.005$] on work. Post-hoc tests (Holm-Sidak) revealed that muscle work at shortening velocities between 0.05-0.20 V_{max} were significantly higher pre-CS than post-CS, ($p < 0.001$). At 0.30 V_{max} there was a crossover effect such that post-CS values were significantly higher than pre-CS, ($p < 0.05$), and this difference increased at 0.35 V_{max} and above, ($p < 0.0001$).

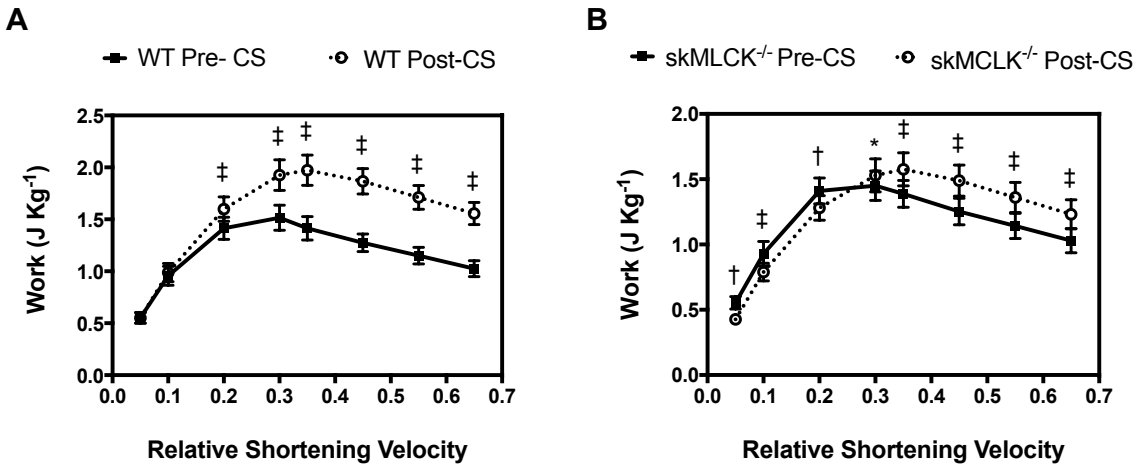

Figure 18. **A)** Absolute work output in WT and **B)** in skMLCK$^{-/-}$ muscles, expressed in Joules per Kilogram of muscle mass. Values are presented as means and ± SEM for each shortening velocity. * Indicates significant difference from other condition (pre-CS vs. post-CS), ($p < 0.05$); † significant difference ($p < 0.001$); ‡ Significant difference ($p < 0.0001$).

4.2.12 Absolute Mean Power Output

A two-way RM ANOVA was conducted to test the hypothesis that WT muscles would produce higher concentric power output after the conditioning stimulus. To assess this outcome we analyzed the influence of shortening velocity (0.05, 0.10, 0.20, 0.30, 0.35, 0.45, 0.55, & 0.65 V_{max}) and activation state (pre-CS vs. post-CS) on concentric power output. Results for WT revealed a significant interaction effect and [F, (7, 63) = 31.04, $p = 0.0003$, $n^2 = 0.027$] significant main effects for shortening velocity [F (7, 63) = 132.7, $p < 0.0001$, $n^2 = 0.64$] and for activation state [F (1, 9) = 76.06, $p < 0.0001$, $n^2 = 0.07$]. Post-hoc comparisons (Holm-Sidak) revealed that post-CS values were significantly higher than pre-CS at 0.20 V_{max} ($p < .001$) and at 0.30 V_{max} and above ($p < 0.0001$), when compared at the same velocity. Furthermore, post-hoc tests were conducted to examine differences in shortening velocity post-CS. Slower speeds of shortening (0.05-0.30 V_{max}) produced significantly lower power output than faster velocities of shortening (0.35-0.65 V_{max}, $p < 0.0001$). However, no discernible peak in power was observed between 0.35-0.65 V_{max}.

Results for skMLCK$^{-/-}$ revealed a significant interaction effect [F, (7, 63) = 26.77, $p < 0.0001$, $n^2 = 0.02$] and significant main effects for shortening velocity [F (7, 63) = 115.7, $p < 0.0001$, $n^2 = 0.68$] and activation state [F (1, 9) = 45.74, $p < 0.0001$, $n^2 = 0.02$]. Post-hoc comparisons (Holm-Sidak) revealed that post-CS values were significantly higher than pre-CS at shortening velocities 0.30 V_{max} and above ($p < 0.0001$). Furthermore, post-hoc tests were conducted to examine differences in shortening velocity post-CS. Slower speeds of shortening (0.05-0.35 V_{max}) produced significantly lower power output than faster velocities of shortening (0.45-0.65 V_{max}, $p < 0.05$). However, no

discernible peak in power was observed between 0.45-0.65 V_{max} and seemed to display a plateau.

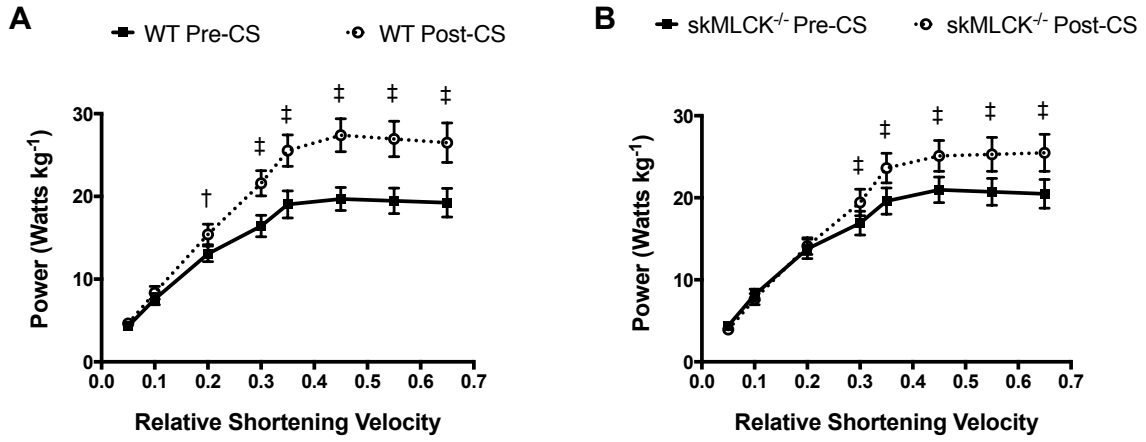

Figure 19. **A)** Absolute mean power output in WT and **B)** in skMLCK$^{-/-}$ muscles, expressed in Watts per Kilogram of muscle mass. Values are presented as means and ± SEM for each shortening velocity. † Indicates significant difference from other condition (pre-CS vs. post-CS), ($p < 0.001$); ‡ significant difference ($p < 0.0001$).

Table 6. Mean power output of mouse EDL in WT and skMLCK-/- mice.

		0.05 Vmax	0.10 Vmax	0.20 Vmax	0.30 Vmax	0.35 Vmax	0.45 Vmax	0.55 Vmax	0.65 Vmax
Before	*skMLCK-/-*	4.40 ± 0.37	8.17 ± 0.70	13.78 ± 1.20	16.91 ± 1.45	19.59 ± 1.60	20.98 ± 1.57	20.73 ± 1.65	20.48 ± 1.76
	WT	4.32 ± 0.32	7.59 ± 0.68	13.06 ± 0.94	16.42 ± 1.31	19.03 ± 1.63	19.68 ± 1.40	19.47 ± 1.55	19.25 ± 1.74
After	*skMLCK-/-*	3.94 ± 0.28	7.63 ± 0.68	14.11 ± 1.02	19.43 ± 1.61‡	23.62 ± 1.81‡	25.10 ± 1.89‡	25.29 ± 2.07‡	25.48 ± 2.26‡
	WT	4.63 ± 0.38	8.36 ± 0.77	15.40 ± 1.24†	21.59 ± 1.53‡	25.53 ± 1.90‡	27.39 ± 2.00‡	26.94 ± 2.15‡	26.49 ± 2.39‡
Relative	*skMLCK-/-*	0.91± 0.04	0.94 ± 0.03	1.04 ± 0.04	1.16 ± 0.04	1.21 ± 0.03	1.20 ± 0.02	1.22 ± 0.02	1.24 ± 0.04
	WT	1.07 ± 0.04*	1.11 ± 0.05*	1.18 ± 0.02	1.33 ± 0.03*	1.37 + 0.05	1.39 ± 0.04§	1.39 ± 0.04*	1.39 ± 0.07

Note: Power output is expressed as W kg^{-1}. Values are presented as means and ± SEM (n = 10). Relative change is calculated as post-CS (**After**) value divided by pre-CS value (**Before**). Muscles were stimulated with 2 pulses.

After: * Indicates a significant increase above pre-CS values, ($p < 0.05$); ‡ ($p < 0.0001$).

Relative: * Indicates a significant increase above $skMLCK^{-/-}$ values, ($p < 0.05$); § ($p < 0.01$).

4.2.13 Absolute Peak Power Output

A two-way RM ANOVA was conducted for each genotype to test the effects of shortening velocity (0.05, 0.10, 0.20, 0.30, 0.35, 0.45, 0.55, & 0.65 V_{max}) and activation state (pre-CS vs. post-CS) on concentric power output, calculated from peak as opposed to mean force. Results for WT revealed a significant interaction effect and [F, (7, 63) = 73.19, $p < 0.0001$, $n^2 = 0.01$] significant main effects for shortening velocity [F (7, 63) = 179.10, $p < 0.0001$, $n^2 = 0.62$] and for activation state [F (1, 9) = 107.00, $p < 0.0001$, $n^2 = 0.08$]. Post-hoc comparisons (Holm-Sidak) revealed that post-CS values were significantly higher than pre-CS at every shortening velocity ($p < 0.0001$), when compared at the same velocity. Furthermore, post-hoc tests (Holm-Sidak) were conducted to examine differences in shortening velocity within conditions. For post-CS values, it was found that at 0.45 V_{max} significantly higher power output was produced compared with any other velocities of shortening ($p < 0.001$). However, for pre-CS values the velocity corresponding to peak power was the same (0.45 V_{max}) and therefore no shift was evident.

Results for skMLCK$^{-/-}$ revealed a significant interaction effect [F, (7, 63) = 13.65, $p < 0.0001$, $n^2 = 0.003$] and significant main effects for shortening velocity [F (7, 63) = 105.5, $p < 0.0001$, $n^2 = 0.57$] and activation state [F (1, 9) = 36.12, $p = 0.0002$, $n^2 = 0.02$]. Post-hoc comparisons (Holm-Sidak) revealed that post-CS values were significantly higher than pre-CS at 0.10 V_{max} ($p < 0.001$) and a greater difference at 0.20 V_{max} and above ($p < 0.0001$), when compared at the same velocity. Furthermore, post-hoc tests (Holm-Sidak) were conducted to examine differences in shortening velocity within

conditions. It was found that no velocity corresponded to peak power in either condition ($p > 0.05$) once again displaying a plateau.

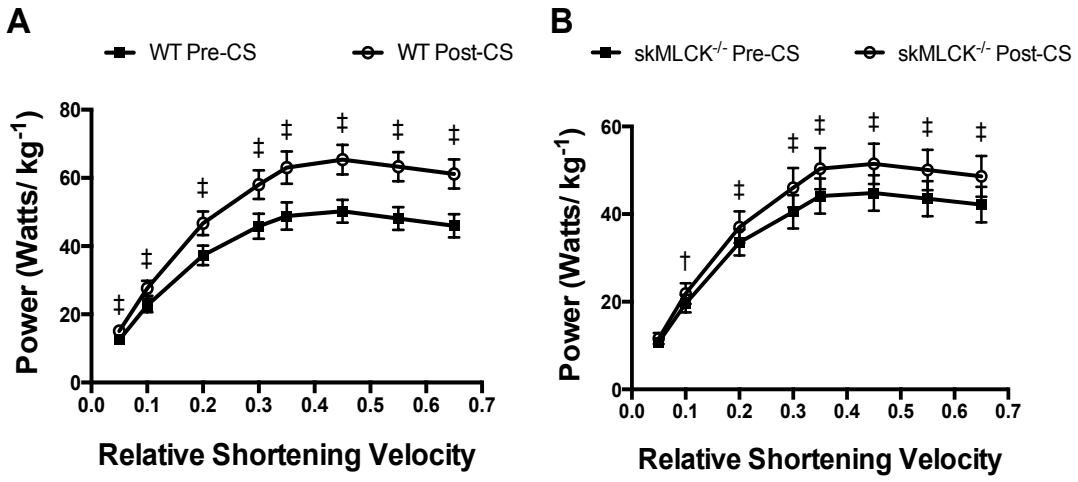

Figure 20. **A)** Absolute peak power output in WT and **B)** in skMLCK$^{-/-}$ muscles, expressed in Watts per Kilogram of muscle mass. Values are presented as means and ± SEM for each shortening velocity. † Indicates significant difference from other condition (pre-CS vs. post-CS), ($p < 0.001$); ‡ significant difference ($p < 0.0001$).

Table 7. Peak power output of mouse EDL in WT and skMLCK-/- mice.

		0.05 Vmax	0.10 Vmax	0.20 Vmax	0.30 Vmax	0.35 Vmax	0.45 Vmax	0.55 Vmax	0.65 Vmax
Before	*skMLCK-/-*	10.7 ± 1.09	19.6 ± 1.99	33.5 ± 2.94	40.5 ± 3.79	44.1 ± 4.02	44.9 ± 4.06	43.5 ± 4.04	42.2 ± 4.07
	WT	12.5 ± 1.03	22.6 ± 2.00	37.3 ± 2.89	45.8 ± 3.68	48.9 ± 4.01	50.3 ± 3.03	48.1 ± 3.34	46.0 ± 3.43
After	*skMLCK-/-*	11.6 ± 1.28	21.9 ± 2.38†	37.0 ± 3.59‡	46.0 ± 4.52‡	50.4 ± 4.72‡	51.5 ± 4.60‡	50.1 ± 4.61‡	48.6 ± 4.67‡
	WT	15.1 ± 1.21‡	27.7 ± 2.22‡	46.7 ± 3.47‡	58.0 ± 4.23‡	63.0 ± 4.74‡	65.4 ± 4.32‡	63.3 ± 4.27‡	61.2 ± 4.27‡
Relative	*skMLCK-/-*	1.07 ± 0.03	1.11 ± 0.02	1.11 ± 0.05	1.13 ± 0.02	1.14 ± 0.02	1.15 ± 0.02	1.15 ± 0.02	1.16 ± 0.02
	WT	1.21 ± 0.02†	1.24 ± 0.03§	1.26 ± 0.02†	1.28 ± 0.02†	1.30 ± 0.04†	1.30 ± 0.03†	1.32 ± 0.03†	1.34 ± 0.03‡

Note: Power output is expressed as W kg^{-1}. Values are presented as means and ± SEM (n = 10). Relative change is calculated as post-CS (**After**) value divided by pre-CS value (**Before**). Muscles were stimulated with 2 pulses.

After: † Indicates a significant increase above pre-CS values, ($p < 0.001$); ‡ ($p < 0.0001$).

Relative: § Indicates a significant increase above $skMLCK^{-/-}$ values, ($p < 0.01$); † ($p < 0.001$); ‡ ($p < 0.0001$).

4.2.14 Power Curve Fitting

A second order polynomial (quadratic) was fit to the data of each condition (pre-CS vs. post-CS) for each genotype (WT & skMLCK$^{-/-}$) for both mean and peak power. The equation describing the curve i.e., $y = a(x^2) + b(x) + c$ was used to extrapolate the curve by solving for a given x value. As shown in figure 23, x values were extrapolated for 0.75, 0.85, and 0.95 V_{max}. The equation was then used to find the peak of each curve to create a better estimate of the corresponding x value (% V_{max}) defining peak power. For mean power, the shortening velocities that corresponded to peak power output in WT were 0.53 & 0.56 V_{max} and in skMLCK$^{-/-}$ were 0.52 & 0.54 V_{max} for pre-CS and post-CS conditions, respectively. For peak power, the shortening velocities that corresponded to peak power output in WT were 0.47 & 0.48 V_{max} and in skMLCK$^{-/-}$ were 0.48 & 0.48 V_{max} for pre-CS and post-CS conditions, respectively. All curves were fit from mean data and the polynomial fits were not tested for normality or confidence intervals. Therefore, we cannot truly claim if a shift in velocity did occur for peak power; regardless, the data and curve fittings suggest no shift was evident. The following equations represent the best fit curves for the data in the panels shown below: **A)** $y = -72.976x^2 + 75.193x + 0.8223$ (pre-CS) and $y = -100.15x^2 + 107.35x - 1.0883$ (post-CS) **B)** $y = -73.361x^2 + 77.253x + 0.9756$ (pre-CS) and $y = -85.845x^2 + 96.266x - 1.019$ (post-CS) **C**) $y = -214.94x^2 + 201.61x + 4.1852$ (pre-CS) and $y = -268.96x^2 + 260.02x + 4.0126$ (post-CS) **D)** $y = -189.6x^2 + 180.69x + 3.2818$ (pre-CS) and $y = -215.02x^2 + 207.67x + 2.895$ (post-CS).

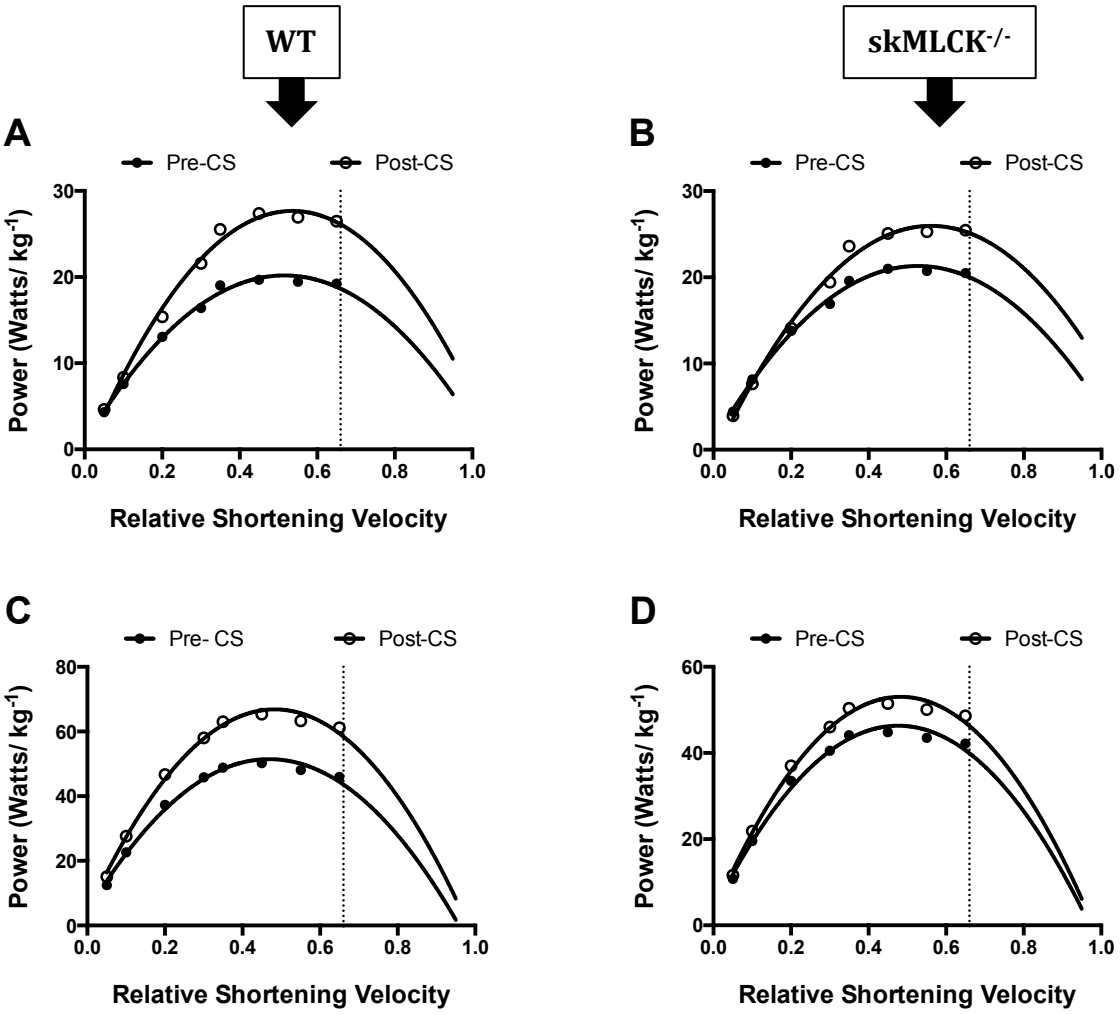

Figure 21. Four panel diagram displaying hypothetical curves for power output. **A)** Mean power in WT and **B)** skMLCK$^{-/-}$ muscles, **C)** Peak power in WT and **D)** skMLCK$^{-/-}$ muscles. Data points from 0.05-0.65 V_{max} represent means (n = 10) and all data to the right of the dashed line represent extrapolated hypothetical data. Curves are best fit to the data using non-linear regression (second order polynomial).

4.3 Biochemical Data

4.3.1 RLC Phosphorylation Content

A two-way ANOVA was conducted to assess the effects of genotype (WT vs. skMLCK$^{-/-}$) and activation state (pre-CS vs. post-CS) on myosin phosphorylation content of mouse EDL muscle. Results of the ANOVA revealed a significant interaction [F (1, 12) = 74.54, $p < 0.0001$, $n^2 = 0.23$] and significant main effects for genotype, [F (1, 12) = 106.70, $p < 0.0001$, $n^2 = 0.37$] and for activation state, [F (1, 12) = 113.10, $p < 0.0001$, $n^2 = 0.37$] on total phosphorylation content. Post-hoc tests were then conducted to reveal the differences between genotypes at rest and after stimulation. The tests (Holm-Sidak) revealed that RLC phosphorylation in WT were significantly higher after stimulation (0.63) than at rest (0.08 mol P/mol RLC), ($p < 0.0001$). skMLCK$^{-/-}$ mice had no significant changes in RLC phosphate content between rest and after stimulation ($p > 0.05$).

Table 8. RLC phosphate content of mouse EDL in WT and skMLCK$^{-/-}$ mice.

GENOTYPE	CONDITION	
	RESTING	**STIMULATED**
WT	0.08 ± 0.01[a]	0.63 ± 0.06[b]
skMLCK$^{-/-}$	0.03 ± 0.01[a]	0.08 ± 0.01[a]

Note: RLC phosphate content expressed in mol P/mol RLC. Muscles were frozen at only one time point i.e., resting or after stimulation. Values are presented as means and ± SEM ($n = 4$).

[a] Indicates a significant difference from other letters

[b] Indicates a significant difference from other letters

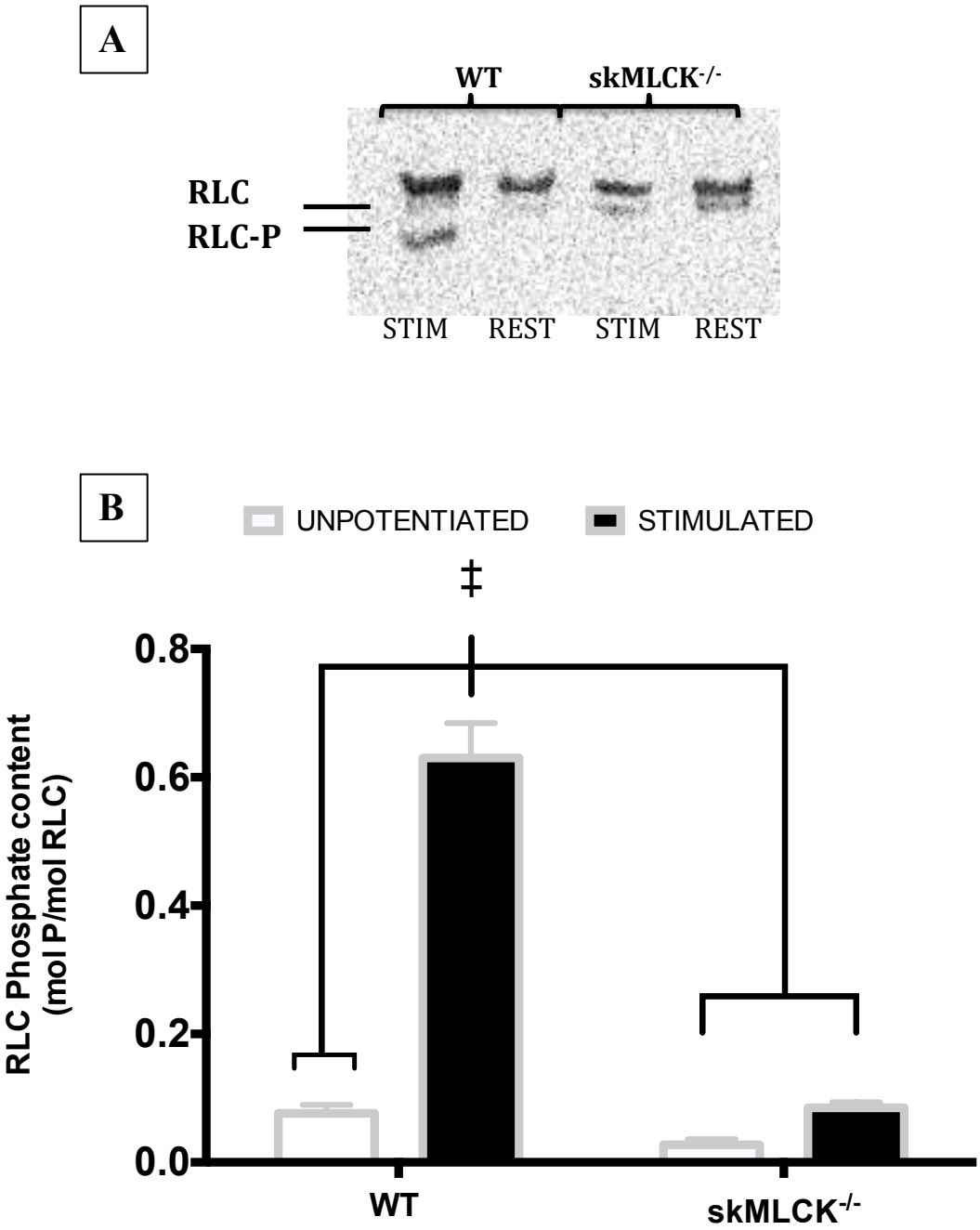

Figure 22. **A)** Representative Urea/Glycerol PAGE blot of monophosphorylated and non-phosphorylated myosin RLC from individual WT and skMLCK$^{-/-}$ mouse EDL muscle. **B)** RLC phosphate content in mouse EDL at rest (open bars) and after stimulation (black bars). Muscles were frozen in liquid nitrogen immediately after the CS or after 15 minutes of quiescence. Values are presented as mean and ± SEM (n = 4). ‡ Indicates significant difference from all other conditions.

4.4 Viability of muscle preparations

4.4.1 Assessment of Tetanic Force

Isometric tetanic force (P_o) was measured during successive conditioning stimuli (CS) to provide information about the viability of the muscle preparation for each muscle (n = 10). The WT force from the first tetanus of the CS was altered by only 2% between the first and last protocol (218.55 ± 22.41 to 220.55 ± 21.51 mN, respectively) and changed by only 5% in skMLCK$^{-/-}$ muscles (184.28 ± 14.44 to 192.57 ± 11.94 mN, respectively). These results indicate that the muscle preparations had not significantly fatigued or been damaged by previous stimulation, as proposed by Barclay, (2005).

DISCUSSION

5.1 General Discussion

The purpose of the current study was to determine the contribution of RLC phosphorylation on peak power of mouse EDL muscle. This was accomplished by comparing the mechanical output of WT and skMLCK$^{-/-}$ muscles, at rest and after tetanic stimulation, over a wide range of shortening velocities (0.05-0.65 V_{max}). Our secondary purpose was to investigate whether stimulation induced increases in RLC phosphorylation would positively impact the force-velocity properties of WT-EDL muscles, effectively increasing the velocity at which peak power occurs.

The skMLCK gene knockout provides a negative control to WT muscles since it does not display any stimulation induced RLC phosphorylation (Zhi et al., 2005; Gittings et al., 2011; 2014) Therefore, the contribution of RLC phosphorylation to force, work and power can be parsed out by subtracting post-CS skMLCK$^{-/-}$ values from that of post-CS

WT values, leaving the force contribution attributable to RLC phosphorylation. The proposed mechanism for phosphorylation mediated force potentiation is covalent binding of a negatively charged phosphate moiety to the RLC of myosin which propels the myosin head away from the thick filament backbone and towards actin (Alamo et al., 2008; Brito et al., 2011; Padron et al., 1991). The closer proximity of myosin to actin increases the rate of crossbridge attachment (f_{app}) leading to an increased fraction of cycling crossbridges in the strongly bound force generating state (aFS) at any given time (Brenner et al., 1988; Sweeney & Stull, 1990). Similar to Ca^{2+} regulated activation of the thin filament, RLC phosphorylation does not alter the rate of transition of crossbridges out of the force generating state (g_{app}). With this in mind, we assumed structural changes to the RLC, resulting from the CS, were the cause of the enhanced force, work and power of WT muscles over skMLCK$^{-/-}$.

5.2 RLC Phosphorylation

The experimental design was consistent with previous work from our lab that utilized a high frequency (100 Hz for 400ms) tetanic conditioning stimulus (CS) repeated four times within 10 s to enhance RLC phosphorylation (Gittings et al., 2012; Caterini et al., 2011). In the present study, the CS increased concentric force of WT muscles in all conditions concurrent with an almost 8 fold increase in phosphorylation above resting levels (0.08 and 0.63 mol Phos/mol RLC, respectively). In skMLCK$^{-/-}$ muscles, no difference was evident between rest and after activation by the CS (0.03 and 0.08 mol Phos/mol RLC, respectively). These results are in confirmation of the effects of stimulation in WT and skMLCK$^{-/-}$ muscles (Bunda et al., 2015; Gittings et al., 2011; 2012; Zhi et al., 2005), however, our results display lower skMLCK$^{-/-}$ resting values for

phosphorylation than those reported above. For example, work by Gittings et al. (2012) in our lab reported no change in values (8-8) mol Phos/mol RLC for resting and stimulated conditions in skMLCK$^{-/-}$ muscles, respectively. These differences may suggest a discrepancy in our sample preparation of individual muscle homogenates, antibody incubation, or blot exposure time.

The residual phosphorylation levels in skMLCK$^{-/-}$ muscles have been suggested to be due to the activity of a non-specific kinase that does not change activity with stimulation (Zhi et al., 2005). Therefore, the concentric force potentiation observed in these mice indicates an alternate source of crossbridge formation i.e., increased myoplasmic [$Ca^{2+}_{resting}$], previously reported by Smith et al. (2013; 2014).

5.3 Shortening Speed Dependence

The potentiation of concentric force is known to be shortening speed dependent, such that potentiation increases with shortening speed (Abbate et al., 2000; Caterini et al., 2011; Gittings et al., 2012; Grange et al., 1998). The current study has extended this finding to include a shortening speed dependence of skMLCK$^{-/-}$ mice, a finding that is consistent with recent work within our lab (Gittings, Bunda, & Vandenboom, 2015: Abstract).

Contrary to results from Gittings et al. 2012, the present study observed the potentiation of concentric force at every shortening speed in WT muscles. Although the reason for this discrepancy is unknown, differences in experimental parameters such as shortening ramp length and activation duration may have contributed to this finding. In lieu of this, we agree with the findings of MacIntosh & Willis (2000) and the suggestion of Vandenboom et al. (2013) that stimulus duration may be a limiting factor for

determining the ability of potentiation to increase peak force. The rate of force development as showed in Table 2 +dF/d*t* shows an apparent increase in WT and skMLCK$^{-/-}$ muscles under all conditions.

A reduction in post-tetanic force at low speeds in skMLCK$^{-/-}$ but not WT muscles was observed, suggesting that RLC phosphorylation may mask the presence of fatigue caused by tetanic stimulation (Grange et al., 1998). However, at shortening speeds 0.20 V_{max} and above, remnant potentiation was still displayed in skMLCK$^{-/-}$ muscles; consistent with previous findings (Gittings et al., 2011; Gittings et al., 2014; Zhi et al., 2005) implying a secondary mechanism is present in these mice. This mechanism is believed to be the result of an increase in resting myoplasmic [Ca^{2+}] due to previous stimulation (Smith et al., 2013). Subsequently, Ca^{2+} buffers such as parvalbumin become saturated enabling a larger portion of free myoplasmic Ca^{2+} to bind Troponin C and increase force production (MacIntosh & Gardiner, 1989).

5.4 Crossbridge Kinetics

It is known that crossbridge kinetics can be altered by several negative (H^+, P_i, and pH) and positive (RLC-P, increased sarcomere lengths) effectors that determine the Ca^{2+} sensitivity of force generation (MacIntosh et al., 2003). Our results suggest that RLC phosphorylation acted as a positive contributor to Ca^{2+} sensitivity by increasing the rate of force development in WT muscles post-CS, which in turn enhanced the peak force of each submaximal contraction, with no distinguishable effect for shortening velocity. As figure 13 displays, similar to the observed effects of PTP on concentric force, the relative change in rate of force development was attenuated in skMLCK$^{-/-}$ (1.14) compared with WT muscles (1.25), when collapsed for shortening velocity. This

difference is consistent with previous work investigating skMLCK$^{-/-}$ mice (Gittings et al., 2011) as well as work examining the effects of RLC phosphorylation on crossbridge dynamics (Metzger et al., 1989; Sweeney & Stull, 1990; Sweeney et al., 1993). Moreover, increases in +dF/d*t* in mouse lumbricals, a fast muscle without RLC phosphorylation, suggests theses changes are not selective to RLC phosphorylation. Therefore, the finding that skMLCK$^{-/-}$ muscles had a smaller yet still increased rate of force development, and peak force post-CS, illustrates that these mechanisms may be additive and/ or complimentary to each other. Indeed, when assessed as a whole, potentiation seems to provide a balanced system that effectively optimizes muscle performance.

The kinetics of -dF/d*t* exhibited a more complex speed dependent effect on contractile measures than did +dF/d*t*. For instance, in both genotypes the relative rate of relaxation was increased above Pre-CS values during slow shortening velocities (0.05-0.20 V_{max}), reaching an almost 2 fold increase above Pre-CS at 0.20 V_{max} (1.90 ± 0.11 & 1.83 ± 0.12) in WT and skMLCK$^{-/-}$, respectively. -dF/d*t* then slowed substantially until 0.45 V_{max} where it was similar to resting values between 0.45-0.65 V_{max}, ($p > .05$). The results for WT may therefore be partly be explained by the findings of Patel et al. (1998) who suggested that RLC phosphorylation eliminates force-dependent effects of relaxation in permeabilized rabbit psoas fibers. Contrarily, however, we did not observe any decrease in -dF/d*t* between genotypes, a result consistent with more recent findings using whole intact skeletal muscle (Gittings et al., 2014). This further indicates that force potentiation resulting from phosphorylation independent mechanisms i.e., increased

myoplasmic [$Ca^{2+}_{resting}$], alter the mechanical output of the contractile unit similar to RLC phosphorylation.

5.5 Modulation of Peak Mechanical Function

We did not observe a significant rightward shift in optimal velocity for peak power. This may indicate a stimulus frequency threshold for this phenomenon. However, it is also important to note that this outcome may have resulted from our selection of experimental conditions, i.e., temperature, muscle, species, etc. For example, Abbate et al. (2000) observed that tetanic stimulation tended to cause a rightward shift in the velocity at which peak power occurred during brief high-frequency contractions. This suggests that modulation of peak power is not limited to an upward shift in power output; but rather, power may also peak at a higher shortening velocity when significant potentiation impacts force production. However, these experiments were conducted using rat gastrocnemius muscle (35^{o}C; at 80 Hz), and therefore, the effects of potentiation are subject to change (Vandenboom et al., 2013). Considering that potentiation decreases with increases in stimulation frequency (Brown & Loeb, 1998; MacIntosh et al., 2008), lower stimulation frequencies (< 100 Hz) may be necessary to induce the shift in velocity for the attainment of peak power. Nonetheless, the tetanic CS resulted in a substantial relative increase in power output across shortening velocities (1.28 and 1.12), in WT and skMLCK$^{-/-}$ muscles, respectively. Our results indicate that RLC phosphorylation is responsible for roughly half of the concentric potentiation of power output across a wide range of shortening velocities. Therefore, without the skMLCK enzyme, optimal muscle performance is impeded.

5.6 In Vivo Applications

A brief but intense warm up before exercise or sport, that activates fast-twitch muscle fibers, may be 'prepping' the body for inducing an optimal level of potentiation (Brown & Loeb, 1998). Furthermore, a prolongation of potentiation as a result of hormonal input from adrenaline may serve a role in the fight or flight response (Decostre, Gillis, & Gailly, 2000). The augmentation of peak power largely by phosphorylation of the RLC will surely add to this biochemical ensemble that seems to function to create optimal mechanical performance. As previously suggested by Grange et al. (1998) and Abatte et al. (2000) an increase in power output during potentiation may be advantageous for several reasons: 1) The muscle will yield greater work and power for a given level of neural activation 2) a mechanical or biochemical feedback loop that decreases motor unit firing rate may permit maintenance of work and power during sustained rapid movements; an effect that may reduce fatigue 3) fewer activating pulses needed for power output will consequently reduce the amount of Ca^{2+} needing to be sequestered by the SR, preserving ATP, and in turn preventing fatigue.

High frequency pulses (>80 Hz) followed by a train of lower frequency pulses e.g., 30 Hz has been previously shown to increase force, work and power of both isometric and concentric contractions (Abbate et al., 2002; Binder-Macleod & Kesar, 2005). Interestingly, the augmented force responses have been attributed to enhanced Ca^{2+} sensitivity and cooperativity irrespective of RLC phosphorylation content (Abbate et al., 2002). This may implicate the role of high frequency pulses at the onset of contraction for increasing transient performance, while the steady increase in RLC

phosphorylation over time may decrease the impact of fatigue (Gittings et al., 2011; Rassier & Macintosh, 2000).

Although our results led us to conclude that no increase in velocity was found for peak power, recent findings characterizing motor unit behavior in mouse LG muscles (lateral gastrocnemius) reveal that sedentary activation occurs within the range of 9-68 Hz (Ritter, Tresch, Heckman, Manuel, & Tysseling, 2014). During active movements it is assumed that fast-fatiguable motor units will be recruited at higher firing rates that may reach 100 Hz or higher. Therefore, our chosen activation frequency may rival the activation of fast-fastiguable motor units in vivo. With this in mind, we conclude that a rightward shift in the optimal velocity for peak power may be selective to experimental conditions that optimize potentiation; but that do not mimic realistic in vivo settings.

5.7 High Velocity for Peak Power

Mouse gait patterns are resoundingly similar to human patterns as they exhibit a walking phase, a trot/jog phase, and a gallop/run phase. The gallop is most relevant to potentiation since fast glycolytic fibres become increasingly important as speed increases during locomotion (Armstrong et al., 1977). Galloping requires muscles to shorten over a longer distance causing the muscle to shorten faster in order to provide smooth rhythmic motion. Consistent with this, The EDL has been shown to shorten between 0.37-0.52 V_{max} during the gallop phase of locomotion (James, 1995). Thus, peak power output at shortening velocities of ~ 0.50-0.55 V_{max}, as observed in our study using curve fitting, may represent the physiological peak of mechanical functioning during shortening in vivo. Although original power calculations based on the Hill model indicated power to fall around 0.30 V_{max} or 0.30 F_{max}, the model also assumed muscles would naturally

operate at an optimal power that corresponded to operating frequency (Hz) i.e., 30 Hz at 0.30 V_{max}. As pointed out by Josephson, (1993) some muscles may operate at a lower or higher percentage of force and velocity depending on their internal characteristics and roles within the body. As such, a muscle such as the EDL with a high content of fast-fatigable (2b) fibers will undoubtedly have a higher peak power output.

Several experimental parameters may have also lead to the culmination of a very rapid V/V_{max} value for peak power. For example, the shortening ramp employed was used to replicate mouse locomotion by minimizing the amplitude of length change of the EDL i.e., 1.05-0.90 L_o (Marsh, 1999). This also deterred changes in the passive elements from altering force and augmenting potentiation (Abbate et al., 2002); however, the use of small length changes may have contributed to the muscles ability to maintain high power output at high speeds. In addition to this, using two pulses for each shortening ramp may have elevated peak power output since fast shortening (0.45-0.65 V_{max}) resulted in force production across the entire shortening ramp; unlike slow shortening (0.05-0.035 V_{max}), where force production had ceased long before shortening had finished. We therefore speculate that length dependent increases in potentiation augmented fast speeds of shortening at the shortest relative muscle lengths (0.95-0.90 L_o) or increased cooperative interactions may have assisted crossbridge binding (Dickenson et al., 1997). Furthermore, the potentiation of force may have been enhanced during fast shortening by sensitizing the contractile apparatus to RLC phosphorylation, via thin filament deactivation, or increases in G_{app} (ADP detachment) at high percentages of V_{max} (Gittings et al., 2012; Piazessi et al., 2007; Stull et al., 2011).

Altogether, any effects that may normally impair force transmission: shortening deactivation, sarcomeric uniformities etc., are less likely to alter force production under these force-enhancing conditions.

5.8 Reductions in Power With Aging

Age related differences in force and velocity properties exist between adult and elderly mouse EDL muscles. These differences are most notably observed by a reduction in power output in elderly mice (Brooks & Faulkner, 1988a, b; 1991). More recent work (Graber et al., 2015) has expanded this finding by observing a reduction in time to peak tension, power output and peak contractile velocity during shortening, coincident with a 21 % decline in the fast-isoform of RLC (MLC3f) in elderly EDL muscles. Interestingly, these aged muscles displayed a downward and leftward shift in the force-velocity curve. This effect is the opposite of what we hypothesized would occur in young adult mice within the current study and would suggest a reduction in MLC3f and type 2b fiber content causes power loss and declining muscle performance with aging. As previously mentioned, there may be a frequency threshold for rightward shifts in force-velocity properties; however, consistent with previous studies (Abbate et al., 2000; Grange et al., 1995; 1998) we did observe an upward shift in power output during potentiation.

Similar deleterious effects in power output are seen in patients with statin myalgia whom display an increased time to peak tension and blunting of power output during exercise (Mallinson et al., 2015). Further examination of the link between RLC phosphorylation, power output, and aging may elucidate its role in the prevention of power loss and muscle weakening associated with sarcopenia and other diseases. Moreover, resistance training programs for older adults may need to include power

movements at high-load to deter the loss of type 2 motor units and underlying changes to skeletal muscle isoforms e.g. RLC3f.

5.9 Significance

The enhancement of power output across an array of physiological shortening speeds, as observed in our study, may result in several benefits for locomotion. For a muscle such as the EDL that is activated, and under strain, largely while the lower limb is in flight, potentiation may positively impact shortening velocity. For example, when running speed increases, the limbs must increase stride length, therefore, shortening velocity must increase while maintaining power output.

Our results show that when power output is collapsed across shortening velocities, the presence of RLC phosphorylation in muscles stimulated with a tetanus (WT), increases power output to 1.28 ± 0.05 compared with 1.11 ± 0.05 in stimulated muscles absent of stimulation induced RLC phosphorylation ($skMLCK^{-/-}$). By comparing these values our study was able to demonstrate that RLC phosphorylation contributed 60 % of the overall effect of PTP on power output. With this in mind, modeling of locomotion should be careful to interpret data of both un-stimulated and stimulated skeletal muscles. Adopting both resting and activated fast-twitch skeletal muscle models to describe the force-velocity relationship will better represent the functional properties of skeletal muscles *in vivo*. The force-velocity properties of skeletal muscles under resting conditions dictates that the force per crossbridge during fast shortening will decrease due to more rapid ADP release, leading to faster cycling as the myosin motor translates force into filament sliding (Piazessi et al., 2007). However, when fast fibers are activated, RLC

phosphorylation, as well as stimulation induced alterations to myoplasmic [$Ca^{2+}_{resting}$], may deter force loss by increasing the attachment rate of cycling crossbridges (F_{app}) (Sweeney & Stull, 1990). Perhaps the most convincing statement supporting the need for this change is that of Brown and Loeb, (1998): "Potentiation may be the working state of fast-twitch skeletal muscle". In sum, without potentiation, and without signaling to trigger RLC phosphorylation, muscle performance and movement is diminished.

5.10 Limitations

The stimulation paradigm used in our study was intended to simulate brief high frequency contractile events previously reported to occur at the onset of locomotion (Binder-Macleod & Kesar, 2005; Garland & Griffin, 1999; Henig & Lomo, 1985). Although we hypothesized this form of activation is physiologically relevant, especially in regards to the EDL muscle, a longer train of lower frequency stimulation may have been more effective in attaining high levels of potentiation and mimicking sustained locomotor movements. However, it should be noted that the purpose of this study was to examine a brief near maximal stimulus/ contraction paradigm to determine peak power; long duration, repeated contractions would have increased fatigue and masked the contribution of potentiation to power output.

The range of shortening velocities used proved to be insufficient in creating adequate power velocity curves for the assessment of peak power. Higher shortening velocities may be needed to achieve a better understanding of modulations to force and velocity properties after repetitive stimulation.

5.11 Summary

Our results were consistent with previous work demonstrating potentiation in the range of what is considered to be physiologically applicable to 'in vivo' stimulation frequencies and length/ speed changes (Abbate et al. 2000; Gittings et al. 2012; MacIntosh, Taub, Dormer, & Tomaras, 2008; MacIntosh & Bryan, 2002). The increases in work and power can be attributed to an increased rate of crossbridge attachment (f_{app}) and changes in kinetics such as the increased +dF/dt. After collapsing across shortening velocities tetanic stimulation elevated concentric force in skMLCK$^{-/-}$ mice to 1.11 ± 0.05 compared with 1.28 ± 0.05 in WT muscles. The present results thus confirm the genotype dependence (Gittings et al., 2014) of concentric force potentiation. By subtracting skMLCK$^{-/-}$ values from WT the portion of power enhancement credited to RLC phosphorylation compared with phosphorylation-independent potentiation was found to be ~61 % across velocities and ~41 % for peak power. This implicates RLC phosphorylation as a major contributor to enhanced power after stimulation. The finding of a high optimal velocity for peak power (~0.50-0.55 V_{max}) in EDL suggests that muscle fiber type composition, as well as the role of the muscle within the body, may lead to different relative peak powers than expected by the Hill equation.

The reduction in force as velocity of shortening increases occurs due to rapid dissociation of myosin from actin, an effect that reduces the population of attached crossbridges. The reduced number of strongly bound crossbridges in turn is associated with reduced Ca^{2+} occupancy of TnC (Vandenboom, Claflin, & Julian, 1998). However, RLC phosphorylation minimizes reductions in crossbridge attachment, displaying the

largest effect during rapid shortening (0.45-0.65 V_{max}) when thin filament activation is low.

5.12 Future directions

The current study did not observe a rightward shift in velocity for the attainment of peak power. More research is needed to examine the effects of low activation frequencies on peak power of skeletal muscle. This is supported by larger increases in potentiation seen at lower compared with higher frequencies (Gittings et al., 2012). Furthermore, a more pronounced deviation in contractile kinetics may emerge between genotypes, at lower frequencies, creating a shift in peak power.

Treadmill gait analysis in rodent models may illuminate locomotor limitations to the skMLCK gene ablation *in vivo*. Previous investigations have already greatly enhanced the ability to infer changes in gait parameters during walking, trotting, and galloping rats and mice (Clarke & Still, 1999; 2001; Herbin, Hackert, Gasc, & Renous, 2007). Thus, comparison of WT with skMLCK$^{-/-}$ mice will determine if any overt physical differences in performance exist stemming from RLC phosphorylation.

References

Abbate, F., Sargeant, A. J., Verdijk, P. W. L., & De Haan, A. (2000). Effects of high-frequency initial pulses and posttetanic potentiation on power output of skeletal muscle. *Journal of Applied Physiology*, *88*(1), 35-40.

Abbate, F., Van Der Velden, J., Stienen, G. J. M., & De Haan, A. (2001). Post-tetanic potentiation increases energy cost to a higher extent than work in rat fast skeletal muscle. *Journal of Muscle Research & Cell Motility*, *22*(8), 703-710.

Abbate, F., Bruton, J. D., De Haan, A., & Westerblad, H. (2002). Prolonged force increase following a high-frequency burst is not due to a sustained elevation of [Ca2+] i. *American Journal of Physiology-Cell Physiology*, *283*(1), C42-C47.

Alamo, L., Wriggers, W., Pinto, A., Bártoli, F., Salazar, L., Zhao, F. Q., ... & Padrón, R. (2008). Three-dimensional reconstruction of tarantula myosin filaments suggests how phosphorylation may regulate myosin activity. *Journal of Molecular Biology*, *384*(4), 780-797.

Allen, D. G., Lamb, G. D., & Westerblad, H. (2008). Skeletal muscle fatigue: cellular mechanisms. *Physiological Reviews*, *88*(1), 287-332.

Askew, G. N., & Marsh, R. L. (1997). The effects of length trajectory on the mechanical power output of mouse skeletal muscles. *Journal of Experimental Biology*, *200*(24), 3119-3131.

Azizi, E. (2014). Locomotor function shapes the passive mechanical properties and operating lengths of muscle. *Proceedings of the Royal Society of London B: Biological Sciences*, *281*(1783), 20132914.

Baldwin, K. M. (1996). Effect of spaceflight on the functional, biochemical, and metabolic properties of skeletal muscle. *Medicine and Science in Sports and Exercise*, *28*(8), 983-987.

Bárány, M. (1967). ATPase activity of myosin correlated with speed of muscle shortening. *The Journal of General Physiology*, *50*(6), 197-218.

Barsotti, R. J., & Butler, T. M. (1984). Chemical energy usage and myosin light chain phosphorylation in mammalian skeletal muscle. *Journal of Muscle Research & Cell Motility*, *5*(1), 45-64.

Beam, K. G., & Bannister, R. A. (2010). Looking for answers to EC coupling's persistent questions. *The Journal of General Physiology*, *136*(1), 7-12.

Binder‐Macleod, S., & Kesar, T. (2005). Catchlike property of skeletal muscle: recent findings and clinical implications. *Muscle & Nerve*, *31*(6), 681-693.

Blumenthal, D. K., & Stull, J. T. (1980). Activation of skeletal muscle myosin light chain kinase by calcium (2+) and calmodulin. *Biochemistry*, *19*(24), 5608-5614.

Botelho, S. Y., & Cander, L. (1953). Post-tetanic potentiation before and during ischemia intact human skeletal muscle. *Journal of Applied Physiology*, *6*(4), 221.

Bottinelli, R., Canepari, M., Reggiani, C., & Stienen, G. J. (1994). Myofibrillar ATPase activity during isometric contraction and isomyosin composition in rat single skinned muscle fibres. *The Journal of Physiology*, *481*(Pt 3), 663-675.

Bozzo, C., Stevens, L., Toniolo, L., Mounier, Y., & Reggiani, C. (2003). Increased phosphorylation of myosin light chain associated with slow-to-fast transition in rat soleus. *American Journal of Physiology-Cell Physiology*, *285*(3), C575-C583.

Brenner, B. (1988). Effect of Ca^{2+} on cross-bridge turnover kinetics in skinned single rabbit psoas fibers: implications for regulation of muscle contraction. *Proceedings of the National Academy of Sciences*, *85*(9), 3265-3269.

Brenner, B. (1990) Muscle mechanics and biochemical kinetics. *Molecular Mechanisms in Muscular Contraction*, 77–149.

Brito, R., Alamo, L., Lundberg, U., Guerrero, J. R., Pinto, A., Sulbarán, G., ... & Padrón, R. (2011). A molecular model of phosphorylation-based activation and potentiation of tarantula muscle thick filaments. *Journal of Molecular Biology*, *414*(1), 44-61.

Brooks, S. V., & Faulkner, J. A. (1988). Contractile properties of skeletal muscles from young, adult and aged mice. *The Journal of Physiology*, *404*(1), 71-82.

Brooks, S. V., Faulkner, J. A., & McCubbrey, D. A. (1990). Power outputs of slow and fast skeletal muscles of mice. *The Journal of Applied Physiology*, *68*(3), 1282-1285.

Brooks, S. V., & Faulkner, J. A. (1991a). Forces and powers of slow and fast skeletal muscles in mice during repeated contractions. *The Journal of Physiology*, *436*(1), 701-710.

Brooks, S. V., & Faulkner, J. A. (1991b). Maximum and sustained power of extensor digitorum longus muscles from young, adult, and old mice. *Journal ofGgerontology*, *46*(1), B28-B33.

Brown, I. E., & Loeb, G. E. (1998). Post-activation potentiation—a clue for simplifying models of muscle dynamics. *American Zoologist*, *38*(4), 743-754.

Brown, I. E., & Loeb, G. E. (1999). Measured and modeled properties of mammalian skeletal muscle. I. The effects of post-activation potentiation on the time course and velocity dependencies of force production. *Journal of Muscle Research & Cell Motility*, *20*(5-6), 443-456.

Brown, W. E., Salmons, S., & Whalen, R. G. (1983). The sequential replacement of myosin subunit isoforms during muscle type transformation induced by long term electrical stimulation. *Journal of Biological Chemistry*, *258*(23), 14686-14692.

Bunda, J., Gittings, B., & Vandenboom, R. (2015). Shortening Speed Dependence of Concentric Force Potentiation in the Absence of Myosin Phosphorylation. Abstract retrieved from *The FASEB Journal*, *29*(1 Supplement), 947-25.

Buller, A. J., Kean, C. J. C., Ranatunga, K. W., & Smith, J. M. (1981). Post-tetanic depression of twitch tension in the cat soleus muscle. *Experimental Neurology*, *73*(1), 78-89.

Burke, R. E., Rudomin, P., & Zajac, F. E. (1976). The effect of activation history on tension production by individual muscle units. *Brain Research*, *109*(3), 515-529.

Butler, T. M., Siegman, M. J., Mooers, S. U., & Barsotti, R. J. (1983). Myosin light chain phosphorylation does not modulate cross-bridge cycling rate in mouse skeletal muscle. *Science*, *220*(4602), 1167-1169.

Caterini, D., Gittings, W., Huang, J., & Vandenboom, R. (2011). The effect of work cycle frequency on the potentiation of dynamic force in mouse fast twitch skeletal muscle. *The Journal of Experimental Biology*, *214*(23), 3915-3923.

Celichowski, J., Dobrzyńska, Z., Łochyński, D., & Krutki, P. (2011). The tetanic depression in fast motor units of mammalian skeletal muscle can be evoked by

lengthening of one initial interpulse interval. *Experimental Brain Research*, *214*(1), 19-26.

Childers, M. K., & McDonald, K. S. (2004). Regulatory light chain phosphorylation increases eccentric contraction–induced injury in skinned fast-twitch fibers. *Muscle & Nerve*, *29*(2), 313-317.

Chin, E. R., Olson, E. N., Richardson, J. A., Yang, Q., Humphries, C., Shelton, J. M., ... & Williams, R. S. (1998). A calcineurin-dependent transcriptional pathway controls skeletal muscle fiber type. *Genes & Development*, *12*(16), 2499-2509.

Chin, E. R. (2004). The role of calcium and calcium/calmodulin-dependent kinases in skeletal muscle plasticity and mitochondrial biogenesis. *Proceedings of The Nutrition Society*, *63*(02), 279-286.

Chin, E. R. (2005). Role of Ca2+/calmodulin-dependent kinases in skeletal muscle plasticity. *Journal of Applied Physiology*, *99*(2), 414-423.

Claflin, D. R., & Faulkner, J. A. (1985). Shortening velocity extrapolated to zero load and unloaded shortening velocity of whole rat skeletal muscle. *The Journal of Physiology*, *359*(1), 357-363.

Claflin, D. R., Morgan, D. L., & Julian, F. J. (1998). The effect of length on the relationship between tension and intracellular [Ca2+] in intact frog skeletal muscle fibres. *The Journal of Physiology*, *508*(1), 179-186.

Close, R., & Hoh, J. F. Y. (1968a). Influence of temperature on isometric contractions of rat skeletal muscles. *Nature, 217*, 1179-1180.

Close, R., & Hoh, J. F. Y. (1968b). The after-effects of repetitive stimulation on the isometric twitch contraction of rat fast skeletal muscle. *The Journal of Physiology*, *197*(2), 461-477.

Close, R., & Hoh, J. F. Y. (1969). Post-tetanic potentiation of twitch contractions of cross-innervated rat fast and slow muscles. *Nature, 221*, 179-181.

Costill, D. L., Daniels, J., Evans, W., Fink, W., Krahenbuhl, G., & Saltin, B. (1976). Skeletal muscle enzymes and fiber composition in male and female track athletes. *The Journal of Applied Physiology*, *40*(2), 149-154.

Craig, R., & Woodhead, J. L. (2006). Structure and function of myosin filaments. *Current Opinion in Structural Biology*, *16*(2), 204-212.

Crow, M. T., & Kushmerick, M. J. (1982a). Chemical energetics of slow-and fast-twitch muscles of the mouse. *The Journal of General Physiology*, *79*(1), 147-166.

Crow, M. T., & Kushmerick, M. J. (1982b). Myosin light chain phosphorylation is associated with a decrease in the energy cost for contraction in fast twitch mouse muscle. *Journal of Biological Chemistry*, *257*(5), 2121-2124.

Crow, M. T., & Kushmerick, M. J. (1982c). Phosphorylation of myosin light chains in mouse fast-twitch muscle associated with reduced actomyosin turnover rate. *Science*, *217*(4562), 835-837.

Davis, J. S., Satorius, C. L., & Epstein, N. D. (2002). Kinetic effects of myosin regulatory light chain phosphorylation on skeletal muscle contraction. *Biophysical Journal*, *83*(1), 359-370.

de Beer, E. D., Grundeman, R. L. F., Wilhelm, A. J., Van Den Berg, C., Caljouw, C. J., Klepper, D., & Schiereck, P. (1988). Effect of sarcomere length and filament

lattice spacing on force development in skinned cardiac and skeletal muscle preparations from the rabbit. *Basic Research in Cardiology*, *83*(4), 410-423.

De Haan, A., Jones, D. A., & Sargeant, A. J. (1989). Changes in velocity of shortening, power output and relaxation rate during fatigue of rat medial gastrocnemius muscle. *Pflügers Archiv*, *413*(4), 422-428.

Decostre, V., Gillis, J. M., & Gailly, P. (2000). Effect of adrenaline on the post-tetanic potentiation in mouse skeletal muscle. *Journal of Muscle Research & Cell Motility*, *21*(3), 247-254.

Dickinson, M. H., Hyatt, C. J., Lehmann, F. O., Moore, J. R., Reedy, M. C., Simcox, A., ... & Maughan, D. W. (1997). Phosphorylation-dependent power output of transgenic flies: an integrated study. *Biophysical Journal*, *73*(6), 3122-3134.

Dominguez, R., & Holmes, K. C. (2011). Actin structure and function. *Annual review of biophysics*, *40*, 169.

Dulhunty, A. F. (2006). Excitation–contraction coupling from the 1950s into the new millennium. *Clinical and Experimental Pharmacology and Physiology*, *33*(9), 763-772.

Endo, M. (1972). Stretch-induced increase in activation of skinned muscle fibres by calcium. *Nature*, *237*(76), 211-213.

Fox, J. G., Barthold, S. W., Davisson, M. T., Newcomer, C. E., Quimby, F. W., & Smith, A. L. (Eds.). (2006). The Mouse in Biomedical Research (2nd ed.). Toronto, ON: Elsevier Science.

Franzini-Armstrong, C., Ferguson, D. G., & Champ, C. (1988). Discrimination between fast- and slow-twitch fibres of guinea pig skeletal muscle using the relative surface density of junctional transverse tubule membrane. *Journal of Muscle Research & Cell Motility, 9*, 403-414.

Garland, S. J., & Griffin, L. (1999). Motor unit double discharges: statistical anomaly or functional entity?. *Canadian Journal of Applied Physiology*, *24*(2), 113-130.

Geeves, M. A., & Holmes, K. C. (1999). Structural mechanism of muscle contraction. *Annual review of biochemistry*, *68*(1), 687-728.

Gittings, W., Huang, J., Smith, I. C., Quadrilatero, J., & Vandenboom, R. (2011). The effect of skeletal myosin light chain kinase gene ablation on the fatigability of mouse fast muscle. *Journal of Muscle Research and Cell Motility*, *31*(5-6), 337-348.

Gittings, W., Huang, J., & Vandenboom, R. (2012). Tetanic force potentiation of mouse fast muscle is shortening speed dependent. *Journal of Muscle Research and Cell Motility*, *33*(5), 359-368.

Gittings, W., Aggarwal, H., Stull, J. T., & Vandenboom, R. (2014). The Force Dependence of Isometric and Concentric Potentiation in Mouse Muscle With and Without Skeletal Myosin Light Chain Kinase. *Canadian Journal of Physiology and Pharmacology*, (ja).

Gordon, A. M., Regnier, M., & Homsher, E. (2001). Skeletal and cardiac muscle contractile activation: tropomyosin "rocks and rolls". *Physiology*, *16*(2), 49-55.

Graber, T. G., Kim, J. H., Grange, R. W., McLoon, L. K., & Thompson, L. V. (2015). C57BL/6 life span study: age-related declines in muscle power production and contractile velocity. *Age*, *37*(3), 1-16.

Grange, R. W., Vandenboom, R., & Houston, M. E. (1993). Physiological significance of myosin phosphorylation in skeletal muscle. *Canadian Journal of Applied Physiology*, *18*(3), 229-242.

Grange, R. W., Cory, C. R., Vandenboom, R., & Houston, M. E. (1995). Myosin phosphorylation augments force-displacement and force-velocity relationships of mouse fast muscle. *American Journal of Physiology-Cell Physiology*, *269*(3), C713-C724.

Grange, R. W., Vandenboom, R., Xeni, J., & Houston, M. E. (1998). Potentiation of in vitro concentric work in mouse fast muscle. *Journal of Applied Physiology*, *84*(1), 236-243.

Hennig R, Lomo T. (1985). Firing patterns of motor units in normal rats. *Nature,* 314, 164–166.

Hennig, R., & Lømo, T. (1987). Gradation of force output in normal fast and slow muscles of the rat. *Acta Physiologica Scandinavica*, *130*(1), 133-142.

Hill, A. V. (1938). The heat of shortening and the dynamic constants of muscle. *Proceedings of the Royal Society of London. Series B, Biological Sciences*, *126*(843), 136-195.

Holt, N. C., Wakeling, J. M., & Biewener, A. A. (2014). The effect of fast and slow motor unit activation on whole-muscle mechanical performance: the size principle

may not pose a mechanical paradox. *Proceedings of the Royal Society B: Biological Sciences*, *281*(1783), 20140002.

Houston, M. E., & Grange, R. W. (1990). Myosin phosphorylation, twitch potentiation, and fatigue in human skeletal muscle. *Canadian Journal of Physiology and Pharmacology*, *68*(7), 908-913.

Huxley, A. F. (1974). Muscular contraction. *The Journal of Physiology*, *243*(1), 1.

Huxley, H., & Hanson, J. (1954). Changes in the cross-striations of muscle during contraction and stretch and their structural interpretation. *Nature*, *173*(4412), 973-976.

Huxley, A. F., & Niedergerke, R. (1954). Interference microscopy of living muscle fibres. *Nature*, *173*(1), 13.

Huxley, A. F., & Taylor, R. E. (1958). Local activation of striated muscle fibres. *The Journal of Physiology*, *144*(3), 426-441.

Inglis, J. G., Howard, J., McIntosh, K., Gabriel, D. A., & Vandenboom, R. (2011). Decreased motor unit discharge rate in the potentiated human tibialis anterior muscle. *Acta Physiologica*, *201*(4), 483-492.

James, R. S., Altringham, J. D., & Goldspink, D. F. (1995). The mechanical properties of fast and slow skeletal muscles of the mouse in relation to their locomotory function. *The Journal of Experimental Biology*, *198*(2), 491-502.

Josephson, R. K. (1985). Mechanical power output from striated muscle during cyclic contraction. *Journal of Experimental Biology*, *114*(1), 493-512.

Josephson, R. K. (1993). Contraction dynamics and power output of skeletal muscle. *Annual Review of Physiology*, *55*(1), 527-546.

Josephson, R. K. (1999). Dissecting muscle power output. *Journal of Experimental Biology*, *202*(23), 3369-3375.

Julian, F. J., & Moss, R. L. (1981). Effects of calcium and ionic strength on shortening velocity and tension development in frog skinned muscle fibres. *The Journal of Physiology*, *311*(1), 179-199.

Kabsch, W., Mannherz, H. G., Suck, D., Pai, E. F., & Holmes, K. C. (1990). Atomic structure of the actin: DNase I complex. *Nature*, *347*(6288), 37-44.

Kakol, I., Kasman, K., & Michnicka, M. (1982). The phosphorylation-dephosphorylation process as a myosin-linked regulation of superprecipitation of fast skeletal muscle actomyosin. *Biochimica et Biophysica Acta (BBA)-Protein Structure and Molecular Enzymology*, *704*(3), 437-443.

Kamm, K. E., & Stull, J. T. (2011). Signaling to myosin regulatory light chain in sarcomeres. *Journal of Biological Chemistry*, *286*(12), 9941-9947.

Krarup, C. (1981). Enhancement and diminution of mechanical tension evoked by staircase and by tetanus in rat muscle. *The Journal of Physiology*, *311*(1), 355-372.

Klug, G. A., Botterman, B. R., & Stull, J. T. (1982). The effect of low frequency stimulation on myosin light chain phosphorylation in skeletal muscle. *Journal of Biological Chemistry*, *257*(9), 4688-4690.

Krendel, M., & Mooseker, M. S. (2005). Myosins: Tails (and heads) of functional diversity. *Physiology-International Union of Physiological Sciences and The American Physiological Society*, *20*, 239-251.

Krueger, J. K., Padre, R. C., & Stull, J. T. (1995). Intrasteric regulation of myosin light chain kinase. *Journal of Biological Chemistry*, *270*(28), 16848-16853.

Lamb, G. D. (2000). Excitation-contraction coupling in skeletal muscle: Comparisons with cardiac muscle. *Clinical & Experimental Pharmacology & Physiology*, *27*(3), 216.

Lee, F. S. (1907). The cause of treppe. *American Journal of Physiology, 18*, 267-282.

Leeuw, T., & Pette, D. (1993). Coordinate changes in the expression of troponin subunit and myosin heavy-chain isoforms during fast-to-slow transition of low-frequency-stimulated rabbit muscle. *European Journal of Biochemistry*, *213*(3), 1039-1046.

Levine, R. J., Kensler, R. W., Yang, Z., Stull, J. T., & Sweeney, H. L. (1996). Myosin light chain phosphorylation affects the structure of rabbit skeletal muscle thick filaments. *Biophysical Journal*, *71*(2), 898-907.

Levine, R. J., Yang, Z., Epstein, N. D., Fananapazir, L., Stull, J. T., & Sweeney, H. L. (1998). Structural and functional responses of mammalian thick filaments to alterations in myosin regulatory light chains. *Journal of Structural Biology*, *122*(1), 149-161.

Lieber, R. L. (1997). Muscle fiber length and moment arm coordination during dorsi-and plantarflexion in the mouse hindlimb. *Cells Tissues Organs*, *159*(2-3), 84-89.

Lin, J., Wu, H., Tarr, P. T., Zhang, C. Y., Wu, Z., Boss, O., ... & Spiegelman, B. M. (2002). Transcriptional co-activator PGC-1α drives the formation of slow-twitch muscle fibres. *Nature*, *418*(6899), 797-801.

Llinas, P., Pylypenko, O., Isabet, T., Mukherjea, M., Sweeney, H. L., & Houdusse, A. M. (2012). How myosin motors power cellular functions–an exciting journey from structure to function. *FEBS Journal*, *279*(4), 551-562.

MacIntosh, B. R., & Bryan, S. N. (2002). Potentiation of shortening and velocity of shortening during repeated isotonic tetanic contractions in mammalian skeletal muscle. *Pflügers Archiv*, *443*(5-6), 804-812.

MacIntosh, B. R., & Gardiner, P. F. (1987). Posttetanic potentiation and skeletal muscle fatigue: interactions with caffeine. *Canadian Journal of Physiology and Pharmacology*, *65*(2), 260-268.

MacIntosh, B. R., Taub, E. C., Dormer, G. N., & Tomaras, E. K. (2008). Potentiation of isometric and isotonic contractions during high-frequency stimulation. *Pflügers Archiv-European Journal of Physiology*, *456*(2), 449-458.

MacIntosh, B. R., Holash, R. J., & Renaud, J. M. (2012). Skeletal muscle fatigue–regulation of excitation–contraction coupling to avoid metabolic catastrophe. *Journal of Cell Science*, *125*(9), 2105-2114.

Mallinson, J. E., Marimuthu, K., Murton, A., Selby, A., Smith, K., Constantin‐Teodosiu, D., ... & Greenhaff, P. L. (2015). Statin myalgia is not associated with reduced muscle strength, mass or protein turnover in older male volunteers, but is allied with a slowing of time to peak power output, insulin resistance and differential muscle mRNA expression. *The Journal of Physiology*, *593*(5), 1239-1257.

Manning, D. R., & Stull, J. T. (1982). Myosin light chain phosphorylation-dephosphorylation in mammalian skeletal muscle. *American Journal of Physiology-Cell Physiology*, *242*(3), C234-C241.

Marsh, R. L. (1999). How muscles deal with real-world loads: the influence of length trajectory on muscle performance. *Journal of Experimental Biology*, *202*(23), 3377-3385.

McCully, K. K., & Faulkner, J. A. (1985). Injury to skeletal muscle fibers of mice following lengthening contractions. *Journal of Applied Physiology*, *59*(1), 119-126.

McKillop, D. F., & Geeves, M. A. (1993). Regulation of the interaction between actin and myosin subfragment 1: evidence for three states of the thin filament. *Biophysical Journal*, *65*(2), 693-701.

Mendell, L. M. (2005). The size principle: a rule describing the recruitment of motoneurons. *Journal of Neurophysiology*, *93*(6), 3024-3026.

Mendez, J., & Keys, A. (1960). Density and composition of mammalian muscle. *Metabolism-Clinical and Experimental*, *9*(2), 184-188.

Metzger, J. M., Greaser, M. L., & Moss, R. L. (1989). Variations in cross-bridge attachment rate and tension with phosphorylation of myosin in mammalian skinned skeletal muscle fibers. Implications for twitch potentiation in intact muscle. *The Journal of General Physiology*, *93*(5), 855-883.

Moore, R. L., & Stull, J. T. (1984). Myosin light chain phosphorylation in fast and slow skeletal muscles in situ. *American Journal of Physiology-Cell Physiology*, *247*(5), C462-C471.

Moore, R. L., Palmer, B. M., Williams, S. L., Tanabe, H., Grange, R. W., & Houston, M. E. (1990). Effect of temperature on myosin phosphorylation in mouse skeletal muscle. *American Journal of Physiology-Cell Physiology*, *259*(3), C432-C438.

Morgan, M., Perry, S. V., & Ottaway, J. (1976). Myosin light-chain phosphatase. *The Journal of Biochemistry*, *157*, 687-697.

Moss, R. L. (1982). The effect of calcium on the maximum velocity of shortening in skinned skeletal muscle fibres of the rabbit. *Journal of Muscle Research & Cell Motility*, *3*(3), 295-311.

Moss, R. L., Diffee, G. M., & Greaser, M. L. (1995). Contractile properties of skeletal muscle fibers in relation to myofibrillar protein isoforms. In *Reviews of Physiology, Biochemistry and Pharmacology, Volume 126* (pp. 1-63). Springer Berlin Heidelberg.

Nyitrai, M., & Geeves, M. A. (2004). Adenosine diphosphate and strain sensitivity in myosin motors. *Philosophical Transactions of the Royal Society-Ser B-Biological Sciences*, *359*(1452), 1867-1878.

Padre, R. C., & Stull, J. T. (2000a). Conformational requirements for Ca^{2+} calmodulin binding and activation of myosin light chain kinase. *FEBS letters*, *472*(1), 148-152.

Padre, R. C., & Stull, J. T. (2000b). Functional assembly of fragments from bisected smooth muscle myosin light chain kinase. *Journal of Biological Chemistry*, *275*(35), 26665-26673.

Palmer, B. M., & Moore, R. L. (1989). Myosin light chain phosphorylation and tension potentiation in mouse skeletal muscle. *American Journal of Physiology-Cell Physiology*, *257*(5), C1012-C1019.

Pemrick, S. M. (1980). The phosphorylated L2 light chain of skeletal myosin is a modifier of the actomyosin ATPase. *Journal of Biological Chemistry*, *255*(18), 8836-8841.

Perrie, W. T., Smillie, L. B., & Perry, S. V. (1973). A phosphorylated light-chain component of myosin from skeletal muscle. *The Journal of Biochemstry*, *135*, 151-164.

Persechini, A., Stull, J. T., & Cooke, R. (1985). The effect of myosin phosphorylation on the contractile properties of skinned rabbit skeletal muscle fibers. *Journal of Biological Chemistry*, *260*(13), 7951-7954.

Person, R. S., & Kudina, L. P. (1972). Discharge frequency and discharge pattern of human motor units during voluntary contraction of muscle. *Electroencephalography and Clinical Neurophysiology*, *32*(5), 471-483.

Pette, D. (2001). Historical perspectives: plasticity of mammalian skeletal muscle. *Journal of Applied Physiology*, *90*(3), 1119-1124.

Pette, D., & Staron, R. S. (1990). *Cellular and molecular diversities of mammalian skeletal muscle fibers* (pp. 1-76). Heidelberg, Berlin: Springer.

Piazzesi, G., Reconditi, M., Linari, M., Lucii, L., Bianco, P., Brunello, E., ... & Lombardi, V. (2007). Skeletal muscle performance determined by modulation of number of myosin motors rather than motor force or stroke size. *Cell*, *131*(4), 784-795.

Ramsey, R. W., & Street, S. F. (1941). Muscle function as studied in single muscle fibres. *Biological Symposium* (Vol. 3, pp. 9-34).

Offer, G., & Ranatunga, K. W. (2013). A cross-bridge cycle with two tension-generating steps simulates skeletal muscle mechanics. *Biophysical Journal*, *105*(4), 928-940.

Rassier, D. E., & Macintosh, B. R. (2000). Coexistence of potentiation and fatigue in skeletal muscle. *Brazilian Journal of Medical and Biological Research*, *33*(5), 499-508.

Rassier, D. E., & MacIntosh, B. R. (2002). Sarcomere length-dependence of activity-dependent twitch potentiation in mouse skeletal muscle. *BMC Physiology*, *2*(1), 19.

Rayment, I., Smith, C., & Yount, R. G. (1996). The active site of myosin. *Annual Review of Physiology*, *58*(1), 671-702.

Rayment, I., Holden, H. M., Whittaker, M., Yohn, C. B., Lorenz, M., Holmes, K. C., & Milligan, R. A. (1993a). Structure of the actin-myosin complex and its implications for muscle contraction. *Science*, *261*(5117), 58-65.

Rayment, I., Rypniewski, W. R., Schmidt-Base, K., Smith, R., Tomchick, D. R., Benning, M. M., ... & Holden, H. M. (1993b). Three-dimensional structure of myosin subfragment-1: a molecular motor. *Science*, *261*(5117), 50-58.

Rebbeck, R. T., Karunasekara, Y., Board, P. G., Beard, N. A., Casarotto, M. G., & Dulhunty, A. F. (2014). Skeletal muscle excitation–contraction coupling: Who are the dancing partners?. *The International Journal of Biochemistry & Cell Biology*, *48*, 28-38.

Ritter, L. K., Tresch, M. C., Heckman, C. J., Manuel, M., & Tysseling, V. M. (2014). Characterization of motor units in behaving adult mice shows a wide primary range. *Journal of Neurophysiology*, *112*(3), 543–551.

Rome, L. C., & Alexander, R. M. (1990). The influence of temperature on muscle velocity and sustained performance in swimming carp. *Journal of Experimental Biology*, *154*(1), 163-178.

Rome, L. C., & Swank, D. (1992a). The influence of temperature on power output of scup red muscle during cyclical length changes. *Journal of Experimental Biology*, *171*(1), 261-281.

Rome, L. C. (1992b). Scaling of muscle fibres and locomotion. *Journal of Experimental Biology*, *168*(1), 243-252.

Rome, L. C., Cook, C., Syme, D. A., Connaughton, M. A., Ashley-Ross, M., Klimov, A., ... & Goldman, Y. E. (1999). Trading force for speed: why superfast crossbridge kinetics leads to superlow forces. *Proceedings of the National Academy of Sciences*, *96*(10), 5826-5831.

Ryder, J. W., Lau, K. S., Kamm, K. E., & Stull, J. T. (2007). Enhanced skeletal muscle contraction with myosin light chain phosphorylation by a calmodulin-sensing kinase. *Journal of Biological Chemistry*, *282*(28), 20447-20454.

Schiaffino, S., & Reggiani, C. (1994). Myosin isoforms in mammalian skeletal muscle. *Journal of Applied Physiology*, *77*(2), 493-501.

Schneider, M. F., & Chandler, W. K. (1973). Voltage dependent charge movement in skeletal muscle: a possible step in excitation–contraction coupling.

Segal, S. S., & Faulkner, J. A. (1985). Temperature-dependent physiological stability of rat skeletal muscle in vitro. *American Journal of Physiology-Cell Physiology*, *248*(3), C265-C270.

Seow, C. Y. (2013). Hill's equation of muscle performance and its hidden insight on molecular mechanisms. *The Journal of General Physiology*, *142*(6), 561-573.

Smith, I. C., Gittings, W., Huang, J., McMillan, E. M., Quadrilatero, J., Tupling, A., & Vandenboom, R. (2013). Potentiation in mouse lumbrical muscle without myosin light chain phosphorylation: Is resting calcium responsible?. *Journal Of General Physiology*, *141*(3), 297-308.

Smith, I. C., Vandenboom, R., & Tupling, A. R. (2014). Juxtaposition of the changes in intracellular calcium and force during staircase potentiation at 30 and 37° C. *The Journal of General Physiology*, *144*(6), 561-570.

Standaert, F. G. (1964). The mechanisms of post-tetanic potentiation in cat soleus and gastrocnemius muscles. *The Journal of General Physiology*, *47*(5), 987-1001.

Staron, R, S., Gohlsch, B., & Pette, D. (1987). Myosin polymorphism in single fibers of chronically stimulated rabbit fast-twitch muscle. *Pflügers Archiv*, *408*(5), 444-450.

Stull, J. T., Kamm, K. E., & Vandenboom, R. (2011). Myosin light chain kinase and the role of myosin light chain phosphorylation in skeletal muscle. *Archives of Biochemistry and Biophysics*, *510*(2), 120-128.

Sweeney, H. L., Yang, Z., Zhi, G., Stull, J. T., & Trybus, K. M. (1994). Charge replacement near the phosphorylatable serine of the myosin regulatory light chain mimics aspects of phosphorylation. *Proceedings of the National Academy of Sciences*, *91*(4), 1490-1494.

Sweeney, H. L. (1995). Function of the N terminus of the myosin essential light chain of vertebrate striated muscle. *Biophysical Journal*, *68*(4), 112-118.

Sweeney, H. L., & Houdusse, A. (2010). Structural and functional insights into the myosin motor mechanism. *Annual Review of Biophysics*, *39*, 539-557.

Sweeney, H. L., & Kushmerick, M. J. (1985). Myosin phosphorylation in permeabilized rabbit psoas fibers. *American Journal of Physiology-Cell Physiology*, *249*(3), C362-C365.

Sweeney, H. L., & Stull, J. T. (1986). Phosphorylation of myosin in permeabilized mammalian cardiac and skeletal muscle cells. *American Journal of Physiology-Cell Physiology*, *250*(4), C657-C660.

Sweeney, H. L., & Stull, J. T. (1990). Alteration of cross-bridge kinetics by myosin light chain phosphorylation in rabbit skeletal muscle: implications for regulation of actin-myosin interaction. *Proceedings of the National Academy of Sciences*, *87*(1), 414-418.

Ter Keurs, H. E. D. J., Luff, A. R., & Luff, S. E. (1984). Force—Sarcomere-Length Relation and Filament Length in Rat Extensor Digitorum Muscle. In *Contractile Mechanisms in Muscle* (pp. 511-525). Springer US.

Rassier, D. E., Tubman, L. A., & MacIntosh, B. R. (1997). Length-dependent potentiation and myosin light chain phosphorylation in rat gastrocnemius muscle. *American Journal of Physiology-Cell Physiology*, *273*(1), C198-C204.

Uyeda, T., Abramson, P. D., & Spudich, J. A. (1996). The neck region of the myosin motor domain acts as a lever arm to generate movement. *Proceedings of the National Academy of Sciences*, *93*(9), 4459-4464.

Vandenboom, R., Grange, R. W., & Houston, M. E. (1993). Threshold for force potentiation associated with skeletal myosin phosphorylation. *American Journal of Physiology-Cell Physiology*, *265*(6), C1456-C1462.

Vandenboom, R., Grange, R. W., & Houston, M. E. (1995). Myosin phosphorylation enhances rate of force development in fast-twitch skeletal muscle. *American Journal of Physiology-Cell Physiology*, *268*(3), C596-C603.

Vandenboom, R. (2004). The myofibrillar complex and fatigue: a review. *Canadian Journal of Applied Physiology*, *29*(3), 330-356.

Vandenboom, R., Gittings, W., Smith, I. C., Grange, R. W., & Stull, J. T. (2013). Myosin phosphorylation and force potentiation in skeletal muscle: evidence from animal models. *Journal of Muscle Research and Cell Motility*, *34*(5-6), 317-332.

Vandenboom, R., Xeni, J., Bestic, N. M., & Houston, M. E. (1997). Increased force development rates of fatigued mouse skeletal muscle are graded to myosin light chain phosphate content. *American Journal of Physiology-Regulatory, Integrative and Comparative Physiology*, *272*(6), R1980-R1984.

Vandervoort, A. A., Quinlan, J., & McComas, A. J. (1983). Twitch potentiation after voluntary contraction. *Experimental Neurology*, *81*(1), 141-152.

Vrbova, G. (1966). Factors determining speed of contraction of striated muscle. *Journal of Physiology (London), 185*(1), 17.

Westerblad, H., Bruton, J. D., & Katz, A. (2010). Skeletal muscle: energy metabolism, fiber types, fatigue and adaptability. *Experimental Cell Research*, *316*(18), 3093-3099.

Westerblad, H., Lee, J. A., Lannergren, J., & Allen, D. G. (1991). Cellular mechanisms of fatigue in skeletal muscle. *American Journal of Physiology-Cell Physiology*, *261*(2), C195-C209.

Wu, H., Kanatous, S. B., Thurmond, F. A., Gallardo, T., Isotani, E., Bassel-Duby, R., & Williams, R. S. (2002). Regulation of mitochondrial biogenesis in skeletal muscle by CaMK. *Science*, *296*(5566), 349-352.

Xeni, J., Gittings, W. B., Caterini, D., Huang, J., Houston, M. E., Grange, R. W., & Vandenboom, R. (2011). Myosin light-chain phosphorylation and potentiation of dynamic function in mouse fast muscle. *European Journal of Physiology*, *462*(2), 349-358.

Yang, Z., Stull, J. T., Levine, R. J., & Sweeney, H. L. (1998). Changes in interfilament spacing mimic the effects of myosin regulatory light chain phosphorylation in rabbit psoas fibers. *Journal of Structural Biology*, *122*(1), 139-148.

Zhi, G., Ryder, J. W., Huang, J., Ding, P., Chen, Y., Zhao, Y., ... & Stull, J. T. (2005). Myosin light chain kinase and myosin phosphorylation effect frequency-dependent potentiation of skeletal muscle contraction. *Proceedings of the National Academy of Sciences of the United States of America*, *102*(48), 17519-17524.

Appendix A: Compilation of Studies Examining Potentiation

Table 9. Experimental data of potentiation in whole-isolated skeletal muscle of various animal models (Vandenboom et al., 2013).

Authors	Species	Muscle	Temp	Rate and duration	Main findings
Abbate et al. (2000)	Rat	MG	34	160 Hz, 1 s	Concentric power ↑ at 80–120 Hz
Bagust et al. (1974)	Cat	FDL, sol	NR	100 Hz, 300 ms	PTP ↓ as time to peak tension ↑
Brown and Loeb (1998)	Cat	CF	37	Various high freq	Pt:Po ↑ five fold
Brown and Loeb (1999)	Cat	CF	37	Various high freq	PTP ↓ as muscle length ↑
Brown and von Euler (1938)	Cat	Gastroc, sol, TA	37	High frequency, 2–20 s	Stimulus duration dependence for PTP
Buller et al. (1981)	Cat	Sol	37	100 Hz, 300–1,000 ms	↓ Pt:Po with ↑ stim number
Close and Hoh (1968a)	Rat	EDL, sol	20–35	Repetitive stimulation	EDL, PTP ↑ with temp; sol, no PTP
Close and Hoh (1968b)	Rat	EDL	35	20 and 300 Hz; various	PTP varies with pulse # at each frequency
Close and Hoh (1969)	Rat	EDL, sol	35	200 Hz, 1 s	Cross-innervation: PTP ↑ sol, ↓ EDL
Grange et al. (1998)	Mouse	EDL	25	5 Hz, 20 s	Work loop area ↑ 25–30 % by PTP
Guttman et al. (1937)	Frog	Gastroc	NR	10–30 Hz, 1–20 s	PTP coexists with fatigue
Krarup (1981a)	Rat	EDL	37–38	2–5 Hz; 125–167 Hz	Biphasic effects of duration and stimuli #
Krarup (1981b)	Rat	EDL	20–38	5 Hz, 50 s	SP ↑ as temp ↑
Krarup (1981c)	Rat	EDL	37–38	5 Hz, 50 s; 167 Hz, 1.5 s	Dantrolene ↑ SP and PTP
Krarup (1983)	Rat	EDL	37–38	3–10 Hz, 1.5–3 s	Potentiation ↓ in myasthenia gravis
MacIntosh and Gardiner (1987)	Rat	Gastroc	37	200 Hz, 1 s	Fat x caff ↑ PTP additively
MacIntosh and Willis (2000)	Rat	Gastroc	37	2–5 pulses at 20–80 Hz	PTP ↓ as force approaches Po
MacIntosh et al. (1988)	Rat	Gastroc[a]	37	10 Hz, 15 s	TTX ↓ SP by ∼75 %
MacIntosh et al. (2008b)	Rat	Gastroc	37	200–400 Hz (2–4 pulses)	↑ Force, work and power at high frequencies
Ramsey and Street (1941)	Frog	Single fibers	22	Tetani 5–180 s	PTP ↑ at low P_t:P_o in isolated fibers
Rankin et al. (1988)	Rat	Sol, EDL	35–37	0.5 Hz 32 s; 100 Hz 500 ms	↑ Pot in ↓ fatigable EDL muscle
Rassier and MacIntosh (2002)	Mouse	EDL	22–35	10 Hz 10 s; 75 Hz 1.5 s	Pot ↓ long lengths at both temps
Rassier and MacIntosh (2000)	Rat	Gastroc	37	5 Hz, 20 s	Dant ↓ Pot but not length dependence
Rassier et al. (1998)	Rat	Gastroc	37	10 Hz, 10 s	Caff ↓ Pot and abolishes length dependence
Rassier and Herzog (2002)	Mouse	EDL	25	10 Hz, 10 s	↓ pH abolishes length dependence
Standaert (1964)	Cat	Sol, gastroc	37	400 Hz 10 s (s);200 Hz 10 s (g)	Fibre and motor unit dependence for PTP
Vergara et al. (1977)	Frog	Semitend	15	20 Hz, 5–200 s	Long lasting PTP with fatigue

Studies examining staircase or PTP in which RLC phosphorylation was not measured arranged alphabetically by first author. Columns (left to right) describe species, muscle(s) and experimental temperature (Temp) as well as the stimulation paradigm used to induce potentiation as frequency in Hz and duration (in ms or sec) with a summary of main findings

CF caudofemoris, *EDL* extensor digitorum longus, *FDL* flexor digitorum longus, *gastroc* gastrocnemius, *MG* medial gastrocnemius, *sol* soleus, *semitend* semitendinosus, *TA* tibialis anterior, *caff* caffeine, *Dant* dantrolene, *#* number, *Po* peak tetanic force, *Pt* peak twitch force, *pot* potentiation, *SP* staircase potentiation, *TTX* tetrodotoxin. (*NR* not reported). Note that due to space constraint not all studies could be included

[a] Tetrodotoxin muscle model used

Table 10. Experimental data of potentiation in whole-isolated skeletal muscle of various animal models in which RLC content was measured (Vandenboom et al., 2013).

Author(s)	Species	Muscle	Temp	Rate and duration	% RLC-P	Main findings
Abbate et al. (2001)	Rat	MG	34	160 Hz, 1 s	13–42–50	PTP ↓ economy of contraction
Barsotti and Butler (1984)	Rat	EDL	23	66 and 100 Hz, 1–10 s	5–73	RLC-P does not alter energy usage
Klug et al. (1982)	Rat	Gastroc	37	5 Hz, 5–20 s	19–63	PTP correlated with RLC-P
MacIntosh and Bryan (2002)	Rat	MG	37	80 Hz, 4–7 s	11–33–50	↑ Isotonic work (shortening)
MacIntosh et al. (2008a)[a]	Rat	Gastroc	37	5 Hz 21 s;	15–42	SP without RLC-P
				200 Hz 1–10 s	11–9[a]	
MacIntosh et al. (1993)	Rat	Gastroc	37	10 Hz 20 s	10–72; 3–19	Fatigue ↓ RLC-P
Manning and Stull (1982)	Rat	EDL sol	23–35	10–200 Hz	14–60	FT and temp dep for RLC-P and PTP
Manning and Stull (1979)	Rat	EDL	23	200 Hz, 1 s	10–75	PTP and RLC-P correlated
Moore and Stull (1984)	Rat	Sol, gastroc	37	1–100 Hz, 10 s	0–34 s; 10–62 g	PTP & skMLCK activity ↓ with ↑ OP
Moore et al. (1985)	Rabbit	Sol, plan	38	100 Hz, 15 s (s)	2–10 s;17–45 p	No PTP (sol); 58 % PTP (plan)
				5 Hz, 20 s (p)		
Rassier et al. (1999)	Rat	Gastroc, plan	37	10 Hz, 10 s	5–26	SP w/o ↑ RLC-P
Rassier et al. (1997)	Rat	Gastroc	37	10 Hz, 10 s	10–15; 35–40	Len Dep of SP not RLC-P dependent
Tubman et al. (1996a)	Rat	Gastroc	37	200 Hz, 0.5–2 s	55 c; 40 f	Fatigue ↓ RLC-P but not PTP
Tubman et al. (1996b)[b]	Rat	Gastroc	37	10 Hz, 10 s	5–9[b]; 21–57	No PTP and no RLC-P with atrophy
Tubman et al. (1997)[a]	Rat	Gastroc	37	200 Hz, 2 s	5–21[a]; 14–49	PTP and RLC-P ↓ with atrophy

Studies examining staircase or PTP in rat and rabbit muscles in which RLC phosphorylation was determined, arranged alphabetically by first author. Columns (left to right) describe species, muscle(s) experimental temperature (Temp), stimulation paradigm used to induce potentiation (as frequency in Hz and duration in ms or sec), the range (minimum and maximum) of RLC phosphorylation (as %) reported at rest and in response to stimulation and a summary of main findings

EDL extensor digitorum longus, *gastroc* gastrocnemius, *GM* medial gastrocnemius *plan* plantaris, *sol* soleus, *FT* fiber type, *len dep* length dependence, *OP* oxidative potential, *PTP* posttetanic potentiation, *skMLCK* skeletal myosin light chain kinase, *SP* staircase potentiation, *temp dep* temperature dependence

[a] Hemisection muscle model used; [b] tetrodotoxin muscle model used

Appendix B: Additional Tables and Figures

Table 11. Experimental design for collection of contractile data during pilot experiments. The table shows the different pairings of shortening ramps from the beginning of an experiment to the end (left to right) between muscle samples.

VELOCITY OF SHORTENING (%Vmax)									
KO+WT (n = 4)		**Pair 1**		**Pair 2**		**Pair 3**		**Pair 4**	
SUBJECT 1	EDL (L)	10	30	5	20	40	70	50	60
	EDL (R)	70	20	50	40	10	30	60	5
SUBJECT 2	EDL (L)	60	10	70	50	30	5	40	20
	EDL (R)	30	40	60	70	5	50	20	10
SUBJECT 3	EDL (L)	5	50	40	10	60	20	70	30
	EDL (R)	40	70	10	30	20	60	5	50
SUBJECT 4	EDL (L)	20	60	30	5	50	40	10	70
	EDL (R)	50	5	20	60	70	10	30	40
TIME →									

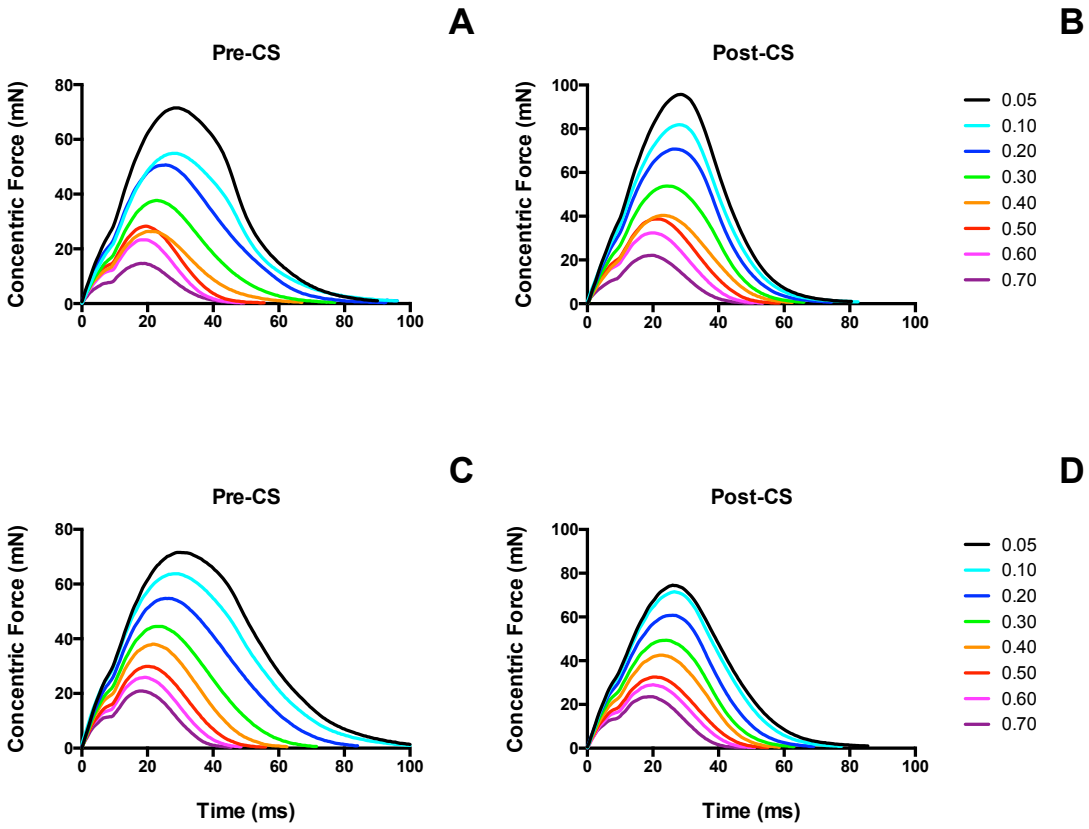

Figure 23. Mean concentric active force traces for each shortening speed, genotype, and condition (pre and post-CS). a) Represents mean force produced by WT muscle at rest (pre-CS); b) represents WT response after stimulation (post-CS); c) represents skMLCK$^{-/-}$response at rest (pre-CS); d) represents skMLCK$^{-/-}$ response after stimulation (post-CS).

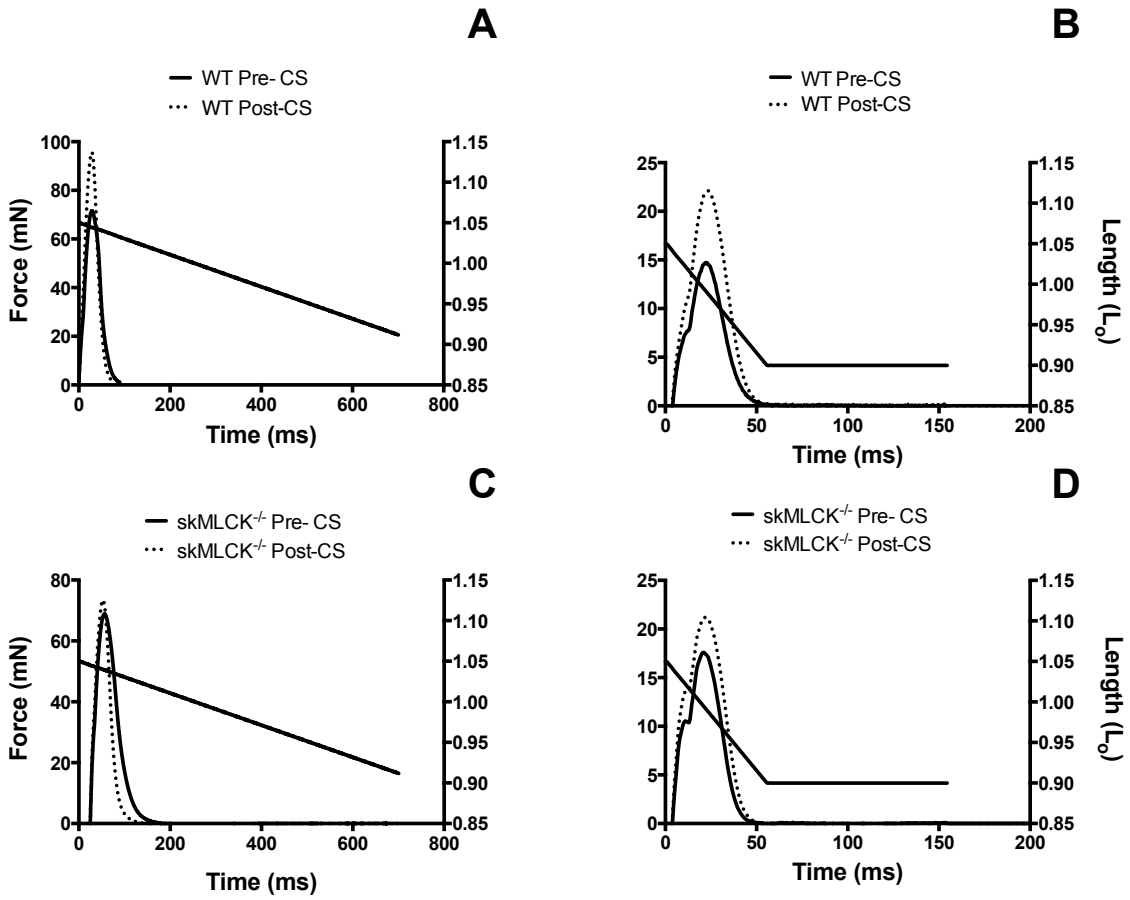

Figure 24. Raw concentric force traces during shortening ramps at 0.05 (A, C) and 0.70 V_{max} (B, D) in WT (upper panels) and skMLCK$^{-/-}$ (lower panels) mouse EDL muscle (n = 1), before (solid line) and after (dashed line) a tetanic conditioning stimulus. Length change (1.05-0.90 L_o) is superimposed to signify complete relaxation from force before the end of shortening.

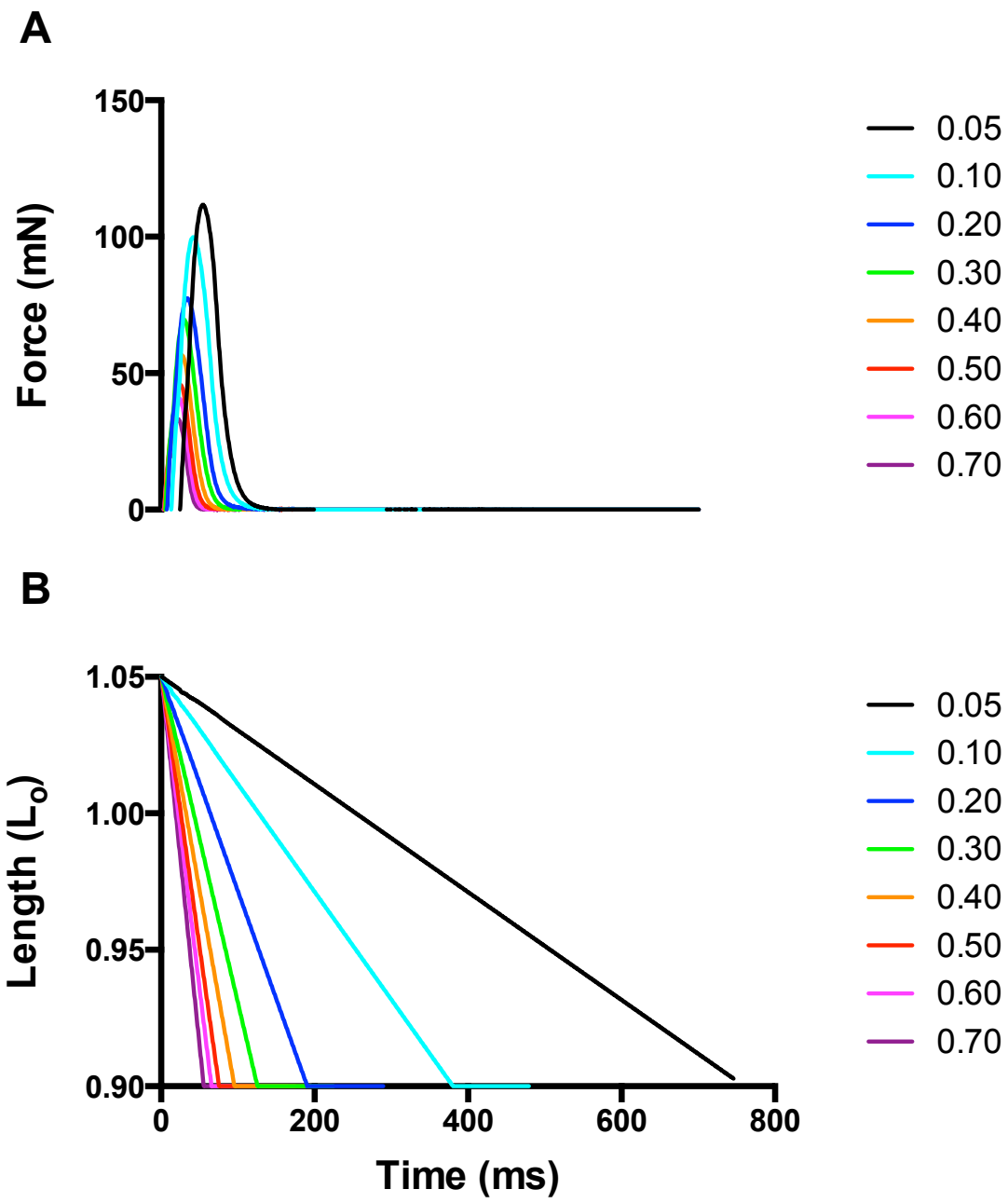

Figure 25. Representative traces of mean force (A) and length (B) during high frequency activation (100 Hz). Traces are taken from pre-CS WT muscle only (n = 1).

Appendix C: Western Blotting

Measurement of Myosin Regulatory Light Chain Phosphorylation by UREA/Glycerol-PAGE with Immunoblotting

Background

Myosin Regulatory Light Chains (RLCs) are small 18-20kDa) acidic proteins that are essential in the conversion of chemical energy into kinetic movement. RLCs migrate easily in polyacrylamide gels containing glycerol for increased density. RLCs are denatured with Trichloracetic acid (TCA) and solubilized in urea to dissociate from their larger myosin heavy chain counterpart. The addition of a phosphate group introduces two additional negative charges at a pH of 8.6 (the pH of the running buffer) so the phosphorylation measurements are in fact quantitative (mol of phosphate per mol RLC) after measurement of the protein band density by Immunoblotting.

The following protocol is an adaptation of the work by Dr. James Stull of the University of Texas Southwestern Medical Centre.

Sample Preparation

1. Freeze tissue samples (quickly with pre-cooled tongs) in liquid nitrogen and store at -80^{o}C (big freezer).
2. Add 0.5mL 10% of Tricholoracetic Acid (TCA; stock is 100% concentrated solid)/ 10mM dithiothreitol (DTT) in acetone to individual polypropylene tubes and freeze in liquid nitrogen.

3. Tubes are to be placed in -20^{o}C cold box (mini fridge), measure weight of frozen muscle tissue in cold box and then place muscle in the tube on top of the mixture from Step 2.
4. Submerge the muscle into the slurry.

   N.B. The frozen TCA and DTT in acetone solution will thaw and form a slurry at -35^{o}C.
5. Remove tubes from cold box and allow them to reach room temperature.
6. Transfer each denatured muscle sample to a ground glass homogenizing tube and add 0.5mL 10%TCA/ 10mM DTT in H_2O.

   N.B. The glass tubes to be used are Wheaton USA Ground Glass Tissue Grinders (3mL)
7. After complete homogenization, transfer homogenate to an Eppendorf tube.
8. Allow the homogenate to sit on ice for 10 minutes or more.
9. Centrifuge the samples at 2000 RPM for 3 minutes at room temperature on tabletop centrifuge.

   N.B. Do not pack the protein too hard or too long because it will become difficult to separate.
10. Carefully decant the supernatant fraction via pouring.
11. Wash protein (now a soft pellet) with 500µL of ether 3 times for 5 minutes each to remove any residue left by TCA (in total 15 minutes of washing).
12. Ether will evaporate from tube under fume hood and let this occur for 5 minutes.

    N.B. If the protein pellet is left in the hood, it will dry out completely
13. Add 30 µL of urea sample buffer per mg of frozen tissue weight (*Appendix I*).
14. Vortex each sample vigorously for 1-2 minutes.

    N.B. This causes the protein pellet to disperse; you should not have to manually disperse the protein pellet.
15. Check to ensure pH has a value of 9 and confirm this by the blue colour of the sample.

    N.B. If the colour is yellow or green, add 5 µL of 2 M Tris Base (basic; pH of 11)
16. Add a few crystals of urea and vortex. Urea may dissolve completely and if it does add more crystals until samples are saturated.

18. Store at -80^{o}C if not running gel the same day.

    N.B. This process is crucial and may take 1-2 hours ensuring all RLC is solubilized. DO NOT heat urea samples on thawing because carbamylation can change the protein's charge. Mix about 1 hour after thawing in water bath.

Preparing Glycerol Gels

1. Mix *Appendix II* and stir for 10 minutes under vacuum.
2. Add 107 µL of 10% APS and 17 µL of TEMED and mix by swirling.
3. Pour quickly into prepared mini-gel apparatus and insert 10 well combs

   N.B. No Stacking Gel. Gel should polymerize after 40 minutes.

Running Buffer

1. Lower Buffer: 83mL of Urea Gel Buffer † / 917mL of H2O
2. Upper Buffer: 73.3mg DTT/ 53.3 mg thioglycholate/ 200mL of Lower Buffer
3. Urea Gel Buffer †

Pre- Electrophoresis

1. Rinse with H_2O to remove any debris.
2. Rinse wells with Upper Buffer (73.3mg DTT/ 53.3 mg thioglycholate/ 200mL of Lower Buffer).
3. Assemble apparatus and pre-electrophorese @ 400V for about 1 hour to get thioglycholate into gel to reduce any residual APS and prevent protein oxidation.

Electrophoresis

1. Load 5-20 µL of each sample; since there is no stacking gel the tip of the pipet should be close to the well of the gel and added slowly with sample in the urea sample buffer.

   N.B. The layer should be a sharp band.

2. Load 15 µL to get good protein bands, if protein is to concentrated, sample can be diluted with urea sample buffer

   N.B. Do not include end wells as they tend to distort.

3. Electrophorese @ 400V for 85 minutes

Membrane Transfer

A. <u>Nitrocellulose</u>

1. Cut off approx. ¼ of the upper part of gel.
2. Rinse gels gently in transfer buffer for 5 minutes each.
3. Immerse nitrocellulose membrane in transfer buffer for 1 minute to wet it.

**How the sponge, blotting paper, nitrocellulose or PVDF and gel should be organized.

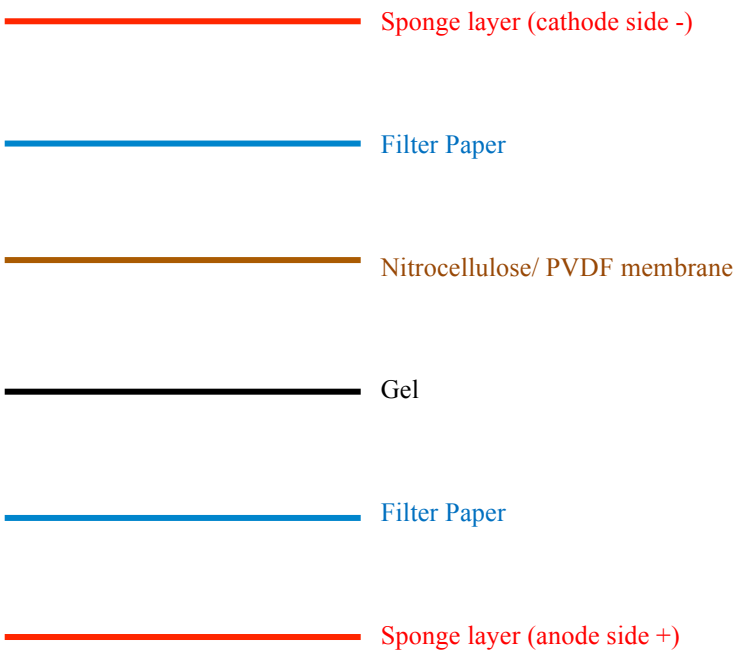

4. Transfer membrane @ 25V for 1 hour.

See *<u>Appendix III</u>* for **Transfer Buffer** and *<u>Appendix IV</u>* for 10x **Transfer Buffer.**

B. <u>PVDF</u>

1. Pre- soak membrane in methanol for 5 minutes.
2. Cut off approx. ¼ of the upper part of gel.
3. Rinse gels gently in transfer buffer for 5 minutes each.
4. Immerse PVDF membrane in transfer buffer for 1 minute to wet it.

N.B. PVDF is done the same as nitrocellulose except it is presoaked in methanol for 5 minutes.

Membrane Preparation after Transfer

A. Nitrocellulose

1. Wash the membrane in TBST 3 times for 10 minutes each.

   N.B. See *Appendix V* for TBST
2. Block with blocking buffer for 1 hour at room temperature to prevent non-specific binding.

   N.B. See *Appendix VI* for Blocking Buffer
3. Add between 1:7500 skRLC polyclonal antibodies to blocking buffer and incubate with rocking overnight at 4^{o}C [1.333 µL skRLC/ 10ml blocking buffer].

B. PVDF

1. Soak membrane in 0.4 glutaraldehyde in PBS [i]for 30 minutes room temperature.
2. Wash membrane 3 times in PBS.
3. Block with 5% Amersham blocking solution for 1 hour.
4. Add 1^{o} antibody in 0.5% blocking solution for 1 hour at room temp with gentle shaking, rocking, or rolling.

Membrane Treatment

****IDENTICAL STEPS EXCEPT TBST AND PBS**

A. Nitrocellulose

1. Remove primary antibody (buffer can be re-used up 3 times) and wash membrane with TBST 3 times for 10 minutes each.
2. Incubate the membrane with 2^{o} (1:10000) goat anti-rabbit IgG- HRP in TBST for 1 hour @ room temperature.

3. Wash membrane 3x for 10 min each time with TBST.
4. Make detection buffer (ECL Plus).
    a. Mix equal volumes of luminol reagent and oxidizing agent i.e., 3ml & 3ml.
5. Incubate the membrane in detection buffer for 3-5 minutes.
6. Drain excess reagent, rinse with dH_2O, and cover with plastic blot protector.

B. <u>PVDF</u>

1. Remove primary antibody (buffer can be used up 3 times) and wash membrane with PBS 3 times for 10 minutes each.
2. Incubate the membrane in 1:10000 goat anti-rabbit IgG- HRP in PBS for 1 hr @ room temperature.
3. Wash membrane 3x for 10 min each time with TBST.
4. Make detection buffer (ECL Plus).
    a. Mix equal volumes of luminol reagent and oxidizing agent.
5. Incubate the membrane in detection buffer for 2 minutes.
6. Drain excess reagent and cover with plastic wrap.

Development (Enhanced Chemiluminescence)

1. Using FlourChem 5500 (Alpha Innotech), select "INSERT" function on the computer and wait for instrument to initialize.
2. Open main door and place your sample on the glass, aligning numbers and letters on the side of glass.
3. Move sample to fit current camera location and make sure membrane is placed protein side down; cover the back with parafilm:
   Click ***Chemiluminescence***
4. Add appropriate exposure time (may vary) to ensure complete image transfer.
5. Click on the ***Scan*** icon, and a save option will pop up
6. Save file as ***name, date and experiment***, under ***Save Scan Data In*** option and specify location where you want saved (use a USB or save to desktop using a separate folder)
7. Then click ***Save*** to continue

8. Analyze later using blot software “Imagej” or “Image Studio Lite” by LI-COR.

Particular Supplies and Reagents

- Secondary antibody- goat anti rabiit IgG HRP
- ECL plus Amersham
- Homogenizing tubes: Wheaton USA Ground Glass Tissue Grinders, 3mL (mortar and pestle)
- Nitrocellulose mem, 0.45 micrometre pore size from Bio- Rad
- PVDF membrane, 0.45 micrometre pore size for Immobilon-P membrane from Milipore

Typical Results

- Different phosphorylated forms of the skRLC are separated in this gel system; nonphosphorylated RLC, mono- (Mono-P RLC), and di- (Di-P RLC)

APPENDIX I

Sample Buffer

REAGENTS	QUANTITY
8 M Urea	1.83 mL
Urea Gel Buffer	167.0 µL
0.5 M DTT	40.0 µL
Saturated Sucrose	100.0 µL
0.2% Bromophenol Blue	40.0 µL
0.4 M EDTA	1.0 µL

Urea Gel Buffer

REAGENTS	QUANTITY
Trizma Base	13.7 g
Glycine	10.0 g
H_2O	Q.S. to 500ml

APPENDIX II

Gel Casting Reagents

REAGENTS	QUANTITY
Ammonium persulfate	0.10 g
dH_20	1.0 mL

Urea/ Glycerol Gel Polyacrylamide Gels

REAGENTS	QUANTITY
dH_2O	4.2 mL
Glycerol	9 mL
30% Acrylamide/ Bis 29:1	7.5 mL
Urea Gel Buffer†	1.9 mL
Stir for 10 minutes under vacuum to degas	
10% APS	~113.0 µL
TEMED	~20.0 µL
Mix by swirling	
Quickly pour into minigel apparatus & insert combs	

APPENDIX III

Transfer Buffer

REAGENTS	QUANTITY
10X Transfer Buffer	100 mL
100% Methanol	200 mL
dH_2O	700 mL

APPENDIX IV

10x Transfer Buffer

REAGENTS	QUANTITY
Glycine	144.12 g
Tris	30.29 g
SDS	5.0 g
dH_2O	500.0 mL
Dissolve	
dH_2O	Q.S. to 1.0 L

APPENDIX V

10x TBS

REAGENTS	QUANTITY
NaCl	87.66 g
2M Tris pH 7.5 (HCL)	15.76 g
10% Tween	30.0 mL
dH_2O	Q.S. to 1.0 L

Tris-Buffered Saline with Tween-20 (TBST)

REAGENTS	QUANTITY
10x TBS	100.0 ml
Tween-20	0.50 mL
dH_2O	Q.S. to 1.0 L

APPENDIX VI

Blocking Solution

REAGENTS	QUANTITY
Carnation fat- free powdered milk	10.0 g
TBST	Q.S. to 200.0 ml